AN ABSTRACT OF THE THESIS OF

David Robert Askren for the degree Master of Ocean Engineering

in Civil Engineering (Major Department) presented on September 15, 1977

Title: NUMERICAL SIMULATION OF SEDIMENTATION AND CIRCULATION IN RECTANGULAR MARINA BASINS

Abstract approved: Redacted for privacy

Dr. Larry S. Slotta

The shear-induced circulation and sedimentation of cohesive particles in rectangular marina basins is simulated using finite-difference and finite element techniques, respectively. The solutions consider the effects of varying 1) basin length, 2) basin width, 3) entrance width, 4) entrance placement, 5) number of entrances, 6) suspended sediment concentration at the entrance, 7) entrance boundary velocity, and 8) strength of transverse dispersion. The results are presented in graphical form to facilitate the estimation of basin-averaged velocities and sedimentation rates for a variety of simple marina configurations. It is suggested that Nobel's (1976) basin-flushing guidelines be used jointly with these results to warn of undesireable flushing characteristics.

The shear-driven vortex circulation may be enhanced by increasing the relative entrance width, or decreasing either the basin width or length. Sedimentation varies directly with the entrance width, the concentration of suspended sediment at the entrance boundary and the strength of transverse dispersion. It varies inversely with the entrance boundary velocity, basin length and basin width.

A square planform with a single entrance, centrally-located in the breakwater produces both maximum basin-averaged circulation and maximum sedimentation. An optimum balance between basin area, circulation and sedimentation should be achieved through increasing the basin length rather than width. Basins with length/width ratios greater than unity and an entrance located downstream of the center of the breakwater will have lower sedimentation rates than an upstream entrance; an upstream entrance is preferable for basins with lower aspect ratios. For a given total entrance width, multiple entrances can be used to measureably improve the velocity distribution without significantly increasing the basin-averaged sedimentation rates.

Numerical Simulation of Sedimentation and Circulation in Rectangular Marina Basins

by

David Robert Askren

A THESIS

submitted to

Oregon State University

in partial fulfillment of
the requirements for the
degree of

Master of Ocean Engineering

Completed September 15, 1977

Commencement June 1978

APPROVED:

Redacted for privacy

Professor of Civil Engineering
in charge of major

Redacted for privacy

Head of Department of Civil Engineering

Redacted for privacy

Dean of Graduate School

Date thesis is presented September 15, 1977

Typed by Carol Askren for David Robert Askren

ACKNOWLEDGEMENTS

This work is the result of research conceived by Dr. Larry S. Slotta and sponsored in part by the Oregon State University Sea Grant College Program, supported by the NOAA Office of Sea Grant, Department of Commerce, under grant number 04-7-158-44085. Special thanks is extended to Dr. Ranjan Araithurai, Niesen Engineering and Research, Inc., Mountain View, California, who donated the computer program used in this research.

TABLE OF CONTENTS

TABLE OF CONTENTS (cont.)

LIST OF FIGURES

LIST OF TABLES

LIST OF SYMBOLS

The following symbols are used in this paper:

a = constant or the vertical cross-sectional area of the entrance at MLLW

A = eddy coefficient or basin plan area at MLLW

Avcon = average suspended sediment concentration over element

b = constant

$b_{i\alpha}$ = element load matrix term

B_i = system load matrix term

c = suspended sediment concentration in mass per unit area of basin planform

c_o = suspended sediment concentration at entrance boundary

C = Chezy friction factor

cosh = hyperbolic cosine

d = depth

D = dispersion coefficient

D_{ne} = domain of all n elements

DH = uniform grid spacing

DT = computational time increment

DXL = distance between points in interpolation polynomial grid

DXR = distance between points in interpolational polynomial grid

DXT = distance between points in interpolational polynomial grid

DYL = distance between points in interpolational polynomial grid

DYU = distance between points in interpolational polynomial grid

DYT = distance between points in interpolational polynomial grid

E = average per-cycle exchange coefficient

$f_{i\alpha}$ = element sink vector term

$F_{i\alpha}$ = system sink vector term

g = acceleration of gravity

G = constant

h = water depth below some datum

I = grid point position in x direction

J = grid point position in y direction

k = constant

$k_{i\alpha}$ = element steady-state matrix term

K = constant or iteration level

$K_{i\alpha}$ = system steady-state matrix term

L = basin length

$L_{1,2,3}$ = area coordinates

m = mass of flocs

MLLW = mean lower-low water

n = number of particles or the Manning friction factor

$\vec{n}$ = surface unit vector

N = constant

N_i = shape function for vertex node i

$N_{i,j}$ = shape function for mid-section node

p = pressure

P = probability of deposition

r = radius of curvature of main flow

R = residual

Re = turbulent or viscous Reynolds number

Re_s = stagnation Reynolds number

S = sedimentation rate or surface when defining integral limits

S.G. = specific gravity of dry sediment

sin = sine

sinh = hyperbolic sine

ss = constant

t = time

$t_{i\alpha}$ = element temporal matrix term

T = non-dimensional shear stress

$T_{i\alpha}$ = system temporal matrix term

TT = depth/average velocity over element

u = velocity component in x direction

$u_m(o) = u_m$ of basin without constricted entrance

u_o = entrance boundary velocity

u_∞ = free-stream velocity

u_* = shear velocity

v = velocity or velocity component in y direction

$\bar{v}(0) = \bar{v}$ of basin without constricted entrance

v_f = filling velocity

$v_m(o)$ = v_m of basin without entrance constriction

v_s = particle settling velocity

V = volume

w = vertical velocity

W = basin width

W_e = entrance width

x_o = x coordinate of gyre center

y_c = y coordinate of gyre center according to Weiss and Florsheim (1965)

$y_o(o)$ = y_o for basin without constricted entrance

z = vertical direction

α = 1/Re

β = mesh aspect ratio

γ = grid constant

δ^* = upstream boundary layer thickness

Δ = constant and equal grid spacing in both x and y directions

Δt = time increment

Δx = grid spacing in x direction

Δy = grid spacing in y direction

η = time-varying water-surface elevation above some datum

η_i = temporal shape function for node i

θ = angle between the x axis and velocity vector

υ = kinematic viscosity

ξ = vorticity

ρ = density

τ = shear stress

Φ = constant or variational functional

ψ = stream function

ω = convergence parameter

ℓ = minimum grid size

Superscripts used:

K = iteration level

$\hat{}$ = approximation

' = perturbation

Subscripts used:

b = bottom

B = boundary

c = central entrance case or coagulation (flocculation) time to equilibrium

cd = critical for deposition

eu = upstream end of entrance

E = entrance

f = final or fluid

h = horizontal

i,J,K, = element node identification

L = lateral

m = maximum

o = initial or unconstricted entrance case

r = rolling

t = transverse

x = in the x direction

xy =in x direction due to processes acting in y direction

xx = in x direction due to processes acting in x direction

y = in y direction

yy = in y direction due to processes acting in y direction

1,2,3 = nodes at vertices of triangular element

4,5,6 = nodes at midpoint in sides of triangular element

||B = parallel to boundary

⊥ B = perpendicular to boundary

||E = parallel to entrance

⊥E = perpendicular to entrance .

α = element node identification

NUMERICAL SIMULATION OF SEDIMENTATION AND CIRCULATION IN RECTANGULAR MARINA BASINS

I. INTRODUCTION

1.1 Problem Statement

Man, in pursuit of commerce and diversion in the sea, has for centuries appreciated the protection offered by bays and estuaries. Within such areas, harbors and marinas have been built which, by design, have traditionally emphasized protection from the environment rather than marina basin water quality. As a consequence, such facilities have frequently suffered from a minimum of exchange between basin and external waters and have acted as traps for suspended and dissolved substances.

Current legal and public pressure to maintain and improve water quality has motivated investigation of the relationship between basin configuration, recirculation, and sedimentation. Most engineering investigations are site specific. In the case of existing marinas, many of which are rectangular in plan form, these investigations consist of field and, possibly, physical model studies of the hydraulics of the marina basin. For new marinas, either physical or mathematical models are often employed to determine circulation characteristics (Tang, 1976). However, due to the difficulties involved in properly scaling both fluid forces and sediment particle properties in physical models, the designer frequently relies on numerical models for prediction of sedimentation. Such models require both substantial computer facilities and a familiarity with mathematical techniques not traditionally in the design engineer's repertoire.

The intent of this study is to investigate, through computer simulation, the functional dependence of basin circulation and sedimentation on various environmental and basin parameters and to provide the design engineer with some first-order predictions of

circulation and sedimentation characteristics for rectangular small-boat basins. The circulation and sedimentation fields are determined numerically, as described briefly in Section 1.3 and in detail in Chapters II, III, and IV, using finite-difference and finite-element programs developed by Araithurai (1974). Non-dimensional plots of velocities and sedimentation rates are presented in Chapter V.

1.2 Generalized Aspects of Shear-Generated Circulation and Sedimentation in Marina Basins

As described by Nece, et al. (1976) and Vollmers (1976), the circulation in a basin adjacent to a tidal channel is driven by density, tidal, and current effects (Figure 1.1). Differences in marina and exterior water temperatures, salinities, or suspended sediment concentrations cause an exchange of water and suspended or dissolved solids between the two water bodies. Since marinas are generally warmer than exterior waters and have equal or lower dissolved and suspended-solids concentrations, the exchange generally occurs through an inflow of external water through the entrance and along the bottom with a compensating outflow of basin water near the surface. Tidal currents periodically flood into or out of the basin, acting over the entire depth of the entrance. Such "flushing" flows are important in determining the over-all water quality of the basin. Equally important are the circulation cells or "vortices" generated within the basin as a consequence of velocity shear between basin and external waters. This present study centers on this last process--shear-generated circulation or current effects--and the sedimentation field that results from the process.

The end of the upstream breakwater or entrance constriction defines a flow-separation point downstream of which develops an interface region (Westrich, 1975) between channel and basin waters (Figure 1.2). This interface region grows laterally in the

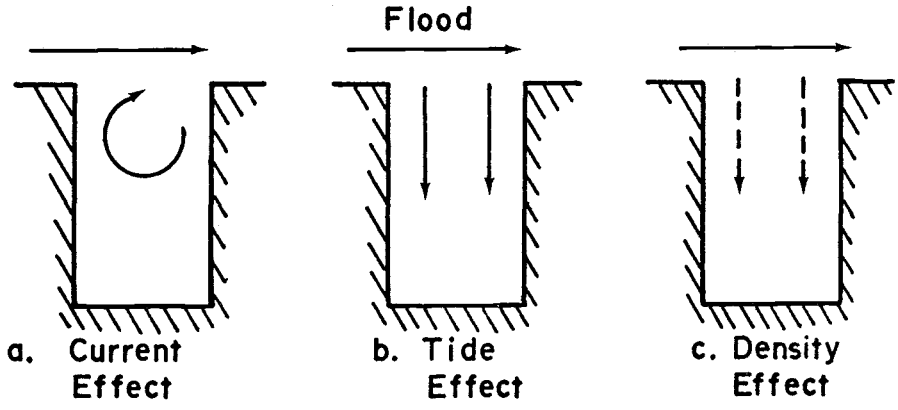

Figure 1.1. Fundamental components of Marina circulation. From Vollmers (1976).

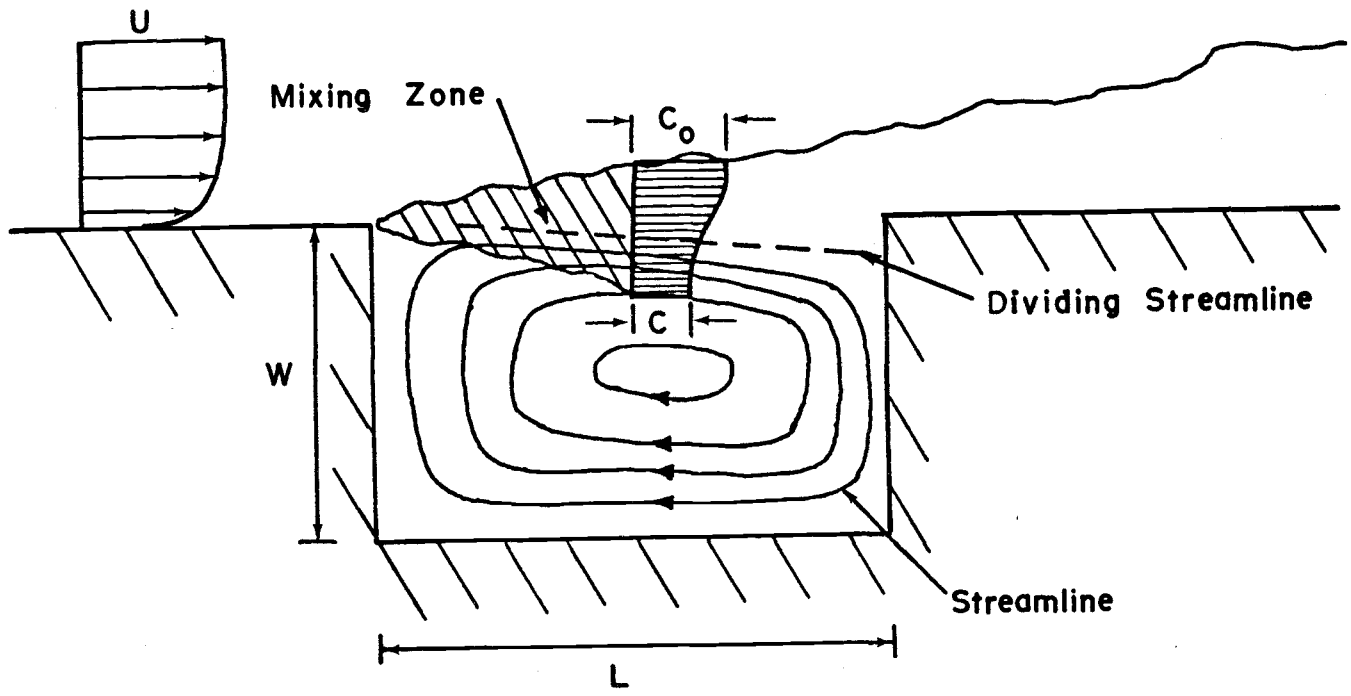

Figure 1.2. Schematic of circulation and mixing between a waterway and an adjacent marina basin. C_o is the suspended sediment concentration in the waterway and C is the concentration within the basin. Modified from Westrich (1975).

downstream direction and is characterized by strong velocity shear and mixing between basin and external waters. The downstream end of the entrance defines a flow stagnation point at which part of the interface flow is diverted into the basin interior. This flow, the shear exerted in the interface zone, and the requirement of mass continuity for the basin as a whole are responsible for the generation of the primary circulation gyre or vortex in the basin. This rotary current may induce secondary circulation cells within a sufficiently-large basin but the circulation of the secondary cells will be relatively weak. On an ebbing flow, channel flows exert less influence upon basin waters due to the outward flow of water from the basin. The outward flux of momentum and reduced interface shear serve to weaken and, possibly, destroy the flood-induced circulation gyre. Chapter II provides a detailed discussion of recent analytical, numerical, and laboratory investigations of this current-generated circulation.

Sedimentation in marina basins occurs as a complex function of basin configuration, entrance velocity and suspended sediment concentration. Sediments enter the basin with inward-flowing density and tidal flood currents and with the inward-diverted arm of the primary vortex. Coarser sediments deposit near the entrance and downstream along the flow path of the diverted current (Zone a, Figure 1.3). Turbulenct flows disperse the sediment laterally. Deposition occurs as increasingly tranquil conditions are encountered, the low velocity core of the primary circulation cell being especially favorable for sedimentation (Zone b, Figure 1.3). Sediments leave the basin with the emptying flow on ebb tide or may be reinjected into the channel when the sediment again encounters the interface zone. Chapter III provides a detailed discussion of recent numerical, laboratory, and field investigations of basin sedimentation characteristics. Chapter IV details the finite-element solution of the sedimentation problem for marina basins.

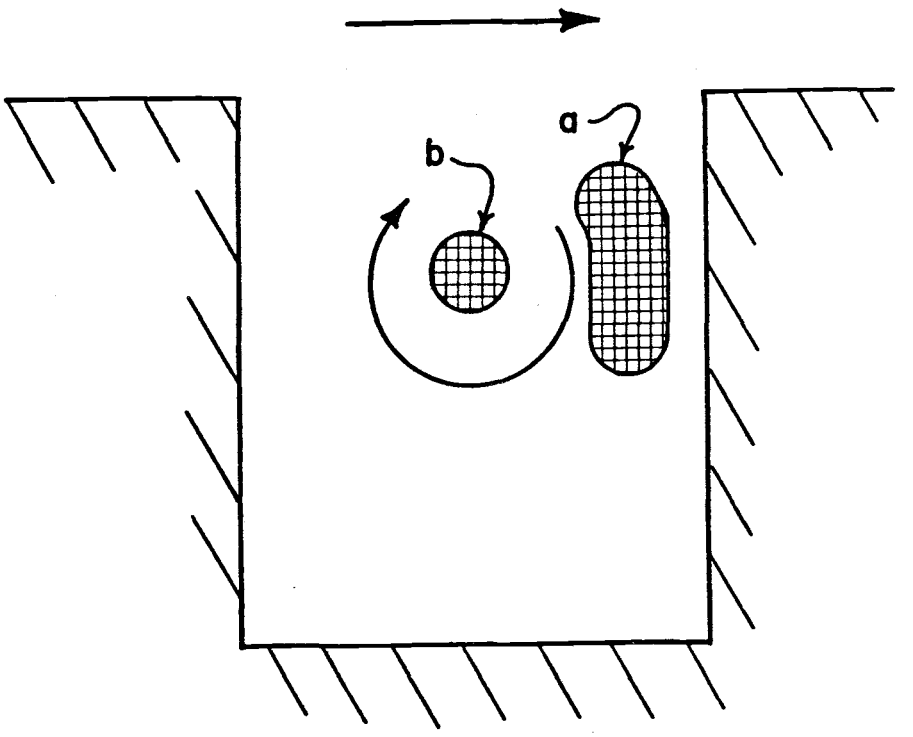

Figure 1.3. Schematic of the sedimentation pattern in a basin connected to a waterway. Cross-hatched areas indicate regions of higher sedimentation rates. From Vollmers (1976).

1.3 Cases Studied

Marina basins have traditionally been rectangular in plan form with relatively steep walls and a dredged, uniform depth. The longest dimension of the basin is frequently oriented parallel to the main channel and a breakwater with one or more entrances provides protection from external waves and currents. Figure 1.4 defines the basic parameters used in this study. Basin length, entrance width, and the x-axis were oriented parallel to the main channel and basin width and the y-axis were oriented towards the interior of the basin.

In marina-design problems, the basin plan area, minimum water depth, and minimum entrance width are generally predetermined by the nature and number of vessels that will use the marina. The design engineer has control over the basin configuration and the orientation, number and width of the entrances. The cases tabulated in Table 1-1 and diagrammed in Figure 1.5 illustrate the effects of varying these parameters as well as the effects of varying entrance boundary velocity and dispersion rates. A rectangular planform was adopted and the velocity and sedimentation rates were computed at specified points--nodes--within the basin. Constant water depths and entrance boundary velocities were also maintained to facilitate the comparison of results and minimize computational expense. Hence, the results of this study are more directly related to the temporal-mean channel velocity than to peak or short-term average velocities. The mean channel velocity for tidal flows is determined by averaging velocity observations over a number of tidal periods and is generally equal to or greater than the velocity that would result purely from river discharge. This velocity is either provided to the design engineer or can be estimated from published river flow data.

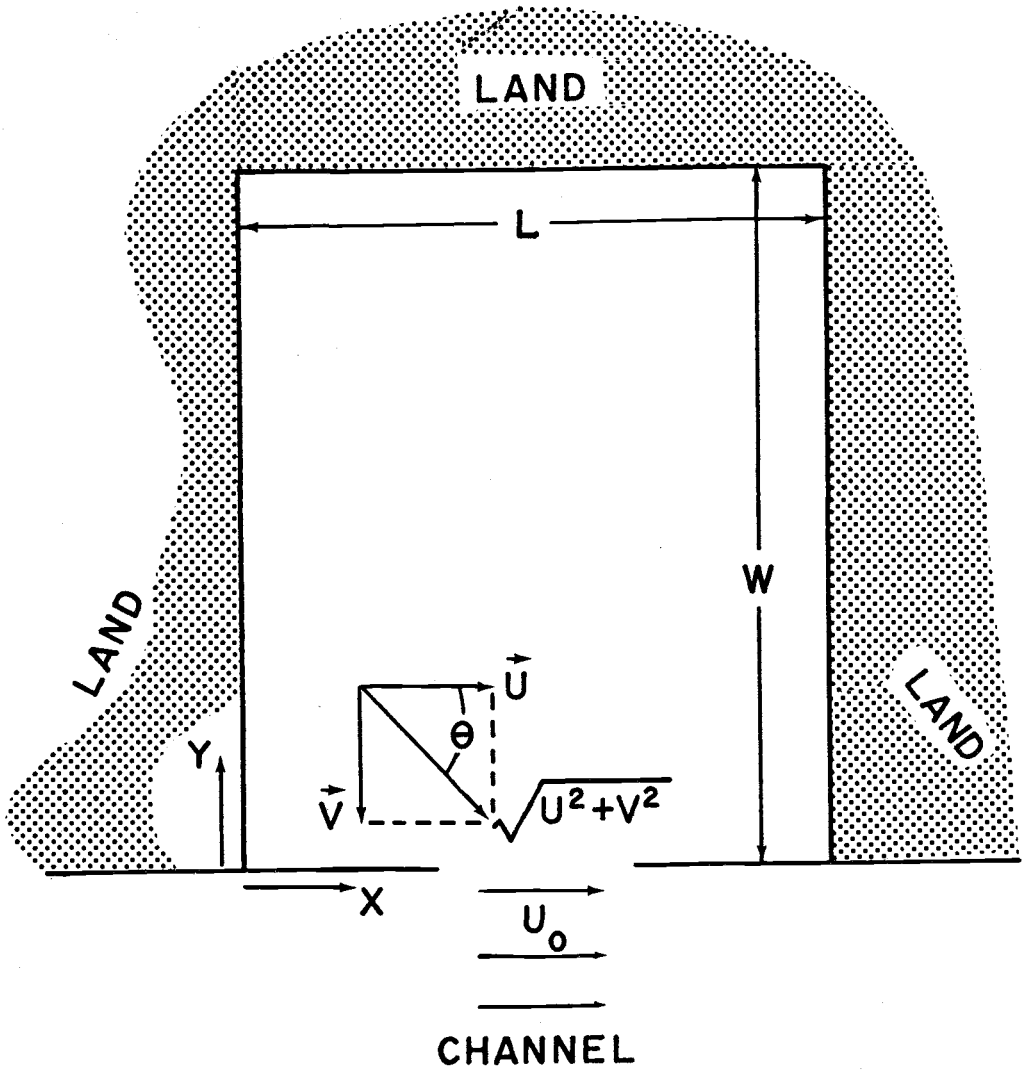

Figure 1.4. Schematic defining terms.

TABLE 1-1. Simulated Cases

Case[1]	Re[2]	Basin Length m	Basin Width m	Special Conditions[3]
O2X2	20	200	200	
U2X2	20	200	200	
C2X2	20	200	200	
D2X2	20	200	200	
C2X3	20	200	300	
O2X2	20	200	400	
U2X4	20	200	400	
C2X4	20	200	400	
D2X4	20	200	400	
C2X6	20	200	600	
O4X2	41	400	200	
U4X2	41	400	200	
C4X2	41	400	200	
C4X2V50	45	400	200	u_o = 0.50 m/s
C4X2V100	47	400	200	u_o = 1.00 m/s
D4X2	41	400	200	
CE4X2	41	400	200	W_e = 132 m
UD4X2	41	400	200	Two entrances
C4X2D100	41	400	200	$D_t = (23d\sqrt{u^2+v^2})/22$
C4X2D1000	41	400	200	$D_t = (230d\sqrt{u^2+v^2})/22$
C6X2	61	600	200	

[1] Entrance location is indicated as O (open or unconstricted), U (upstream), C (center), or D (downstream) end of breakwater. CE denotes a central entrance of doubled width.

[2] Eddy basin Reynolds number; $Re = u_o L/A_h$, $A_h = 60\, u_* d$.

[3] Unless otherwise noted: $D_L = (60\sqrt{u^2+v^2})/22$, $D_t = (0.23d\sqrt{u^2+v^2})/22$, $d = 4.5$ m, $c_o = 5\times10^{-5}$ kg/l, $W_e = 66$ m, $U_o = 0.15$ m/s

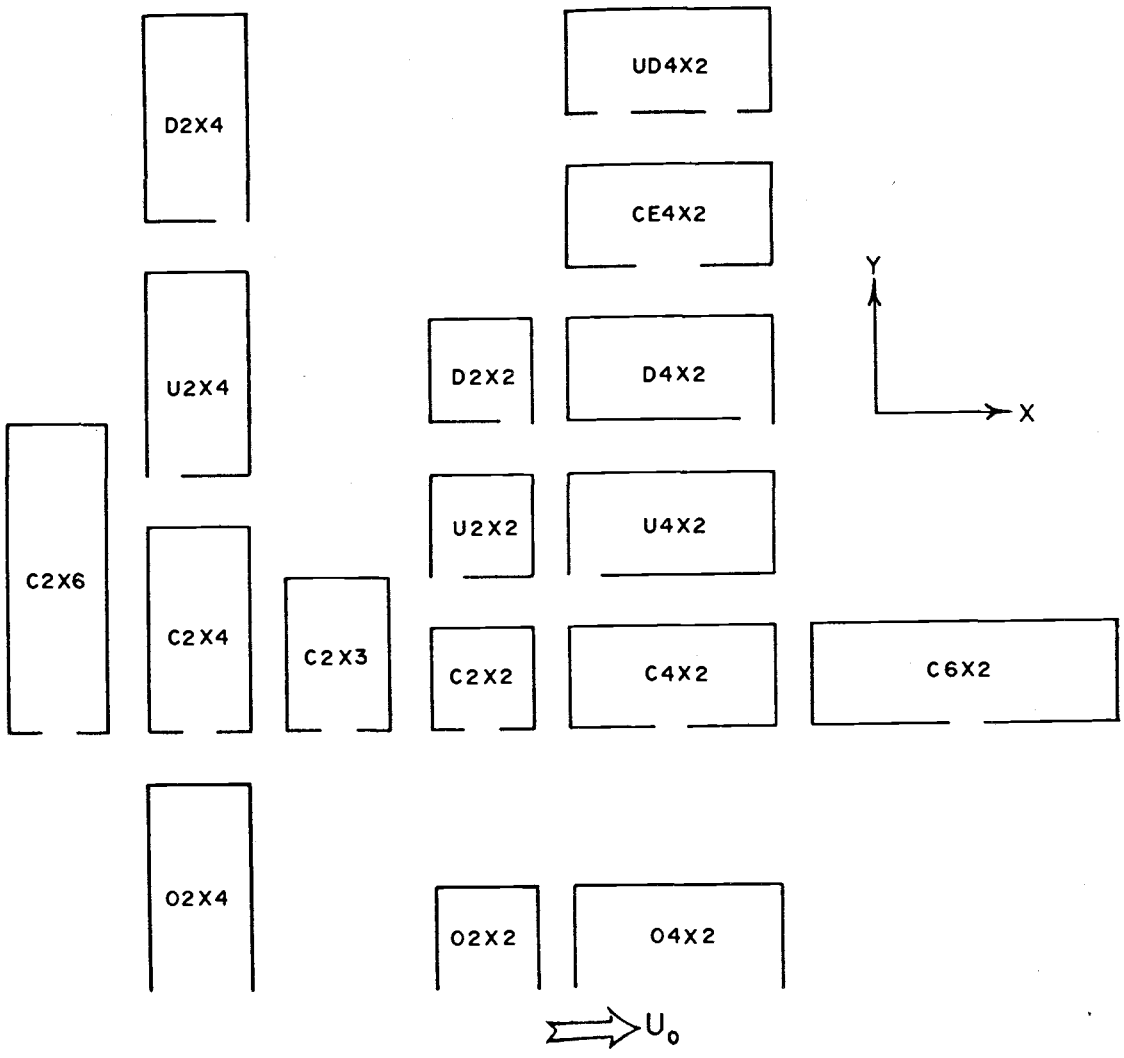

Figure 1.5. Marina-study case geometry. Entrance location is indicated as open (unconstricted), upstream, central or downstream by O, U, C, or D, respectively. Basin length and width are given in hundreds of meters by the first and second numbers, respectively, of the code identifying each case.

The range of parameters was characteristic of Oregon's coastal marains (Nobel, 1976). The unit basin dimension chosen was 200 m and aspect ratios--the ratio of basin length to width--of 3:1, 2:1, 1:1, 1:2, and 1:3 were considered. A respresentative average depth of 4.5 m was chosen and held constant throughout this study. Since many marinas have aspect ratios greater than unity, basins with aspect ratios of two were used to investigate the effects of entrance velocity (15, 50, 100 cm/s), entrance concentration (50, 100, 1000 mg/l), entrance width (66, 132 m), and transverse dispersion (100 and 1000 times standard level). Except for cases CE4X2 and UD4X2, a single 66 m wide entrance was situated at either the upstream or downstream end of the breakwater or at its center. For case CE4X2 the central entrance was 132 m wide and in case UD4X2 two 66 m entrances were placed one entrance length away from the land ends of the breakwater.

In all cases, the entrance boundary velocity acted only tangent to the entrance boundary and no fluid was advected into the basin. Since the symmetry of the problem made the downstream entrance solutions equivalent to the solution for the upstream entrance under reversed flow conditions and vice versa, the superposition of both solutions permits the first order estimation of average sedimentation rates under "oscillating" flow conditions.

1.4 Solution Technique

The solution for each case was achieved in two phases. First, the circulation field was determined. Secondly, the associated sedimentation field was computed. This section considers the general formulation and solution of each problem. Detailed descriptions of the solution techniques may be found in Chapters II, III, or IV.

The circulation problem for a basin connected to a passing waterway was posed by the two-dimensional, horizontal, vorticity-transport equation (momentum transport), the Poisson equation (vorticity), and by no-slip, impermeable boundary conditions at solid boundaries and strictly tangential uniform velocity conditions at the entrance boundary. Equations 2.2.11 and 2.2.12 and the boundary conditions equations explicitly formulate the problem. The principal assumptions implicit in these formulations include:

1) incompressible, steady or slowly-varying flow;
2) velocities, dispersion coefficients, etc., were taken as vertical averages;
3) turbulent perturbations of density and pressure were neglected;
4) the Reynolds shear stress analogy was applicable to terms involving products of turbulent velocity fluctuations, permitting each term to be replaced by the customary Fickian analog employing turbulent diffusion coefficients;
5) vorticity dispersion coefficients were locally constant;
6) vertical velocities and accelerations were neglected;
7) the flow within the basin was strictly recirculating and there was no velocity component perpendicular to the entrance boundary;
8) vertical gradients in the horizontal velocity vanished near the water-air interface;
9) the stream function was identically zero at solid boundaries but had a value at the entrance of $\psi_e = u_o \Delta y$, where Δy is the finite difference grid length parallel to the y-axis at the entrance;
   and that
10) first order spacial derivatives of the stream function must be continuous and finite.

The governing differential equations were approximated using truncated, three-point Lagrangian polynomials (Figure 1.6). The vorticity transport equation was solved for the vorticity field at each new time level using the alternating direction method and Thomas algorithm. The Poisson equation was then solved iteratively for the corresponding stream function field via the successive over-relaxation technique. Time was incremented and the above procedure repeated until a given time period had elapsed or other convergence criteria were satisfied. Initial conditions specified zero velocity in the interior of the basin. A non-dimensional time increment, $\Delta t u_o/L$, of 0.02 was adopted and a total elapsed time of 5.00 was considered sufficient for convergence to steady-state conditions. Subsequent to convergence, numerical differentiation of the stream function yielded the velocity field.

The sedimentation/transport problem for a marina basin was specified by the sediment advection-dispersion equation (Equation 3.1.1) and the requirement that the entrance boundary concentration be continuous and remain constant. The problem was formulated using the Galerkin weighted residuals technique and solved via the finite element method following the flow chart of Figure 1.7. The principal assumptions involved include the following:

1) the velocity field was stationary;
2) suspended sediment floc size was in equilibrium with fluid shear effects;
3) concentrations, velocities, etc., were taken as vertical averages;
4) sediment dispersion coefficients were considered to have distinct components parallel and perpendicular to the local velocity vector;

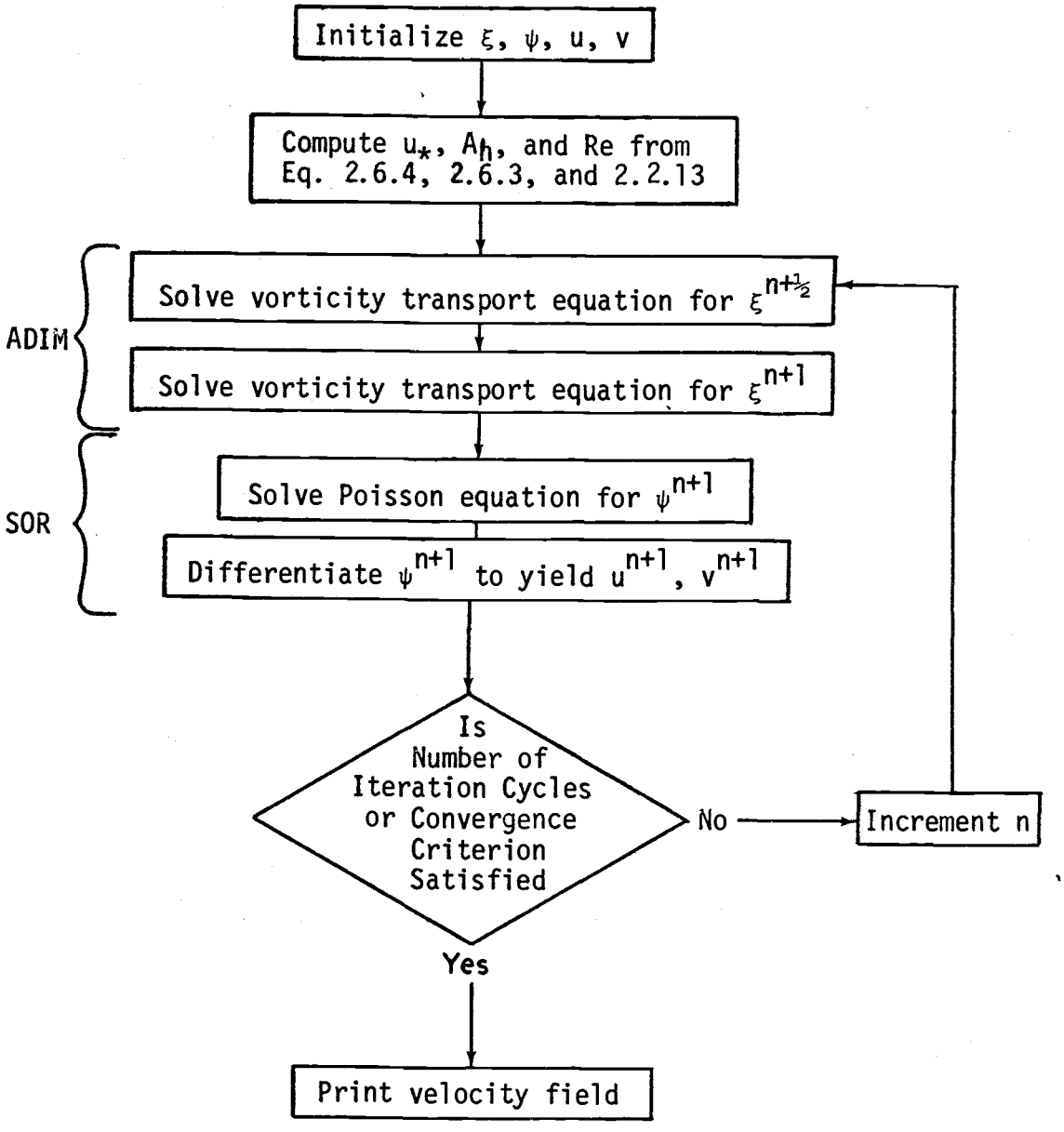

Figure 1.6. Flow chart for the finite-difference solution of the circulation problem.

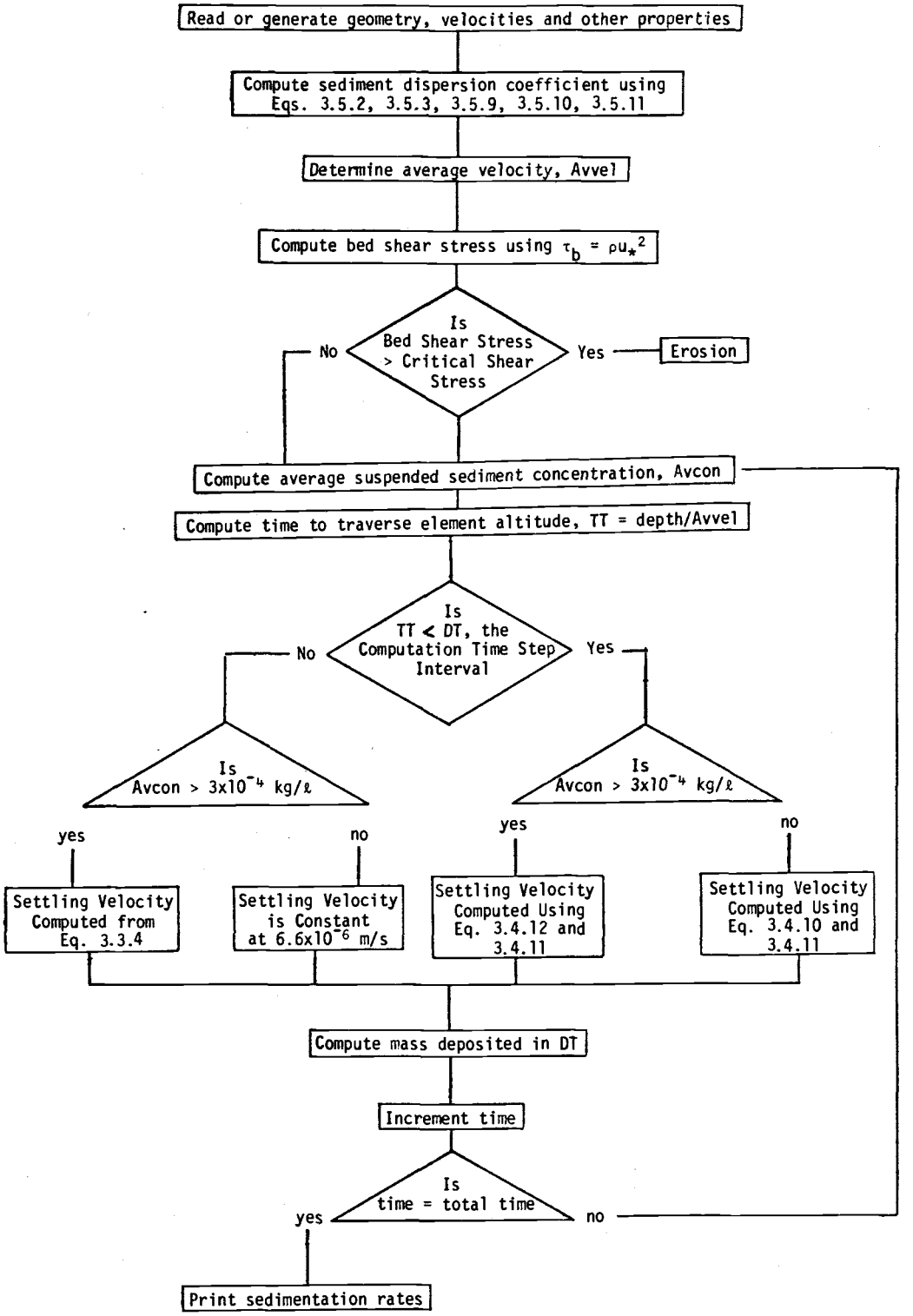

Figure 1.7. Flow chart for the finite-element solution of the sedimentation problem. Modified from Araithurai (1974).

5) the dispersion coefficients may be adjusted to partially account for the effects of secondary currents; and
6) the settling velocity was linearly proportional to suspended sediment concentrations below 0.3 gm/l.

Initial conditions specified a uniform concentration over the entire domain. A time increment of one-half hour was found to ensure computational stability and smooth convergence. Computation proceeded until the sedimentation rate for a specified interior element changed less than 0.5% over one time increment. The coarseness of this criterion was necessitated by the slowness of convergence for basins having interiors which were far removed from the entrance. Except for case D4X2 and cases with aspect ratios of 0.5 or less, the upstream interior corner element was used since it characteristically exhibited the slowest rate of convergence. For the remaining cases, the isolation of the interior resulted in very low concentrations (less than 10^{-6} kg/l) and unavoidable numerical instabilities. Consequently, the computation was allowed to proceed until the concentration in the upstream interior element dropped to 10^{-6} kg/l.

II. THE FLUID FLOW PROBLEM

2.1 Introduction

Since an estuary may be defined as the zone of transition from unidirectional, time-varying freshwater flows to the tidally-varying ocean, one may expect to find a gradation in salinity, suspended sediment load, and current velocity along the estuary. The marina location will then necessarily have a substantial effect on marina circulation, water quality, and sedimentation characteristics. If the marina is located close to the estuary head, basin salinity will be low, stream flows relatively steady and basically unidirectional, and sedimentation processes will occur with a minimum of particle interaction. If the marina is located close to the mouth, circulation will be tidal in nature, i.e., varying periodically in direction and strength, and the salinity will be high and relatively constant. Since fine clays and silts tend to flocculate in the presence of salts, sedimentation rates along the estuary will depend not only upon the advection of bed load and suspended load, but also upon the local salinity and character of the suspended load. Hence, a given location of the marina in the estuary will result in correspondingly unique characteristics of sedimentation, water circulation, and water quality.

Once potential marina or harbor sites have been selected or designated, the design engineer is often faced with predicting the marina basin circulation and flushing characteristics. Such predictions require a relatively detailed knowledge of local flow conditions for various seasons. Frequently, only the general character of the flow can be determined from published data and either physical or numerical models are necessary for more detailed

analysis. Fluid flow in estuaries and river channels is generally turbulent. The flow within marinas will generally also be turbulent, though at a greatly reduced level; thus, such fluid flows should be described by the equation of turbulent motion. Analytical solutions for these nonlinear equations have been obtained only for highly-simplified conditions. Various solution techniques have been applied, including: 1) reduction to ordinary differential equations which permit numerical integration; 2) linearization techniques applied to reduce the equations where analytical solutions may be obtained; 3) finite-difference and 4) finite element methods to reduce the equations to a set of algebraic equations which can be solved simultaneously.

The first two techniques (reduction of order and linearization) are limited in application because they are restrictive and involve much analytical work. A stringent restriction placed on fluid problems by these techniques is that of steady flow, i.e., time derivatives of variables must vanish. This is clearly an unrealistic restriction for oscillatory flow problems. The latter two methods, however, are applicable to most flow conditions including those with unsteady flow. The following sections consider the formulation of a finite-difference circulation model limited to rectangular basins of constant depth having a constant velocity past the entrance. Previous attempts by other investigators to solve similar circulation problems are then reviewed. Finally, the finite-difference problem-solution technique used in this present study is discussed in detail.

2.2 The Vorticity Transport Equation

The two-dimensional, vertically-averaged equations of turbulent motion are

$$\frac{\partial u}{\partial t} + u\frac{\partial u}{\partial x} + v\frac{\partial u}{\partial y} = -\frac{1}{\rho}\frac{\partial p}{\partial x} - \frac{\tau_{bx}}{(h+\eta)} + A_x\left[\frac{\partial^2 u}{\partial x^2} + \frac{\partial^2 u}{\partial y^2}\right] \quad (2.2.1a)$$

$$\frac{\partial v}{\partial t} + u\frac{\partial v}{\partial x} + v\frac{\partial v}{\partial y} = -\frac{1}{\rho}\frac{\partial p}{\partial y} - \frac{\tau_{by}}{\rho(h+\eta)} + A_y\left[\frac{\partial^2 v}{\partial x^2} + \frac{\partial^2 v}{\partial y^2}\right] \quad (2.2.1b)$$

$$p = \rho g(h+\eta) \quad (2.2.1c)$$

where all terms represent vertical averages,

η = water surface elevation relative to some datum,

and h = water depth relative to that datum.

Here the internal and bottom shear stresses have been combined in an equivalent quadratic function of the velocity

$$\tau_b(x,y) = K(u,v)\sqrt{u^2 + v^2} \quad (2.2.2)$$

where K is a friction coefficient usually between 0.002 and 0.005 in estuaries (Dyer, 1973). A value of 0.003 was adopted in this study, corresponding to a Chezy coefficient, C, of 146 and a Manning's n of 0.019 $cm^{1/6}$ since

$$K = \frac{\rho g n^2}{(h+\eta)^{1/3}} = \frac{\rho g}{C^2}$$

When shear stresses are expressed as in Eq. 2.2.2, Eqs. 2.2.1 contain two unknowns, pressure and velocity. Pressure may be eliminated from the problem by forming the vorticity transport equation. By cross differentiating the first and second equations (Eq. 2.2.1) with respect to y and x and subsequently subtracting the resulting equations, one obtains the vorticity transport equation

$$\frac{\partial \xi}{\partial t} = -u\frac{\partial \xi}{\partial x} - v\frac{\partial \xi}{\partial y} - \frac{1}{\rho(h+\eta)}\left[\frac{\partial \tau_{bx}}{\partial y} - \frac{\partial \tau_{by}}{\partial x}\right] + A_h\left[\frac{\partial^2 \xi}{\partial x^2} + \frac{\partial^2 \xi}{\partial y^2}\right] \quad (2.2.3)$$

Here ξ is the vorticity

$$\xi = \frac{\partial u}{\partial y} - \frac{\partial v}{\partial x} \quad (2.2.4)$$

If it is assumed that the eddy coefficients are locally uniform, and introducing the stream function, ψ, such that

$$\frac{\partial \psi}{\partial x} = v \qquad \frac{\partial \psi}{\partial y} = -u \tag{2.2.5}$$

then Eq. 2.2.4 is expressed as the elliptic Poisson equation

$$\nabla^2 \psi = -\xi \tag{2.2.6}$$

The vorticity transport equation is parabolic in time, hence posing a "marching" or initial-value problem wherein the solution is stepped out from some initial condition. The Poisson equation, being elliptic, poses a boundary value problem which may be solved by iterative means. These equations, when combined with selected boundary conditions, define the circulation problem. The boundary conditions include the following:

1) no-slip physical boundaries, i.e., the velocity parallel to the boundary is zero at the boundary

$$\vec{v}|_B = 0 \tag{2.2.7}$$

2) physical boundaries are impermeable, i.e., the velocity perpendicular to the boundary is zero at the boundary

$$\vec{v}_\perp|_B = 0 \tag{2.2.8}$$

3) constant stream function along physical boundaries, a consequence of boundary conditions 1) and 2)

$$\psi_B \equiv 0 \tag{2.2.9}$$

4) a "moving, no-slip" wall boundary (Roach, 1972, p. 150) at the basin entrance

$$\left.\begin{aligned} \vec{v}||_E &= u_o \\ v_\perp|_E &= 0 \end{aligned}\right\} \quad \text{or} \quad \psi_E \doteq u_o \Delta y \tag{2.2.10}$$

and 5) zero velocity at the tips of the breakwaters.
The fourth boundary condition (Eq. 2.2.10) requires that the value of the stream function at the entrance be different from that at adjacent solid boundaries by $u_0\Delta y$; Δy being the distance between the entrance and the first interior node of the finite difference spacial grid (Figure 2.6).

Equations 2.2.1 and 2.2.3 to 2.2.6 are recast in dimensionless form using the boundary velocity u_0 and basin length measured parallel to the entrance as the characteristic velocity and length measures, e.g., $u \equiv u/u_0$, hence

$$\xi \equiv \frac{\partial(u/u_0)}{\partial(y/L)} - \frac{\partial(v/u_0)}{\partial(x/L)} \quad , \text{ etc.}$$

Then the complete non-dimensionalized boundary value problem becomes

$$\frac{\partial \xi}{\partial t} = -u\frac{\partial \xi}{\partial x} - v\frac{\partial \xi}{\partial y} - \frac{1}{d}\left[\frac{\partial T_x}{\partial y} - \frac{\partial T_y}{\partial x}\right] + \frac{1}{Re}\left[\frac{\partial^2 \xi}{\partial x^2} + \frac{\partial^2 \xi}{\partial y^2}\right] \qquad (2.2.11)$$

DE:

$$\nabla^2\psi = \xi \qquad (2.2.12)$$

BC: $\vec{v}\,|\,|_B = 0$

$\vec{v}_\perp|_B = 0$

$\psi_B = 0$

$\vec{v}\,|\,|_E = u_0/u_0 = 1$

$\vec{v}_\perp|_E = 0$

$\psi_E = u_0\Delta y \qquad (2.2.13)$

where $Re = u_o L/A_h$ is the basin "eddy" Reynolds number,

L = basin length,

A_h = the horizontal eddy coefficient,

$d = (h+n)/L$,

$t = tu_o/L$

and $T = \tau_b/\rho u_o$.

The following section reviews the results of previous investigations of recirculating flows. Following that, the solution technique for the above-posed circulation problem is discussed in detail.

2.3 Review of Flow Models for Rectangular Basins

A review of published literature regarding shear-induced circulation in basins adjacent to a waterway revealed that while analytical solutions for viscous flow conditions are available (Weiss and Florsheim, 1965; Burggraf, 1966), corresponding solutions for turbulent flow conditions are not presently available. Most investigators rely upon physical or numerical models to study turbulent flow conditions but only a limited number of laboratory or field investigations have been conducted. The following pages review some of the more pertinent contributions.

For low viscosity fluids, Prandtl (1904) and Batchelor (1956) showed analytically that steady, high-Reynolds-number flows within closed streamlines generally consist of an inviscid core having uniform vorticity with viscous effects confined to infinitesimally thin shear layers along the boundary.

Weiss and Florsheim (1965) analytically and experimentally investigated steady, viscous flow characteristics in rectangular cavities for low Reynolds numbers. Neglecting the advective terms in the steady vorticity transport equation and applying variational

techniques, the stream function was determined to be

$$\psi = \frac{u_o \sin^2 \pi x/L}{a\Phi \sinh bW \cos aW} \left(\frac{b}{a} \cosh by \sin ay - \sinh by \cos ay + \left[\frac{1 - bk/a}{\tan aW} \right] \sinh by \sin ay \right) \quad (2.3.1)$$

where

u_o = boundary velocity at opening,

x,y = point coordinates measured from innermost upstream corner (Figure 2.1),

$\Phi = (1 + b^2/a^2) \tan aW + (1 - b^2k^2/a^2)(1/\tan aW)$, (2.3.2)

$a = \frac{2\pi}{3^{\frac{1}{4}}L} \sin(\arctan \sqrt{2})$,

$b = \frac{2\pi}{3^{\frac{1}{4}}L} \cos(\arctan \sqrt{2})$,

L = basin length parallel (in $\vec{x}$) to the opening,

W = basin width perpendicular (in $\vec{y}$) to the opening,

$k = \tan aW/\tanh bW$.

Assuming a linear change in velocity across the entrance boundary layer and that the boundary layer thickness did not change across the opening u_o was estimated as

$$u_o \simeq u_\infty/(1 + N\delta^*/L) \quad (2.3.3)$$

where

u_∞ = free-stream velocity,

δ^* = upstream boundary layer thickness,

$$N = \frac{3^{\frac{1}{4}}}{\pi} \left(\frac{abL^2}{G}\right)\left[\cos aW \sinh bW + k \sin aW \cosh bW\right]$$

in which,

$$G = \sin\left(\tfrac{1}{2} \arctan \sqrt{2}\right) \cosh bW \cos aW + \cos\left(\tfrac{1}{2} \arctan \sqrt{2}\right) \sinh bW \cdot \sin aW - \frac{\tan aW}{\tan bW}\left[\cos\left(\tfrac{1}{2} \arctan \sqrt{2}\right) \cosh bW \cos aW - \sin\left(\tfrac{1}{2} \arctan \sqrt{2}\right) \sinh bW \sin aW\right]$$

Also determined was the location of the zero-velocity point of the recirculating gyre (Fig. 2.1). Since the opening extended completely across the cavity, the x location of this center is L/2. The y location, y_c, is determined from

$$\frac{1}{\tan ay_c} + \frac{b/a}{\tanh by_c} = \left[\frac{b^2/a^2 + 1}{bz/a - 1}\right] \tan aW \qquad (2.3.4)$$

This equation predicts the existence of multiple recirculation cells. A single cell exists up to a L/W ratio of about 0.59 and a third cell forms when L/W is about 0.25. Successive interior cells necessarily decrease in strength. Table 2-1 gives the relative locations of cell centers for four different basin aspect ratios.

For a "stagnation" Reynolds number defined as

$$Re_s = \frac{u_\infty(W - y_c)}{\nu} \qquad (2.3.5)$$

with a magnitude of about 150, Weiss and Florsheim (1965) found that model tests indeed produced multiple cells. The positions of the theoretical and actual stagnation points agreed to within 19%, from which the investigators concluded that the omission of the advective terms from the problem was acceptable.

TABLE 2-1

Location of Cell Centers

L/W	y_c/W	y_o/W
2.00	0.70	0.30
1.00	0.79	0.21
0.50	0.20, 0.90	0.80, 0.10
0.33	0.44, 0.93	0.56, 0.07
0.25	0.23, 0.59, 0.95	0.77, 0.41, 0.05

Weiss and Florsheim (1965) also suggested that the complete nondimensionalized vorticity diffusion equation

$$\nabla^4\psi - Re \cdot \nabla(\nabla^2\psi) = 0 \qquad (2.3.6)$$

could be solved using a series expansion in the Reynolds number, Re being defined by the characteristic parameters, ν, L, and u_o.

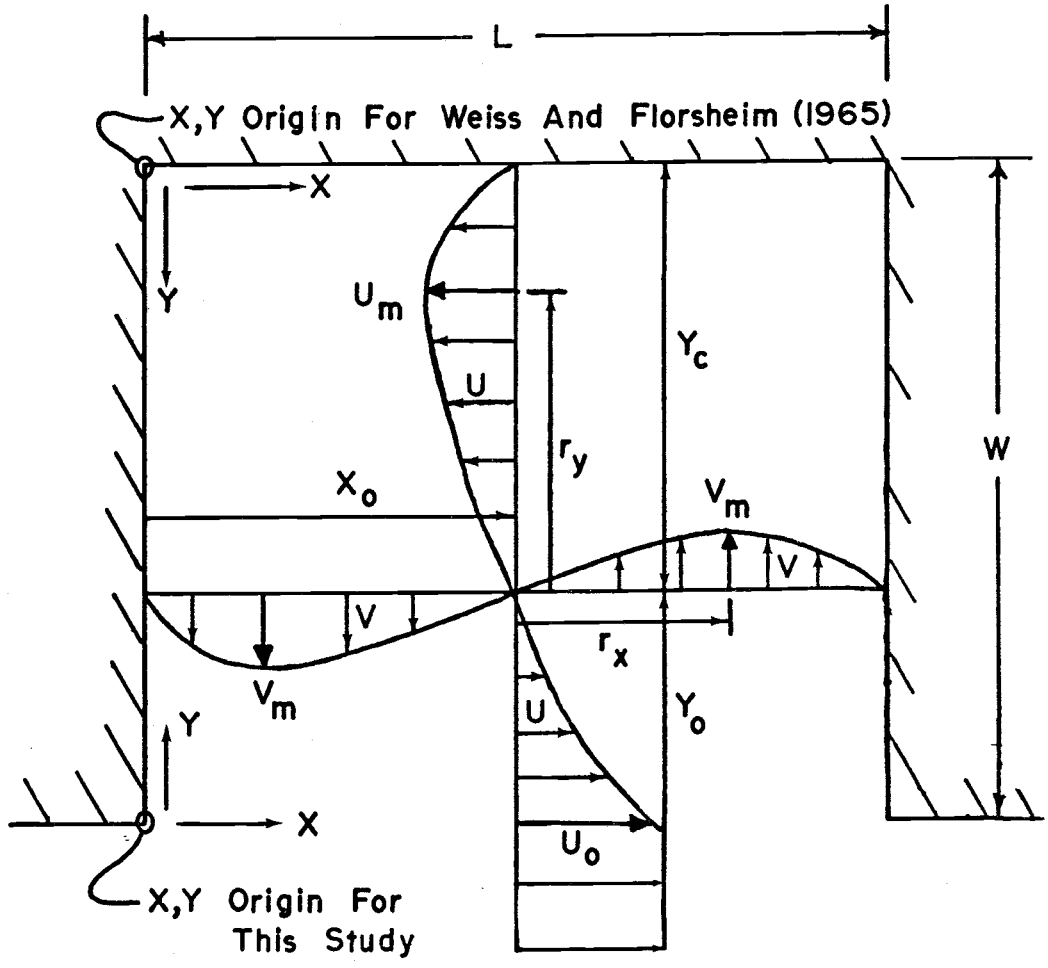

Figure 2.1. Parameters used to describe vortex flow in a rectangular basin. The vortex center is located at (x_o, y_o). The terms r_x and r_y measure the distance from the vortex center to the maximum velocity components u_m and v_m that act across transects paralleling the coordinate axes and passing through the vortex center.

The series

$$\psi = \psi_o + Re\ \psi_1 + Re^2\psi_2 + \ldots + Re^n\psi_n \qquad (2.3.7)$$

should be expected to be convergent for $Re < Re_{max}$ where Re_{max} is given by the requirement that the second term in Eq. 2.3.7 is less than the first, i.e.

$$Re_{max} = Min(\psi_o/\psi_1)$$

for the whole domain. Such an expansion would result in a set of linear equations in ψ, allowing ψ to be determined to any desired accuracy. The first two members of that set are

$$\nabla^4\psi_o = 0$$

$$\nabla^4\psi_1 = \vec{v} \cdot \nabla(\nabla^2\psi_o).$$

Burggraf (1966) investigated the behavior of circular unconfined eddies and eddies within a square cavity. Linearization and perturbation of the Navier-Stokes equations permitted a first-order analytical solution to be determined for a circular boundary. In the limit as the Reynolds number approached infinity, viscous shear effects were confined to a thin shear layer near the boundary and the inviscid core exhibited constant vorticity. As predicted analytically by Batchelor (1956) for such inviscid flows, the vorticity was proportional to the root-mean-square velocity past the boundary.

Burggraf (1966) also used relaxation techniques to solve the vorticity transport equation for a square cavity with one moving wall. Flows having Reynolds numbers from zero to 400 were used, characteristic scales being the basin length, the moving wall velocity, and molecular kinematic viscosity, ν. As Re was slowly increased, the vortex center was observed to shift first in the downstream direction as a consequence of viscous and inertial effects and then towards the center of the cavity as the inviscid core developed. The inviscid case was approached asymptotically as the non-linear convective terms increased in importance over the viscous diffusion terms. Figure 2.2 shows the velocity profile along the centerline, perpendicular to the entrance. As the Reynolds

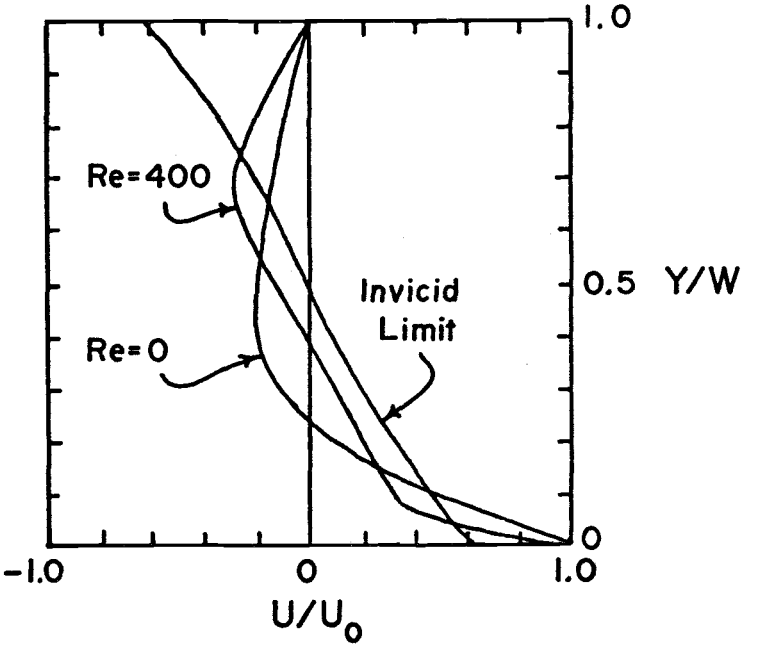

Figure 2.2. Viscous flow velocity profiles as a function of the Reynolds number. From Burggraf (1966).

number and/or velocity was increased, convective effects smoothed the velocity profile until at the inviscid limit, a state of constant vorticity, and hence, constant velocity gradients, was achieved. Secondary eddies were also observed in the inner corners of the square cavity. The downstream corner eddy grew with increasing Re whereas the upstream corner eddy remained stable. Burggraf concluded that the growth of these corner eddies would prevent the primary vortex from approaching the geometric center of the cavity.

Pan and Acrivos (1967) found that for creeping flow, the stagnation point predictor of Weiss and Florsheim was in reasonable agreement with laboratory observations under different entrance boundary conditions. They also considered the dependence of corner vortices on Reynolds number. They noted that previous applications of the variational technique (Weiss and Florsheim, 1965) and Galerkin's method (Snyder, Spriggs, and Stewart; 1964) had not been applied on a grid scale fine enough to accurately describe this phenomenon. Defining vortex size as the fraction of wall width, W, covered by the upstream vortex, the size was observed to increase from 0.1 W under creeping flow conditions to a maximum of 0.35 W around Re = 500 for a basin aspect ratio of 0.62. Further increases of the Reynolds number caused the vortex to shrink.

Concommittant with such behavior of the corner vortices was an initial shrinkage of the primary vortex to a Reynolds number of approximately 800. For higher Reynolds numbers, the eddy grew in size, becoming linear with $Re^{\frac{1}{2}}$ in the range $1500 \leq Re \leq 4000$.

In summary, the recirculating flow within a rectangular cavity will consist of a main vortex and, for relatively low Reynolds flows in which viscous effects are important, secondary cells will develop in the interior of the basin. As the Reynolds number increases, the principal vortex center will migrate first downstream and then towards the interior of the basin. Expansion of the principal vortex will occur at the expense of any secondary cells present, but may be opposed in a cavity of finite width by the growth of corner vortices. As the inviscid limit is approached, circulation will

consist essentially of the primary vortex in which vorticity is constant. Viscous effects will be confined to the thin boundary layer along the walls.

Westrich (1975) conducted laboratory models of turbulent exchange between a river and a rectangular backwater area. The flows were turbulent and the entrance was unconstricted. A channel Reynolds number, $u_o d/\nu$ was given as 10^6, d being the depth. For basin length/width ratios between 0.3 and 6, the mean circulation consisted of a single gyre, but for ratios smaller than 0.3, a second gyre developed with lower velocities and rotation opposite to that of the main gyre. Such observations conform with those of the previously discussed papers which addressed non-turbulent flow conditions. This suggests that the turbulent flow problem may be approached in a manner similar to the preceeding analyses.

Nece, et al. (1976) used physical models to investigate tidal flushing of rectangular harbors with a single entrance located at one end of the breakwater. The authors concluded that the strength and uniformity of basin flushing depends upon the angular momentum established within the basin by flooding flow and that optimum flushing conditions correspond to a relatively narrow entrance placed at one end of the breakwater of a square basin. In model tests, a single circulation cell was observed for basin aspect rations (L/W) between 0.6 and 3.0. The gyre developed during the flooding stage and continued to expand under high slack conditions, filling much of the basin. For aspect ratios larger than 3, multiple circulation cells formed.

Nece, et al. (1976) defined basin flushing efficiency as the ratio of the average per-cycle exchange coefficient, E, to the ideal tidal prism ratio. The exchange coefficient is the fraction of the water in the basin at high water slack which is removed from the basin and replaced by ambient water during the following flood cycle. The tidal prism ratio is the ratio of the difference of the water volume in the basin at high and low tides to the volume at high tide.

Figure 2.3 presents the conclusions of Nece's study. Best overall flushing occurred for a given tide range for basin aspect ratios between 0.6 and 3.0 in which a single circulation cell fills most of the basin. The secondary minimum in the exchange coefficient using an aspect ratio (L/W) of 0.8 was considered to be the result of the approximate equality of the gyre circulation period and half the tidal period. Water injected into the basin during flood stage circulates around the basin with a relative minimum of mixing. Should it arrive back at the entrance at high slack, part of this water will be deflected out of the basin and will not effectively contribute to the mixing process, thereby reducing the measured exchange coefficient. Narrower entrances were also considered to increase jet entrance velocities, internal circulation and mixing processes. Nece, et al. (1976) also considered the effect of rounding the interior basin corners to minimize the momentum and energy drain associated with corner eddy development. They concluded that although rounded corners did improve local exchange processes, it had little effect on the flushing process of the basin as a whole.

Noble (1976) attempted to relate the water quality of Oregon's coastal marinas to basin geometry via sediment chemistry. He concluded that basin configuration for optimum flushing was one in which the non-dimensional parameters AREA and ENTR were kept below 400 and 100, respectively. These parameters as defined as:

$$AREA = A/a \tag{2.3.8}$$

$$ENTR = A/\sqrt{a}\ W_e \tag{2.3.9}$$

where

A = basin horizontal area (MLLW),

a = entrance vertical cross-sectional area (MLLW),

and W_e = entrance width (MLLW).

Combining both criteria requires that

$$a > 0.0625\ W_e^2. \tag{2.3.10}$$

Vollmers (1976) considered basin circulation to be the consequence of three dynamic factors which account for boundary shear, tidal effects and internal density gradients. Boundary shear effects

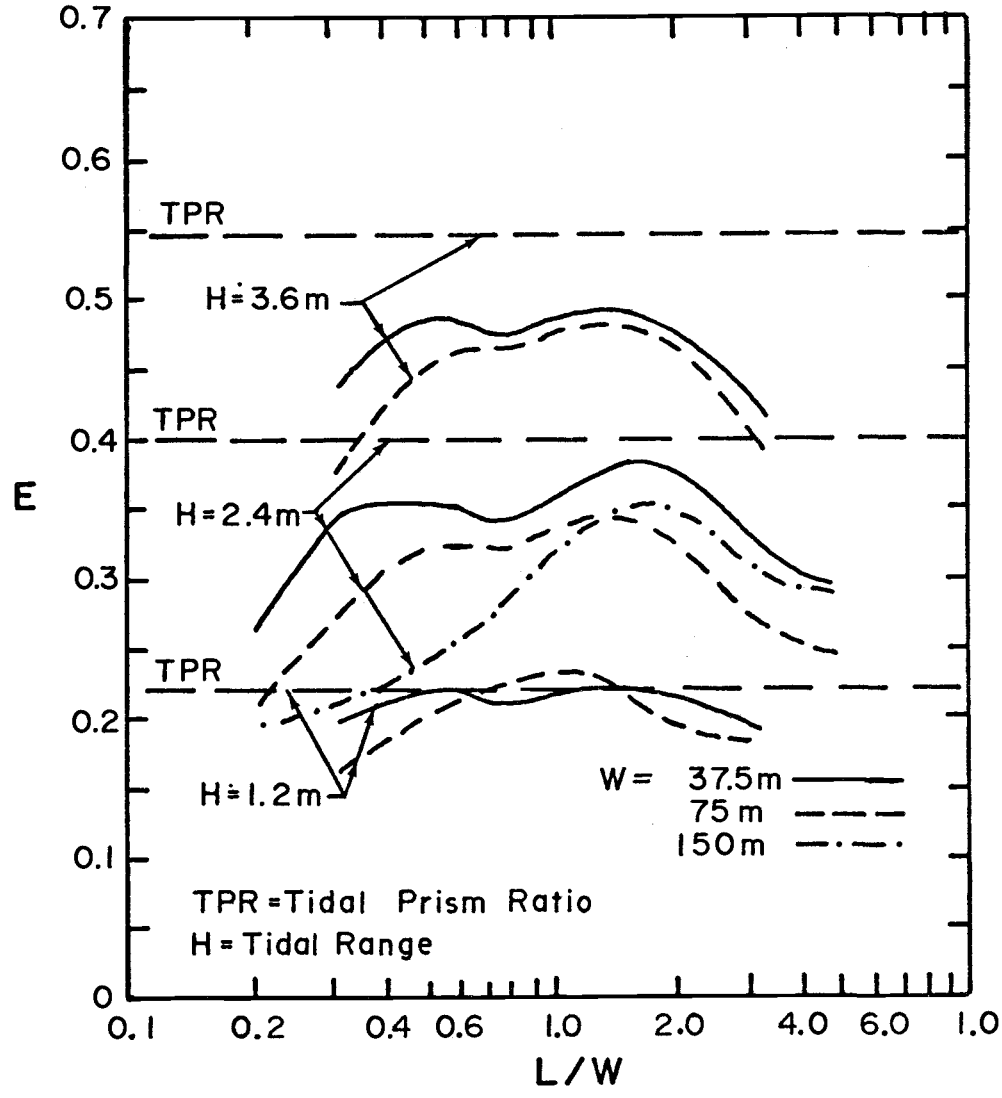

Figure 2.3. The average per-cycle exchange coefficient, E, versus the basin aspect ratio for three tidal ranges. From Nece, et al. (1976).

induce the vortex circulation described by Weiss and Florsheim (1965), Burggraf (1966), and others and is superimposed upon the tidal flow into and out of the basin, depending upon the stage of the tide. During the flood tide the "filling current" adds to the flood-generated vortex to produce enhanced current velocities along the downstream boundary (Figure 1.1). During the ebb stage, however, the outward flux of momentum from the basin and the opposition of flood-generated vortex and "emptying current" serve to reduce the strength of the vortex. Vollmers (1976) suggested that the vortex flow may even vanish during this stage.

Vollmers (1976) conducted physical model studies to improve circulation in the Delfzijl harbor, Netherlands. The harbor is extremely elongated and although two entrances were provided, one near each end of the basin, the vortex action only occurred near the entrances and the basin interior suffered from poor circulation. By modifying the breakwaters, a through-flowing current was generated during flood tide which was strong enough to destroy the vortex formation at the entrances, thereby improving basin circulation. The use of multiple entrances to generate such through-flowing currents is advantageous for many marinas which are elongated parallel to the river or estuary channel.

Abbott (1977) numerically simulated the flow interaction between a channel and a rectangular basin (Fig. 2.4). Unlike most previous investigations, the basin entrance was restricted to one-half of the basin length and positioned at upstream, central, and downstream locations. Entrance effects were also included since the model incorporated part of the river channel both upstream as well as downstream. Flow conditions were defined at the upstream and downstream ends of the channels and both steady and non-steady, oscillatory flow conditions were considered. It was found that proper simulation of entrance effects required that the dispersion coefficients at nodes near the entrance be somewhat higher than in

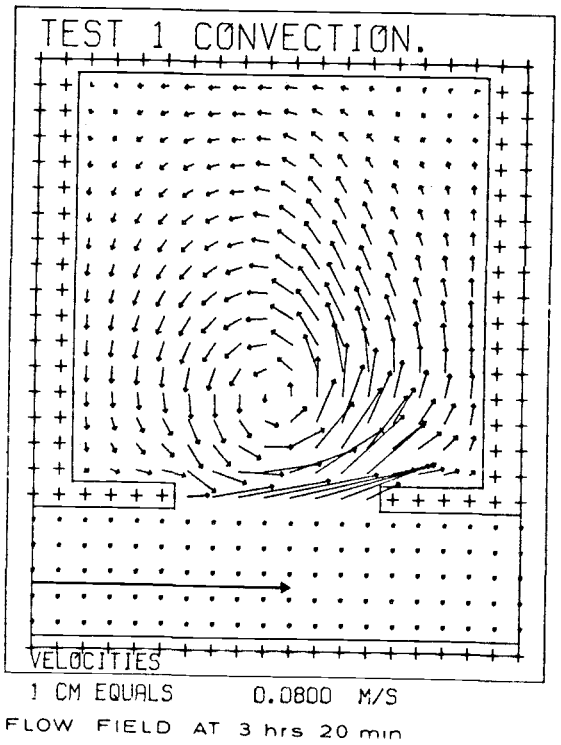

(A)

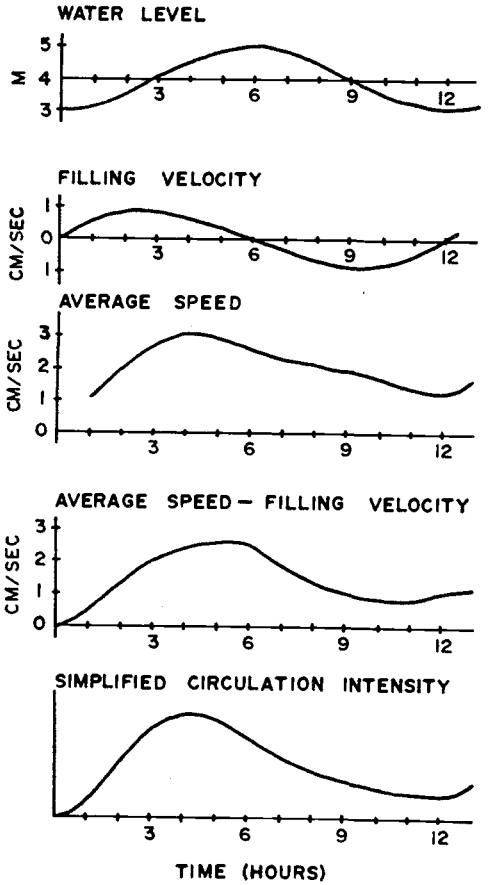

(B)

Figure 2.4. Example of Abbott's (1977) method of estimating the circulation intensity or flushing of a rectangular basin connected to a waterway. (A). Basic geometry and finite difference schemetization. (B). Example of data analysis for a non-steady flow problem.

the interior. The dispersion coefficients frequently appear in the equations of motion and derived equations as inflated diffusion coefficients, e.g. the Austauch coefficients A_x and A_y in Eq. 2.2.1. Such coefficients are used in numerical and analytical models to account for effects not directly accounted for by the advective terms, i.e., terms involving the velocity. In the above breakwater entrance case, the enhanced dispersion accounted for effects due to a particular vertical distribution of velocity, secondary current development or some other process. Abbott cautioned that the definition of entrance conditions can greatly influence the solution for flow inside the marina. In order to obtain reliable results, it may be necessary to define the entrance geometry and dispersion characteristics using a finer computation grid near the entrance than in the interior.

Abbott (1977) investigated the separate effects of dispersion and advection of momentum between the channel and basin under steady-flow conditions. Advective tests used velocities sufficiently high to mask out any secondary dispersive effects. Dispersion tests showed that the center of the circulation eddy was not located at the center of the basin. This is to be expected since continuity requires that the flows between this center and any wall be equal. Given the difference in velocity gradients over the basin, the center would be expected to be closer to the channel entrance.

Abbott separated basin-filling effects from the computed flow field by defining the "filling velocity"

$$v_f = \frac{d}{t}\frac{W}{2d} \tag{2.3.11}$$

where

d = the water depth as a function of time

t = time

W = width of basin

v_f = filling velocity

The difference between the short-term average velocity for the basin and the filling velocity was assumed by Abbott to be a measure of the circulation intensity, and thereby of the flushing obtained from the river flow. Under early flood conditions, the circulation increased parabolically with time (Fig. 2.4). Due to inertial effects, the maximum flushing appeared to occur after both maximum filling and maximum average basin velocities were realized. Such a condition occurred prior to the weakening of the circulation gyre during ebb conditions described by Vollmers (1976). During the ebb cycle, the outward flux of momentum from the basin and the opposition of entrance shear to the flood-induced circulation produced an exponential type of decay in the circulation intensity.

Abbott's calculations showed that the effect of entrance location was only important in the convective case; dispersive effects for central and non-central entrance cases being similar. For entrances located in the downstream sector, the filling velocity became oriented in the same direction as the interior circulation, thereby intensifying circulation. For entrances located in the upstream sector, these two processes were in opposition, which produced a weaker internal velocity field. These characteristics were earlier described by Vollmers (1976).

Abbott (1977) also considered a circular basin with an offset entrance (Fig. 2.5). Unexpectedly, this configuration resulted in a body of stagnant water in the interior and downstream portion of the marina that, during the falling stage, made the circulation break into two smaller circulations. A lower circulation speed was also realized than for the square, central-entrance case. This was presumably due to damping effects at the entrance and to the increased effects of friction in the more uniform flow field within the marina.

2.4 Numerical Solution Techniques

The circulation problem may be specified in one of two ways. In one, the differential equations governing the behavior of a

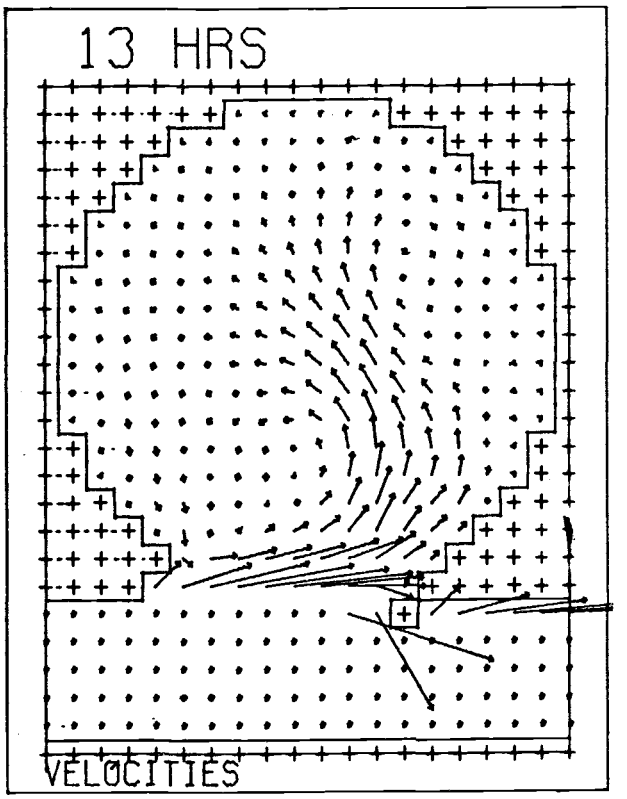

Figure 2.5. Circular planform and velocity field. From Abbott (1977).

typical, infinitesimal, region are given, i.e. as illustrated in the boundary value problem outlined above. In the other, a variational (extremum) principle, valid over the whole region, is postulated and solved by some quantity, Φ, which is defined by suitable integration of the unknown quantities--velocity and pressure for the problem of flows into, around and out of marina entrances.

Both approaches are equivalent; differences arise in the approximate solution procedures. Finite difference techniques approach the solution of differential equations directly by approximating the equations in a discrete manner. The variational approach, on the other hand, deals directly with an approximate minimization of the functional, Φ. The circulation problem in this study is solved using the finite difference approach. Chapters III and IV consider the solution of the sedimentation problem via the variational, finite-element technique.

2.5 The Finite Difference Approximation

Finite difference methods are by far the most widely used numerical method for solving fluid flow problems, although the finite element method is rapidly increasing in popularity. The finite difference approach involves a minimum of analytical work as compared to any other method. The continuous fluid domain is replaced by a discrete grid of points at which governing differential equations are evaluated (Fig. 2.6). Spatial derivatives are approximated using truncated three-point Lagrangian polynomials. The result is a set of approximated differential equations.

In the basin interior the centered forms of the three-point formuli are used (Abramowitz and Stegun, 1965). Conforming to the notation of Figure 2.6, these formuli when applied to the vorticity property are:

$$\xi(x) \doteq \left[\frac{(x-x_1)(x-x_2)}{(x_0-x_1)(x_0-x_2)}\right] \xi(I-1,J) + \left[\frac{(x-x_0)(x-x_2)}{(x_1-x_0)(x_1-x_2)}\right]\xi(I,J)$$

$$+ \left[\frac{(x-x_0)\ (x-x_1)}{(x_2-x_0)\ (x_2-x_1)}\right] \xi(I+1,J) \qquad (2.5.1)$$

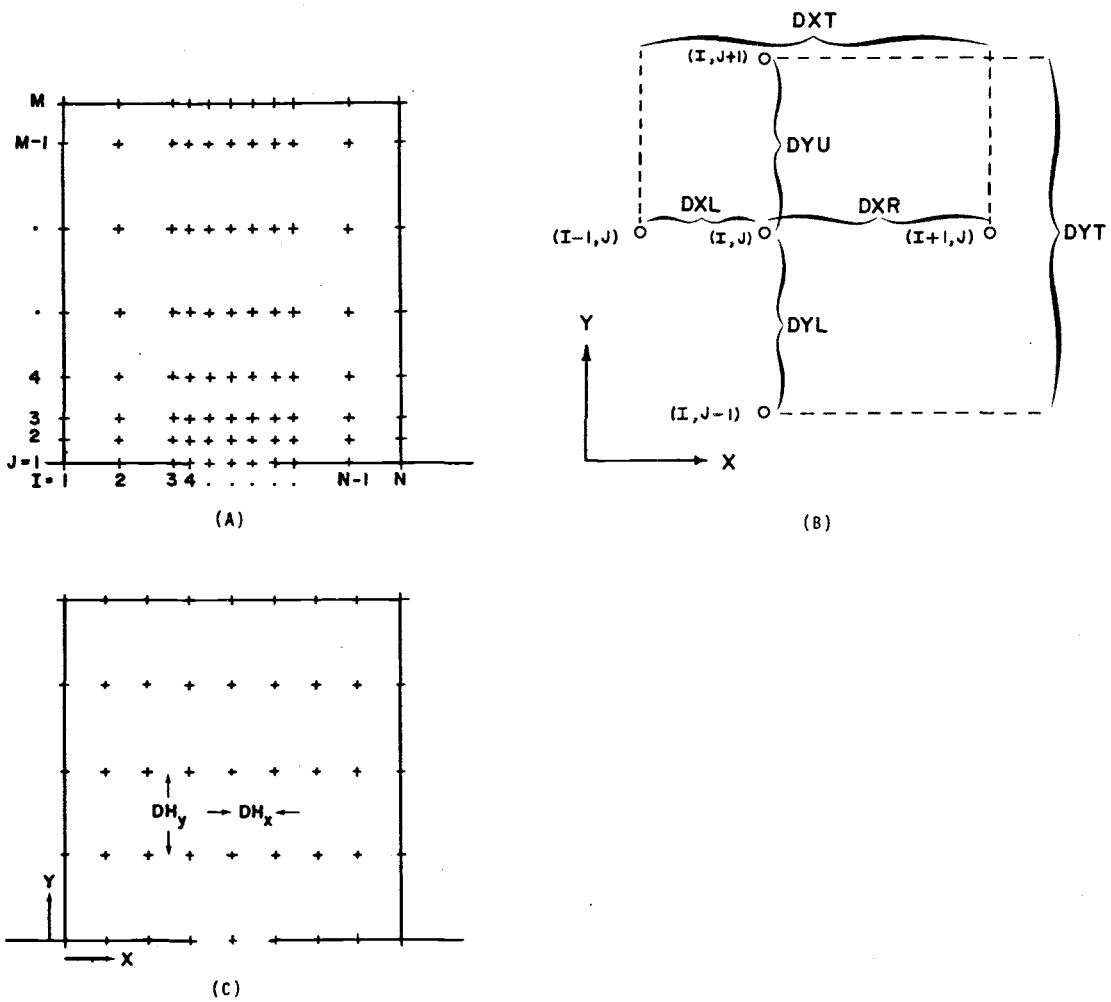

Figure 2.6. Spacial discretization of a rectangular planform. (A). General schemetization using variably-spaced nodal points identified by (I,J). (B). Notation for non-uniform nodal spacing. (C). Schemetization using constant (but not necessarily equal) intervals DH_x and DH_y.

with:

$$\frac{\partial \xi}{\partial x}(I,J) \doteq \frac{\Delta \xi}{\Delta x}(I,J) = \left[\frac{x_1-x_2}{(x_o-x_1)(x_o-x_2)}\right]\xi(I-1,J) + \left[\frac{(x_1-x_2)+(x_1-x_o)}{(x_1-x_o)(x_1-x_2)}\right]\xi(I,J) + \left[\frac{x_1-x_o}{(x_2-x_o)(x_2-x_1)}\right]\xi(I+1,J) \quad (2.5.2)$$

and

$$\frac{\partial^2 \xi}{\partial x^2}(x) \doteq \frac{\Delta^2 \xi}{\Delta x^2}(x) = \left[\frac{2}{(x_o-x_1)(x_o-x_2)}\right]\xi(I-1,J) + \left[\frac{2}{(x_1-x_o)(x_1-x_2)}\right]\xi(I,J) + \left[\frac{2}{(x_2-x_o)(x_2-x_1)}\right]\xi(I+1,J) \quad (2.5.3)$$

For the special case in which the grid is evenly spaced with DH the distance between nodes (Fig. 2.6), Eq. 2.5.1 to 2.5.3 become:

$$\xi(x) \doteq \left[\frac{(x-x_1)(x-x_2)}{2DH^2}\right]\xi(I-1,J) + \left[\frac{(x-x_o)(x-x_2)}{DH^2}\right]\xi(I,J) + \left[\frac{(x-x_o)(x-x_1)}{2DH^2}\right]\xi(I+1,J) \quad (2.5.4)$$

$$\frac{\partial \xi}{\partial x}(I,J) \doteq \left[\frac{-1}{2DH}\right]\xi(I-1,J) + \left[\frac{1}{2DH}\right]\xi(I+1,J) \quad (2.5.5)$$

and

$$\frac{\partial^2 \xi}{\partial x^2}(x) = \left[\frac{1}{DH^2}\right]\xi(I-1,J) + \left[\frac{-2}{DH^2}\right]\xi(I,J) + \left[\frac{1}{DH^2}\right]\xi(I+1,J) \quad (2.5.6)$$

with corresponding equations developed for the y-direction.

Boundary conditions are imposed upon the solution due to the involvement of boundary node values in the approximation of derivatives at the first interior nodal points. Applying the non-slip moving wall boundary condition, then for nodes lying in the fluid portion of the boundary

$$\psi_E = u_o \Delta y \quad (2.5.7)$$

The approximated Poisson equation then defines the vorticity for the entrance nodes

$$\xi_E \doteq \frac{2\left[\psi_{E+1} - u_o \Delta y\right]}{\Delta y^2} \quad (2.5.8)$$

and for nodes just interior of the land or breakwater boundaries

$$\xi_B \doteq \frac{2\psi_B+1}{\Delta y^2} \qquad (2.5.9)$$

The solution of Equations 2.2.3 and 2.2.6 is determined according to the following procedure (Figure 1.5):

1) the vorticity transport equation is solved for one time step via the alternating direction method to yield a new vorticity field;
2) the Poisson equation, $\nabla^2\psi = -\xi$, is solved iteratively for a new stream function field via the successive over-relaxation technique;
3) numerical differentiation of the new stream function yields a corresponding velocity field;
4) boundary vorticity and stream function values are interpolated by Eqs. 2.5.7 to 2.5.9; and
5) steps 1-4 are repeated until the vorticity field is stationary, representing convergence to the specified boundary conditions.

The finite difference solution of the vorticity transport/stream function problem is considered next.

2.6 The Alternating Direction Solution of the Vorticity Transport Equation

The alternating direction (ADI) method splits each time step to obtain a multi-dimensional, implicit form which requires only the inversion of simple tridiagonal matrices. The split-level ADI formulation of the vorticity transport equation is:

$$\frac{\xi^{\kappa+\frac{1}{2}}-\xi^{\kappa}}{\Delta t/2} = -\frac{u^{\kappa}\Delta\xi^{\kappa+\frac{1}{2}}}{\Delta x} - \frac{v^{\kappa}\Delta\xi^{\kappa}}{\Delta y} - \frac{1}{d}\left[\frac{\Delta T_x}{\Delta y} - \frac{\Delta T_y}{\Delta x}\right]^{\kappa} +$$

$$\frac{1}{Re}\left[\frac{\Delta^2\xi^{\kappa+\frac{1}{2}}}{\Delta x^2} + \frac{\Delta^2\xi^{\kappa}}{\Delta y^2}\right] \qquad (2.6.1)$$

$$\frac{\xi^{k+1}-\xi^{k+\frac{1}{2}}}{\Delta t/2} = \frac{-u^{k}\Delta\xi^{k+\frac{1}{2}}}{\Delta x} - \frac{v^{k}\Delta\xi^{k+1}}{\Delta y} - \frac{1}{d}\left[\frac{\Delta T_x}{\Delta y} - \frac{\Delta T_y}{\Delta x}\right]^{k} +$$

$$\frac{1}{Re}\left[\frac{\Delta^2\xi^{k+\frac{1}{2}}}{\Delta x^2} - \frac{\Delta^2\xi^{k+1}}{\Delta y^2}\right] \qquad (2.6.2)$$

where $\frac{\Delta\xi}{\Delta x}$ and $\frac{\Delta^2\xi}{\Delta x^2}$ are point approximations of their corresponding partial derivatives and superscripts identify the time level.

Equation 2.6.1 is solved for $\xi^{k+\frac{1}{2}}$ at each node using the Thomas algorithm (Roach, 1972, p. 345). These $\xi^{k+\frac{1}{2}}$ values are then entered into Eq. 2.6.2 and ξ^{k+1} similarly determined. The stream function problem, Eq. 2.2.12, is solved next; the velocity components and boundary vorticity and stream function values are calculated and substituted into Eq. 2.6.1. This sequence is repeated until some criterion is met, usually the achievement of steady state conditions or the passage of a prescribed period of time.

Ideally, the "eddy" Reynolds numbers should vary with both space and time in the ADI solution of the vorticity transport equation. However, to minimize computer storage, it is often assumed that the eddy coefficients, A_{hy}, A_{hx}, could be considered quasi-constant and computed using the shear velocity, u_*, at the entrance. Assuming that

$$A_h \doteq 60\, u_* d \qquad (2.6.3)$$

d being the water depth in cm, u_* is determined from the Newton-Rhapson solution of the logarithmic velocity profile equation at the entrance:

$$u_o = u_*(16.0 + 5.75 \log_{10} d\, u_*) \qquad (2.6.4)$$

The use of a constant coefficient, A_h, would result in enhanced dispersion of momentum and hence, in somewhat higher velocities than would result for non-uniform coefficients. The difference would not be expected to be significant considering the uncertainties involved in any attempt to apply a spacially-varying coefficient.

2.7 The Successive Over-Relaxation Solution for Stream Function

The stream function problem, Eq. 2.2.12, is solved via the successive over-relaxation (SOR) technique as per Frankel, 1950 (Roache, 1976). The Poisson equation is expanded in terms of the point formuli and solved for $\psi(I,J)$. Following the Richardson method (Roache, 1976), the left hand side of the equation is evaluated at iteration level K+1 and the right hand side is evaluated at level K; the vorticity values are constants. The Richardson algorithm is then

$$\psi^{K+1}(I,J) = \frac{1}{2\gamma}\left(2\left[\frac{\psi^{K}(I-1,J)}{DXL\cdot DXT} + \frac{\psi^{K}(I+1,J)}{DXR\cdot DXT} + \frac{\psi^{K}(I,J-1)}{DYL\cdot DYT} + \frac{\psi^{K}(I,J+1)}{DYU\cdot DYT}\right]\right) \tag{2.7.1}$$

where spacial parameters are defined in Figure 2.6 and

$$\gamma = \left[\frac{1}{DXL\cdot DXR} + \frac{1}{DYL\cdot DYU}\right] \tag{2.7.2}$$

To speed convergence, it is useful to involve newly-computed (K+1)-level values in the continuing computations at the same level but for neighboring points whose parameters are still at the Kth level. For example, the computations proceed nodal row by nodal row towards the basin interior and node by node in the positive x-direction. Having completed the (K+1)-level computation for the first row, the second and third row values are at the Kth level but the first row is at the (K+1) level. Point approximations of derivatives in the y-direction involve both levels, hence accelerating the convergence of the solution. Similar remarks apply to derivatives in the x-direction.

The successive over-relaxation technique further accelerates convergence through the use of a relaxation factor, ω, whose value is a function of the grid spacing, the shape of the domain, and the boundary conditions. By adding $\psi^{K}(I,J)-\psi^{K}(I,J) = 0$ to the Richardson equation (Eq. 2.7.1) and rearranging, the SOR solution algorithm is

$$\psi^{K+1}(I,J) = \psi^{K}(I,J) + \frac{\omega}{2\gamma}\left(2\left[\frac{\psi^{K+1}(I-1,J)}{DXL\ DXT} + \frac{\psi^{K}(I+1,J)}{DXR\ DXT} + \right.\right.$$

$$\left.\left. + \frac{\psi^{K+1}(I,J-1)}{DYU\ DYT} + \frac{\psi^{K}(I,J+1)}{DYU\ DYT} - \gamma\ \psi^{K}(I,J) \right] - \xi(I,J) \right) \qquad (2.7.3)$$

for a rectangular domain of size $(I-1)\Delta x$ by $(J-1)\Delta y$ with constant Δx and Δy, Frankel (1950) determined that

$$\omega = 2\,\frac{1 - \sqrt{1-ss}}{ss} \qquad (2.7.4)$$

$$ss = \left[\frac{\cos\left(\frac{\pi}{I-1}\right) + \beta^2 \cos\left(\frac{\pi}{J-1}\right)}{1+\beta^2} \right]^2 \qquad (2.7.5)$$

$\beta = \Delta x/\Delta y$, the mesh aspect ratio

I,J = the number of nodes in the $\vec{x}$ and $\vec{y}$ directions.

No analytical expressions exist for ω with varying grid shape or basin geometry. The optimum value for ω is then generally determined experimentally using the computer. As the geometries considered in this study are rectangular and constant grid spacings Δx and Δy were employed, Frankel's formulation was adopted.

2.8 Stability and Convergence of the Flow Solution

In any numerical solution effort two processes are of concern, stability and convergence. Convergence means that the computation approaches limiting values which nearly represent an exact answer. The difference between the exact and limiting values is then the error of the method. Computational stability simply means that the convergence process occurs relatively smoothly and that errors due to round-off, truncation of series or in the specification of initial conditions do not grow in an unbounded manner. Two methods exist for determining the degree of stability of any model. Firstly, in simple models, a perturbation analysis (Roache, 1972) of the governing equations will demonstrate whether or not arbitrary perturbations in any parameter will result in instability. Secondly, and more frequently, stability requirements are determined empirically by

varying the magnitude of parameters and observing the effects. Generally, decreasing the grid spacing decreases truncation errors and improves stability (Fig. 2.7). Roundoff errors increase, however, and depending upon the problem, may adversely affect computational stability.

From perturbation analyses, the von Neuman stability requirements (Roache, 1972) for the steady-state two-dimensional vorticity transport equation are that:

$$\alpha \frac{\Delta t}{\Delta x} + \frac{\Delta t}{\Delta y} \leq \frac{1}{2} \tag{2.8.1}$$

and

$$\frac{u\Delta t}{\Delta x} + \frac{v\Delta t}{\Delta y} \leq 1 \tag{2.8.2}$$

where

$\alpha = \frac{1}{Re} = \frac{D}{\vec{v}L}$,

$\vec{v}$ = velocity,

L = basin length,

D = a viscosity or diffusion coefficient, depending on the problem,

Re = local basin Reynolds number based on local velocity, basin length and D,

and $\frac{u\Delta t}{\Delta x}$ and $\frac{v\Delta t}{\Delta y}$ are Courant numbers.

For the special case in which $\Delta x = \Delta y = \Delta$, Eq. 2.8.1 reduced to

$$\frac{\alpha\Delta t}{\Delta} \leq \frac{1}{4} \tag{2.8.3}$$

Alternatively, if $u\Delta t/\Delta x = v\Delta t/\Delta y$, then Eq. 2.8.2 reduced to

$$\frac{u\Delta t}{\Delta x} = \frac{v\Delta t}{\Delta y} \leq \frac{1}{2} \tag{2.8.4}$$

Equations 2.8.3 and 2.8.4 are in fact twice as restrictive as would be indicated by a similar one-dimensional analysis of the vorticity transport equation. For a uniform grid, Eq. 2.8.4 will normally be

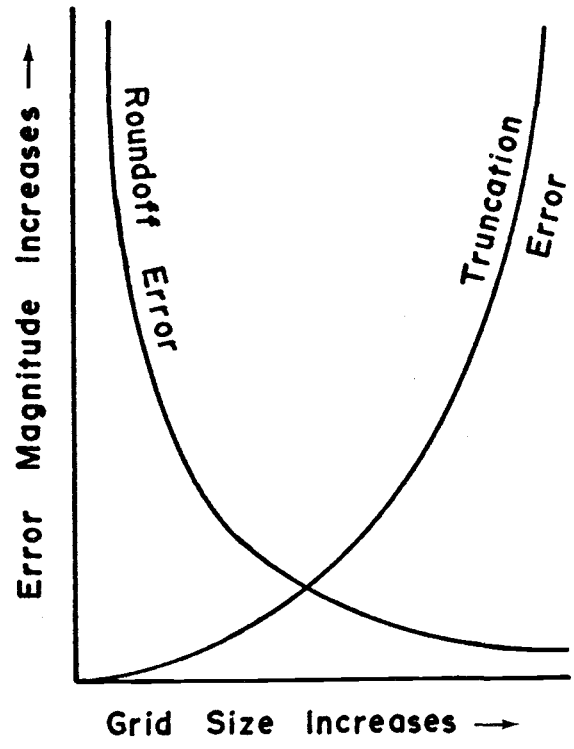

Figure 2.7. Illustration of the variation of round-off and truncation errors as a function of the size of grid employed.

more restrictive than Eq. 2.8.3. For a normalized velocity, $\vec{v}/u_o$, of unity and the grid length, Δ, of 1/12 used in this study, the computation Δt must be less than 0.04.

The ADI method is unconditionally stable and is formally second order accurate in space and time, i.e., the truncation error originating in the approximation of the spacial derivatives is $O(\Delta x^2, \Delta y^2, \Delta t^2)$. Some computational instabilities associated with high Reynolds numbers have been noted, but are attributed to insufficient convergence in the iterative solution for boundary vorticity at the K+1 level or to the equation used to evaluate boundary vorticity values from internal point values of the stream function (Roach, 1972). The ADI method is actually less accurate than second order in time due to the use of Kth level bed shear and velocity terms in the split-level Equations 2.6.1 and 2.6.2 where formally (K+½)th level terms should be used. Boundary conditions also pose a limit to accuracy. Equations 2.6.1 and 2.6.2 require that $\xi^{K+\frac{1}{2}}$ and ξ^{K+1}, respectively, be specified on the boundary. Since for no-slip boundaries these values depend on values of ξ^{K+1}, an implicit solution of the form $\nabla^2\psi^{K+1} = \xi^{K+1}$ would be required. This is not practically tenable. As an approximation, values from the preceeding time level are used. An exact determination of the errors resulting from these substitutions is only possible when an analytic solution to the problem exists. If, however, the time step Δt is chosen sufficiently short, the flow may be considered to be slowly varying and the roundoff and truncation errors may approach their theoretical limits. In this study, preliminary runs demonstrated that little change occurred in the vorticity field if the time step was less than 0.92. Since the computations were also stable, a normalized Δt of 0.02 was used throughout this study.

2.9 Summary

A literature review indicated that an analytic solution is lacking for the problem of shear-generated, turbulent flow within a

rectangular basin adjacent to a waterway. Most investigators have adopted numerical or physical modeling techniques to study this phenomenon. Little substantiating field work has been previously conducted.

A finite-difference solution to the vorticity-transport/stream function boundary value problem of shear-driven circulation was also presented in this chapter. The results of this solution are reviewed in light of previous investigations in Chapter V.

III. THE SEDIMENT TRANSPORT PROBLEM

3.1 Introduction

This chapter reviews previous efforts to model sediment transport phenomena in tidal water. A brief review is given of the salient aspects of the two-dimensional, horizontal, sediment-transport model developed by Araithurai (1974).

The problem of defining the sediment dispersion coefficients which greatly influence the dispersal of suspended sediments, is also considered at length. Araithurai's finite element model formulation is described in detail in Chapter IV and the model was used to generate the data discussed in Chapter V.

3.2 Review of Transport Models

Several comprehensive reviews of hydrodynamic and transport models have been published in recent years (e.g. TRACOR, 1970; Callaway, 1971; Hinwood and Wallis, 1975a and b). The last authors noted that two-dimensional plan-view models are restricted to vertically well-mixed estuaries or embayments, and that the effects of vertical density gradients are not represented satisfactorily. Westrich (1977) has also suggested that such models may not accurately reproduce the transportive effects of strong, vertical, secondary currents which result from flow curvature.

The two-dimensional plan-view transport models are based on the vertically-integrated mass conservation equation

$$\frac{\partial c}{\partial t} + \frac{\partial (uc)}{\partial x} + \frac{\partial (vc)}{\partial y} = \frac{\partial}{\partial x}\left(D_x \frac{\partial c}{\partial x}\right) + \frac{\partial}{\partial y}\left(D_y \frac{\partial c}{\partial y}\right) + S \qquad (3.2.1)$$

(1) (2) (3) (4) (5) (6)

where

$c = \overline{\rho c d}$ = the vertically-integrated concentration (mass per unit projected area),

ρ = carrier fluid density,

d = depth,

D_x,D_y = directional turbulent dispersion coefficients,

and S = source/sink term accounting for erosion and deposition.

Attempts to solve the sediment transport analytically have generally been unsuccessful. Only in certain simplified cases--e.g. reduction in the degrees of freedom of movement; conservative, neutrally-buoyant material; etc.--has any measure of success been achieved (O'Connor, 1960; Okubo, 1967; Fisher, 1970). More success has been realized through numerical modeling efforts and O'Connor and Zein (1974), Araithurai (1975), O'Connor (1975) Westrich (1975), Nece (1976), Vollmers (1976), and Abbott (1977) have investigated sediment transport and deposition processes in a basin connected to a passing waterway. These works are reviewed below with other works dealing with salt, mass or energy transport, but which utilize the same basic equation (Eq. 3.2.1) and serve to illustrate the variety of solution techniques employed.

TRACOR (1970) developed a steady state model with terms (2), (3), (4), and (5) of Eq. 3.2.1. The magnitudes of the dispersion coefficients were assumed and tidally-averaged velocities were used. The concentration field was determined using the relaxation technique.

Odd and Owen (1972) developed a two-layer, two-dimensional (vertical and longitudinal) model of circulation and mud transport of well-mixed estuaries. Distinct sediment concentration gradients were assumed in each layer, thereby better approximating reality than do single layer models. Sediment transport was determined from the solution by the method of characteristics of the mass balance equations for mud transport in two layers.

Masch, et al. (1971), Leendertse (1971), Beoricke and Hall (1974), Taylor and Davis (1975), Araithurai (1974), and Leimkuhler, et al. (1975) have solved the complete Eq. 3.2.1. Masch, et al. (1971) used an implicit finite difference formulation. Leendertse (1971) employed an alternating direction implicit-explicit formulation to obtain time-centered derivatives. Unlike most other models,

Leendertse's dispersion coefficients were calculated from the instantaneous velocities and depths. Boericke and Hall (1974) used an explicit predictor-corrector numerical scheme to model thermal dispersion from several heat sources and sinks. An irregular grid was obtained using coordinate transformation.

O'Connor and Zein (1974) applied a two-dimensional, (vertical and longitudinal), suspended-sediment model to problems having analytical solutions as well as to laboratory and field situations. Horizontal eddy diffusion was neglected in comparison with vertical diffusion and vertical water motion was assumed negligible compared with the sediment fall velocity. Although the model was intended for quasi-steady depth and flow conditions, the currents and the vertical sediment-diffusion coefficient were varied sinusoidally in time. O'Connor (1975) subsequently modified this model to include tidally-varying depths and showed that the error in neglecting such variation was generally less than 10%. O'Connor and Zein also incorporated time-variable longitudinal grid spacing to minimize pseudo-dispersion, i.e., interpolative errors arising from the convective term under low-flow conditions. Since this model assumes a constant depth while permitting time varying velocities, dispersion coefficients, etc., it is a useful tool for first-order engineering applications.

O'Connor (1975) also considered siltation rates in channels dredged at right angles to the main direction of flow. The rate of deposition per unit area was expressed as:

$$S = v_s C_{bed}$$

where v_s is the sediment's settling velocity and C_{bed} is the sediment concentration at the bed. The term C_{bed} was computed from the two-dimensional (horizontal and vertical) sediment transport equation using physical model velocity data as input. Substantial difficulties were encountered in matching computer and physical model results. Reentrainment was considered to be the cause of the disparity.

Westrich (1975) presented a one-dimensional model describing the exchange process between a channel and an adjacent basin of rectangular shape. The model allowed for unsteady exchange and varying water depth as associated with floods and tidal flows. Westrich stated that the mean residence time of a tracer particle would be a characteristic measure for judging the rate of deposition within the basin. From physical model tests using neutrally-buoyant tracers, Westrich determined that the residence time for basins with large aspect ratios (length/width) was constant and independent of length. As the aspect ratio approached zero, however, the exchange processes and residence time are controlled by secondary eddies generated on the interior of the basin. In all cases, the basins were completely open to exchange flows with the channel.

Vollmers (1976) briefly described the sedimentation patterns resulting from such conditions. He divided the sedimentation regime into two parts, one for the coarser fraction that deposits in the downstream portion of the main vortex (a, Fig. 1.3) and a second area for the finer material that deposits in the low-velocity core of the main vortex (b, Fig. 1.3).

Guymon, et al. (1970) solved the two-dimensional advection-diffusion equation by the Rayleigh-Ritz finite element method. This method requires the specification and minimization of a variational functional derived from the advection-diffusion equation. In contrast, Taylor and Davis (1975) Liemkuhler, et al. (1975), and Araithurai and Krone (1976) employed the Galerkin finite element method to solve the transport problem. This method directly solves a set of weighted advection-diffusion equations without the need to specify a functional.

The finite element method is replacing the finite difference approach in many problems since it permits maximum flexibility in expressing boundary conditions, geometry and input parameters. Prakash (1977) has reaffirmed the existence of variational

functionals for the general linear second-order differential equation with variable coefficients and has presented the functional appropriate for the two-dimensional advection-diffusion sediment transport problem.

Either the Rayleigh-Ritz or Galerkin method may be adopted. The former method involves the replacement of the problem-defining differential equation (Eq. 2.2.11) by an equivalent variational functional which is subsequently minimized for the prescribed boundary conditions. The Galerkin method avoids the direct use of the variational functional by minimizing the residual between the exact and approximate solutions. Direct use is made of the problem-defining differential equation and special "shape functions" or interpolating ploynomials which are functions of the geometry of the problem. According to Araithurai (1974), severe roundoff errors may result when applying the Rayleigh-Ritz technique to problems dominated by advective effects. Prakash (1977) has suggested that the roundoff error, which results from exponents involving overly-large Peclet numbers, uL/D, will not be a problem in estuarine flows due to the low velocities and large dispersion coefficients involved. However, Prakash (1977) acknowledges that the Galerkin technique does not suffer from such a limitation and is, therefore, more stable and versatile. The Galerkin technique, however, generally does not produce symmetrical matrices, as does the Ritz method, thereby increasing computer storage requirements. The work presented in this study predates Prakash's (1977) publication and is based upon the Galerkin method of Araithurai and Krone (1976). Substantial reductions in computer memory requirements and in computation time could result from using the Rayleigh-Ritz variational technique, should it be proven to have acceptable roundoff error characteristics. Chapter IV considers the details of the Galerkin method and of the alternative variational technique.

Although the Araithurai-Krone (1976) model worked well for channel flows, Westrich (1977) has suggested that any two-dimensional (horizontal) model may be incapable of accurately reproducing material

transport by secondary currents. The data to be presented herein should be cautiously reviewed in light of this observation. For cases where secondary currents are of importance, a complete three-dimensional solution would then be required, necessitating increased computer storage requirements and subsequently higher computation costs which might rise to unacceptable levels.

3.3 Deposition

Since erosion is not expected to occur in the protected areas considered in this study, the source/sink term of Eq. 3.2.1 may be simply stated as

$$S = -\frac{dc}{dt} \tag{3.3.1}$$

Metha and Parthenaides (1974) and Araithurai (1974) discuss the processes governing deposition and suspension of sediments in the estuarine environment. The rate of sedimentation of cohesive sediments depends upon

1) the chemical composition of the sediment, i.e., its tendency to cohere,
2) the salinity and chemical composition of the transporting fluid,

and 3) the degree of internal and bed shear.

Given the proper clay chemistry and fluid salinity, the individual particles may flocculate and tend to settle out. The ultimate floc size and settling velocity depend upon the degree of internal shear. The net balance between downward settling and upward dispersion of flocs then determines the local sedimentation rate.

Krone (1962) observed in flume studies that the rate of deposition for cohesive sediments varied with suspension concentration. For suspended sediment concentrations less than 3×10^{-4} kg/l, the sediment concentration decreased exponentially with time, the particles settling more or less independently. For concentrations

between 3.10^{-4} and 10^{-2}kg/l, the settling rate would increase due to the increasing frequency of particle collisions and faster growth of larger flocs. At higher concentrations, hindered settling would be found to occur due to the restriction of escaping interfloc water. Consequently, the rate of deposition was lower in this range than in the $3x10^{-4}$ to 10^{-2} kg/l range.

Krone (1962, 1963) postulated a growth model for floc formation in suspended cohesive sediments which was adopted by Araithurai (1974) in the preparation of the program used in this present study. Krone's model assumed that flocs were composed of basic "primary particle aggregates" of uniform porosity. The porosity, strength, etc., of a floc depended, however, upon the arrangement or order of these primary aggregates which itself depends on environmental parameters, especially fluid shear. Viscosimeter tests of a number of cohesive sediment samples and observation of floc growth rates permitted Krone (1963) to determine representative sediment shear strengths and densities for various levels of sediment aggregation. Aggregate shear strength was observed to decrease with increasing aggregation as a result of an increasing void ratio.

In the absence of continuing aggregation, i.e., when either particle concentration is low or equilibrium has been reached between floc size and turbulence level, the rate of deposition is given by Krone (1962) as

$$\left.\frac{dc}{dt}\right|_d = - \frac{P\, v_s c}{\bar{d}} \qquad (3.3.2)$$

where

$P = 1 - \tau_b/\tau_{cd}$ is the probability of deposition (Krone, 1962; Partheniades, 1962).

τ_b = the actual bed shear,

τ_{cd} = the critical shear stress at which deposition begins,

v_s = settling velocity,

c = suspended sediment concentration,

and $\bar{d}$ = average depth through which the particles settle.

That the settling velocity also depends on concentration has been long known. For particle concentrations less than 3×10^{-4} kg/l, the settling velocity may be adequately determined from Stoke's law for the terminal settling velocity of individual particles as

$$v_s = \frac{gd^2}{18\nu} (S.G.-1) \qquad (3.3.3)$$

where

d = equivalent grain diameter,

ν = kinematic viscosity of the fluid,

and S.G.= specific gravity of dry sediment.

Hence, clay particles ranging in "diameter" from 2.4×10^{-7} to 4×10^{-6} m, with a specific gravity of 2.64, will have a settling velocity

$$4 \times 10^{-7} < v_s < 10^{-4} \text{ m/s}$$

in 8° C water. A value of 6.6×10^{-6} m/s was used for cases of independent settling in this study, as would be considered representative for sediments accumulating in Oregon estuaries.

Above the 3×10^{-4} kg/l level, aggregation proceeds even in tranquil flows. However, once equilibrium is achieved between floc size and internal shear, Krone (1962) has shown that the terminal settling velocity may be expressed as:

$$v_s = K C^{4/3} \qquad (3.3.4)$$

where K is an empirical constant depending on the type of sediment, and C is the suspended sediment concentration in the inflowing waters.

A suspended sediment concentration of 5×10^{-5} kg/l is representative of average conditions for the Sacramento River at Rio Vista just upstream of San Francisco Bay (Klingeman and Kaufman, 1965). St. Louis Bay (Hoskins, 1971), the lower Columbia estuary (Hubbell and Glen, 1971), and the Savanna estuary (Krone, 1972) also exhibited average concentrations of a few tens of milligrams per liter. Peak concentrations associated with river floods or peak tidal velocities may exceed 10^{-3} kg/l for a period of hours, but on an annual basis have a relative short-term effect. Since this study is directed

towards understanding the general sedimentation problem, such an extreme concentration case will not be considered farther, and a moderate suspended sediment concentration of 5×10^{-5} kg/l was adopted in most cases.

3.4 Concentration and Sedimentation Rates

When continuing aggregation occurs, there is a decrease in the number of individual particles and an increase in the apparent diameter of the suspended flocs. Kruyt (1952) expresses the number of particles, n, as a function of time by

$$n = \frac{n_o}{(1 + t/t_c)} \tag{3.4.1}$$

where

n_o = initial number of particles,

and t_c = time of coagulation or flocculation to the equilibrium size. Krone (1962) derived an expression for the concentration of suspended sediment in terms of the accumulated time, t, since the sediment was introduced to the flow. Taking the average mass of the flocs at any time to be

$$\overline{m} = m_o(n_o/n)$$

with

m_o = initial mass of individual particles,

n_o = the initial number of particles per unit volume,

and n = the number of flocs at any time, t, per unit volume,

then substutition of the Kruyt function gives

$$\overline{mn} = m_o n \left(\frac{n_o}{n}\right)\left[\frac{1}{1 + t/t_c}\right] = c \tag{3.4.2}$$

where $\overline{mn}$ is the concentration of suspended sediment. Substituting Eq. 3.4.1 into 3.3.1 and integrating over time yields

$$\ln\frac{c}{c_o} = -\frac{v_s t_c}{d}\left(\frac{n_o}{n}\right)\left[1 - \frac{\tau_b}{\tau_{cd}}\right]\ln\left[1 + \frac{t}{t_c}\right] \qquad (3.4.3)$$

where c_o is the initial concentration of the inflowing waters.

The term (n_o/n) will approach a limiting value because floc size will be limited by shear effects associated with the flow velocities. When aggregation proceeds slowly, $t < t_c$ and the time dependence can be expanded as

$$\ln\left[1 + \frac{t}{t_c}\right] = \frac{t}{t_c} - \frac{(t/t_c)^2}{2} + \frac{(t/t_c)^3}{3} - \ldots$$

which permits the first order form of Eq. 4.4.3

$$\ln\frac{c}{c_o} = -K_o t \qquad (3.4.4)$$

where

$$K_o = \frac{v_s}{d}\left[1 - \frac{\tau_b}{\tau_{cd}}\right] \qquad (3.4.5)$$

For $t >> t_c$, a fully-aggregated floc size is achieved and Eq. 3.4.3 becomes approximately

$$\ln C = -K_1 \ln t + \text{const.} \qquad (3.4.6)$$

where K_1 is an empirical constant.

Computations in this study assumed that a fully-aggregated condition exists. Equation 3.4.3 was used to describe the variation of the suspended sediment concentration during each time step of the finite element computation.

The sink term from Eq. 3.1.1 and 3.3.2 is

$$S = -\frac{dc}{dt} = \frac{P\, v_s c}{d} \qquad (3.4.7)$$

For concentrations below 3×10^{-4} kg/l, Eq. 3.4.7 becomes

$$S = -\frac{v_s}{d}\left[1 - \frac{\tau_b}{\tau_{cd}}\right] c \qquad (3.4.8)$$

where v_s is the Stoke's settling velocity, Eq. 3.3.2. For concentrations greater than 3×10^{-4} kg/l, Eq. 3.3.2, 3.3.3, and 3.3.4 yield

$$S = -\frac{2K}{d}\left[1 - \frac{\tau_b}{\tau_{cd}}\right] c^{7/3} \qquad (3.4.9)$$

For the higher concentration case, the S term becomes non-linear in the advection-dispersion equation. Araithurai (1974) claims that except under almost stagnant conditions, the sink term will be at least an order of magnitude smaller than the dispersion or advective terms and thus should not unduly effect the stability or convergence of the solution. The proper choice of limits of lengths and velocities for spatial and temporal descritizations in approximate solutions will further mitigate the non-linear effects (see Section 4.5).

Sedimentation is assumed in this analysis to occur at a constant rate over a given time interval, Δt, e.g. following Eq. 3.4.8 or 3.4.9. Since this rate is concentration dependent, the value of c at the beginning of the time interval is used throughout the interval. For a sufficiently short time increment, the computed solution approaches the exact solution for the sedimentation problem.

Where the velocity is so small that in the Δt interval the fluid does not cross the element, the assumption of deposition from constant concentration is invalid. Araithurai (1974) defined a time TT as the ratio of the element mean depth to the element average velocity. If this TT exceeds Δt, then deposition is assumed to occur from a stagnant fluid, the concentration within the element decreasing with time according to Eq. 3.3.3. The rate of deposition can then be computed from the difference between the initial and final concentrations.

For TT > Δt and the initial concentration, c_o, less than 3×10^{-4} kg/l, the settling velocity is treated as constant. Integrating Eq. 3.4.8 over the time increment gives

$$c_f = c_o \exp \left(- \frac{2 v_s}{\bar{d}} \left[1 - \tau_b / \tau_{cd} \right] \Delta t \right) \qquad (3.4.10)$$

where c_f is the final concentration and c_o the initial concentration.

The sedimentation rate is then

$$\frac{\partial c}{\partial t} = -\left(\frac{c_o - c_f}{\Delta t}\right) \tag{3.4.11}$$

For concentrations in excess of 3×10^{-4} kg/l, the integration of Eq. 3.4.9 yields

$$c_f = \left[\frac{8}{3}\,\frac{K}{d}\left(1 - \frac{\tau_b}{\tau_{cd}}\right)\Delta t + c^{4/3}\right]^{-3/4} \tag{3.4.12}$$

with the sedimentation rate as defined in Eq. 3.4.11.

3.5 Dispersion

The sediment transport equation (Eq. 3.2.1) includes terms proportional to turbulent sediment-dispersion coefficients which account for the movement of sediments by processes other than can be accounted for by the velocity terms on the left-hand side of Eq. 3.2.1. Effects of secondary currents and of the vertical distribution of velocity and diffusion are some of the processes accounted for by the dispersion terms in Eq. 3.2.1. This section reviews currently-available estimates of the sediment dispersion coefficient.

It is often assumed that the mass dispersion coefficient for entrained particles, D_s, can be related to that of the fluid, D_f, by

$$D_s = K D_f \tag{3.5.1}$$

where K is a constant (Johnson, 1974). Most investigators have assumed that $D_s < D_f$ because particles do not respond fully to turbulent velocity fluctuations. Singamsetti (1966), in studies of the diffusion of sediment diffusion in a submerged water jets, has concluded the opposite. He reasoned that in turbulence composed of vortices, the centrifugal force acting on the sediment particles would be greater than that acting on the fluid particles. Due to the greater centrifugal force, the solid particles move towards the outside of the eddies, resulting in an increased rate

of dispersion. Results from numerical modeling of sediment transport by O'Connor and Zein (1974) also indicate that the dispersion of suspended sediments is more rapid than for fluid "particles" alone. Most investigators nonetheless prefer to use fluid dispersion coefficient obtained from field or flume studies of dye dispersion which is understandable considering the limited amount of field and laboratory data available regarding particle dispersion.

Most modelers attempt to approximate the dispersive effects through the use of kinetic energy or momentum correction factors and "adjusted" diffusion coefficients, also known as dispersion coefficients. These coefficients were originally described by Talyor (1954). Proceeding in direct analogy to the derivation of the Reynolds stress terms, the parameters of interest were espressed as the sum of the temporal, profile, or cross-sectional mean values and corresponding perturbations. The relevant equations were then integrated over either time or space, leaving only mean values and terms involving the products of perturbations. Applying the Prandtl mixing length hypothesis, these products were equated to the product of a dispersion coefficient and the gradient of the mean parameter. Hence, for substance s, and perturbations s' and u'.

$$D_x \frac{\partial \bar{s}}{\partial x} = \overline{u's'} \qquad (3.5.2)$$

is the flux per unit area due to either spatial or temporal nonhomogeneities in the field of s(s,y,z,t), relative to its temporal or spatial average value.

The magnitude of dispersion coefficients is generally considered case-specific but numerous attempts have been made to express the dispersion coefficient in terms of measurable quantities. Appendix B lists many of the expressions derived for open-channel, estuarine, and coastal flow conditions (Choi, 1975). Taylor's (1959) analysis has been applied to open-channel flows by Elder (1959) and Fisher (1967) and to coastal waters by Bowden (1965). Araithurai (1974), Westrich (1975), O'Connor (1975), and Abbott (1977) have applied these and other estimators developed for open channel flows to studies of circulation and sedimentation in basins and backwater

areas along river margins. As no work has been examined which deals directly with dispersive conditions in large, recirculating, turbulent flows, the Taylor-Elder-Fischer relationships were adopted for this study.

A direct comparison of the magnitudes of reported dispersion coefficients is not strictly valid since such coefficients are strongly dependent upon local flow conditions which vary from estuary to estuary and over time in a given estuary. If one assumes, however, that such conditions average out if a sufficiently large number of estuaries are considered, then a "representative" magnitude can be estimated. Longitudinal dispersion coefficients reported for 16 estuaries in the United States and Europe had a mean of approximately 3×10^2 m^2/s with a standard deviation of similar magnitude (Haag and Bedford, 1971; Thomann, 1972; Nihoul and Adam, 1975; Choi, 1975; Ward, 1976). Choi (1975) and other authors have noted that reported coefficients are generally one or more orders of magnitude larger than that predicted from the often-used Elder (1959) equation

$$D_L = 5.9\, u_* d \tag{3.5.3}$$

Consequently, this study used the modified Elder estimator for the longitudinal dispersion coefficient:

$$D_L = 60\, u_* d \tag{3.5.4}$$

This formulation was also used to compute the eddy viscosity coefficients for the ADI solution of the vorticity transport equation (see Section 2.6).

Transverse dispersion in steady, open-channel flows is generally estimated using Elder's (1959) relationship

$$D_t = 0.23\, u_* d \tag{3.5.5}$$

as determined from flume studies. Glover (1964) has observed that in open channel flows

$$D_L \approx 300\, D_t$$

where the subscripts L and t identify the longitudinal or transverse dispersion coefficient. This supports the use of the amplified expression (Eq. 3.5.4) for the longitudinal dispersion coefficients.

Such a magnitude, however, does not account for any secondary flow effects.

Similarly, little information is available regarding the vertical dispersion coefficient. Holley, et al. (1970), O'Connor (1975), and others have used Glover's (1964) expression

$$D_v \simeq 0.067\ u_* d \tag{3.5.6}$$

Engelund (1974) described the effects of secondary flows on horizontal momentum transfer at river bends Abbott (1977) extended parts of Engelund's work to define two dispersive processes: advective and rolling dispersion. Advective dispersion specifically accounts for deviations from the assumed velocity profile and is given as

$$D_a = \left[\frac{\alpha - \beta^2}{2}\right] V_* V d \tag{3.5.7}$$

where $\alpha = \dfrac{\int_{h_o}^{0} u^3 dz}{v^3 d}$, a kinetic energy correction coefficient,

$\beta = \dfrac{\int_{h_o}^{0} u^2 dz}{v^2 d}$, a momentum correction coefficient,

V_* = V/u_*, a non-dimensional Chezy number or shear velocity.

V = depth averaged velocity,

u_* = friction velocity,

and d = water depth.

Abbott observed that this formulation yields values similar to those derived from Elder's (1959) Eq. 3.5.1. Rolling dispersion accounts for the secondary flow field effects such as occur at river bends or, possibly in confined recirculating flows. In such cases

$$D_r = \frac{V_*^3}{18} \left(\frac{d}{r}\right)^2 Vd \tag{3.5.8}$$

where r is the radius of curvature of the main flow.

The magnitude of the advective and rolling dispersion processes obviously depends on local flow conditions and will in some cases need to be included in the formulation of the transport model. For

example, for recirculating flow in a 4.5 m deep marina with a basin-mean velocity of 0.05 m/s, a friction velocity of 1.9×10^{-3}, and a radius of curvature of 50 m, one obtains $D_a \doteq 2.96 \times 10^{-2}$ m^2/s and $D_r = 1.85$ m^2/s.

For vertically-averaged velocities, advective dispersion may be expected to act in the vertical plane containing the local velocity vector. The rolling dispersion on the other hand, may contribute to both downstream and transverse dispersion. Most simply, however, one may assume that the rolling dispersion acts only in the transverse direction.

Dispersion in oscillating flows has been investigated by Bowden (1965) and Holley, et al. (1970). Bowden has shown that dispersion in oscillatory flows occurs at only half the rate in steady flows. Holley, et al. suggested expressions for transverse dispersion under oscillatory flow which unfortunately require detailed prior knowledge of the velocity field. Bowden's formulations hence are more frequently used.

The definition of dispersion in terms of spatial or temporal perturbations of parameters as in Eq. 3.5.4 admits the possibility of directionally-varying dispersion coefficients since the perturbations of velocity, concentration, etc. can be broken into components parallel to the principle coordinate axes or parallel to and perpendicular to the local velocity vector, for example. The latter condition would permit the modeler of recirculating flows in rectangular basins, for example, to enhance dispersion perpendicular to the local velocity vector and hopefully, more correctly simulate the effects of secondary currents which are generated by flow curvature and flow towards the basin center.

Pollock (1973) applied a random-walk technique in an attempt to retain the "directionality" of the dispersive process. Particles representing parcels of waste were assumed to move with an advective step and a dispersive step in each time increment. The dispersive step was determined by the random selection of a point on the dispersion ellipse whose principal axes are the magnitudes of the longitudinal and transverse dispersion coefficients.

Leimkuhler, et al. (1975) formulated dispersion coefficients as functions of temporal mean velocities and terms equivalent to the Reynolds stresses in the perturbed equations of motion. These coefficients were then decomposed into axial components as

$$D_{xx} = D_L \cos^2\theta + D_t \sin^2\theta \tag{3.5.9}$$

$$D_{yy} = D_L \sin^2\theta + D_t \cos^2\theta \tag{3.5.10}$$

$$D_{xy} = (D_L - D_t) \sin\theta \cos\theta \tag{3.5.11}$$

where

$D_{L,t}$ = longitudinal and transverse dispersion coefficients as functions of local velocity,

and θ = angle between local velocity vector and the x-axis.

The directional dispersion coefficients for this present study were computed using the vector components (Fig. 3.1) of the previously-derived estimates, Eqs. 3.5.4 and 3.5.5,

$$D_L = 60\, u_* d \tag{3.5.4}$$

and

$$D_t = 0.23\, u_* d \tag{3.5.5}$$

as:

$$D_x = D_L \cos\theta + D_t \sin\theta = \left| \frac{D_L\, u + D_t\, v}{\sqrt{u^2+v^2}} \right| \tag{3.5.12}$$

and

$$D_y = D_L \sin\theta + D_t \cos\theta = \left| \frac{D_L\, v + D_t\, u}{\sqrt{u^2+v^2}} \right| \tag{3.5.13}$$

Here D_L and D_t, respectively, indicate dispersion acting parallel and perpendicular to the local velocity vector whereas D_x or D_y indicate dispersion acting parallel to the x or y axes.

Strictly, u_* should be computed iteratively from Eq. 3.6.4 for each nodal point. To reduce computer computation requirements in this present study, a representative u_* was computed for each node using the expression

$$u_* \doteq \frac{\sqrt{u^2+v^2}}{22} \tag{3.5.14}$$

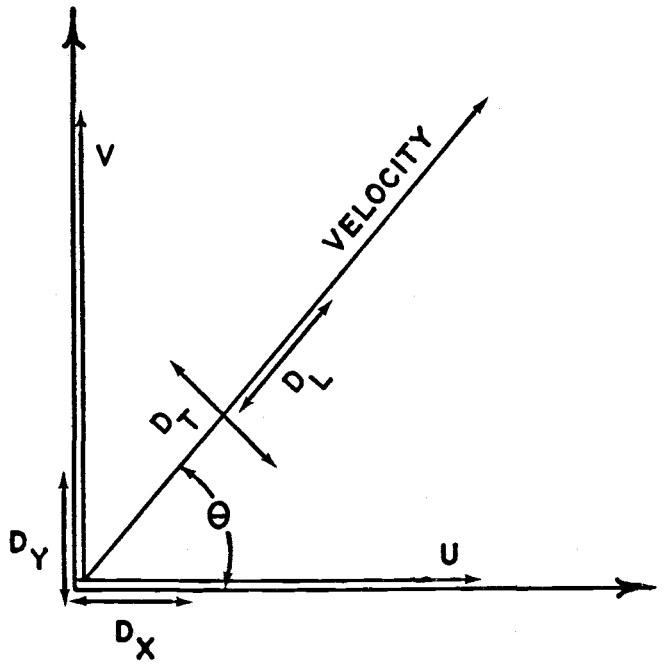

Figure 3.1. Vector representation of sediment dispersion. D_T and D_L are the transverse and longitudinal dispersion coefficients, respectively. The double-headed arrows indicate the directions in which the transverse and longitudinal dispersion processes act relative to the local velocity vector. D_x and D_y similarly indicate dispersion processes acting parallel to the coordinate axes.

The factor 1/22 was determined as follows. The average basin velocity, $\bar{v}$, was determined for a number of cases and the corresponding u_* values determined from Eq. 2.6.3. For these pairs of values, the relation

$$u_* \doteq K \bar{v} \tag{3.5.15}$$

was determined where K was approximately 22. Since local velocities for the majority of cases did not differ from the mean by more than a factor of 5, the approximation of u_* in Eq. 3.5.14 was considered acceptable.

3.6 Summary

In this chapter, the two-dimensional, horizontal, sediment-transport boundary-value problem was posed for a rectangular basin connected to a waterway. A review of the literature dealing with the general transport equation illustrated various methods for solution of this problem. As the finite-element model developed by Araithurai (1974) was adopted for use in this study, a brief review was presented of the conceptual framework of that model relating concentration, settling velocity, and sedimentation rate. Finally, a synopsis was given of alternative ways of computing the dispersion coefficients which, in part, determine the distribution of suspended sediments.

IV. THE FINITE ELEMENT METHOD

Most problems in engineering physics can be specified in one of two ways. In the first, differential equations describing the process within the domain of interest are given. In the second, a variational principle is determined for the whole region. Both approaches then require the minimization of some quantity such that the resulting set of differential equations will yield the best approximation of the unknown, desired function after standard matrix solution techniques are applied.

The finite element method simply provides the spatial and temporal framework for either method of analysis. In this chapter, each of the above-mentioned techniques is investigated. The first case is represented by the Galerkin method of weighted residuals and the second by the variation principle.

4.1 Sequence of Analysis

The finite element method has been described in detail by Zienkiewicz (1971) for structural engineering applications and more recently by Pinder and Gray (1975) for fluid problems. The basic sequence of analysis is as follows

a) identify the parameter of interest and the governing differential equations, i.e. Eq. 3.2.1, and boundary conditions;
b) replace the continuous domain of solution by discrete points or nodes at which the function is to be determined;
c) group these points into subdomains or finite elements with the nodal points located on the interelement boundaries;
d) approximate the dependent variables on the interior of each element in terms of their unknown nodal point values, insuring continuity of dependent variable values between elements;

e) minimize an appropriate measure of error so that a set of simultaneous equations results; and

f) solve the resulting set of equations for the node point unknowns.

The net result is that a continuous function is approximated and solved for over some domain using functions defined over subdomains, without regard to the specific location of any subdomain.

4.2 Global and Element Coordinate Systems

Figure 4.1 displays a hypothetical domain which has been partitioned into a number of triangular quadratic elements. The global coordinate system, x-y, applies continuously over the entire domain, but is distinct from the element or local coordinate system, α_1, α_2, α_3, which applies only within a given element.

The element coordinates may also be defined as area coordinates which are more easily used in the computational process (Zienkiewicz, 1971). The area of the element shown in Figure 4.1 is divided into sub-areas about the arbitrary point, P. The area coordinates of point P, with respect to the corner nodes are:

$$L_1 = \frac{\text{Area P23}}{A}, \tag{4.2.1}$$

$$L_2 = \frac{\text{Area P31}}{A}, \tag{4.2.2}$$

$$L_3 = \frac{\text{Area P12}}{A}, \tag{4.2.3}$$

where A is the total area of the triangular element and Area PNM is the area contained within the triangle defined by points P, N and M. These local coordinates are related to the global coordinates of the corner nodes by:

$$x = L_1x_1 + L_2x_2 + L_3x_3, \tag{4.2.4}$$

$$y = L_1y_1 + L_2y_2 + L_3y_3, \tag{4.2.5}$$

$$1 = L_1 + L_2 + L_3, \tag{4.2.6}$$

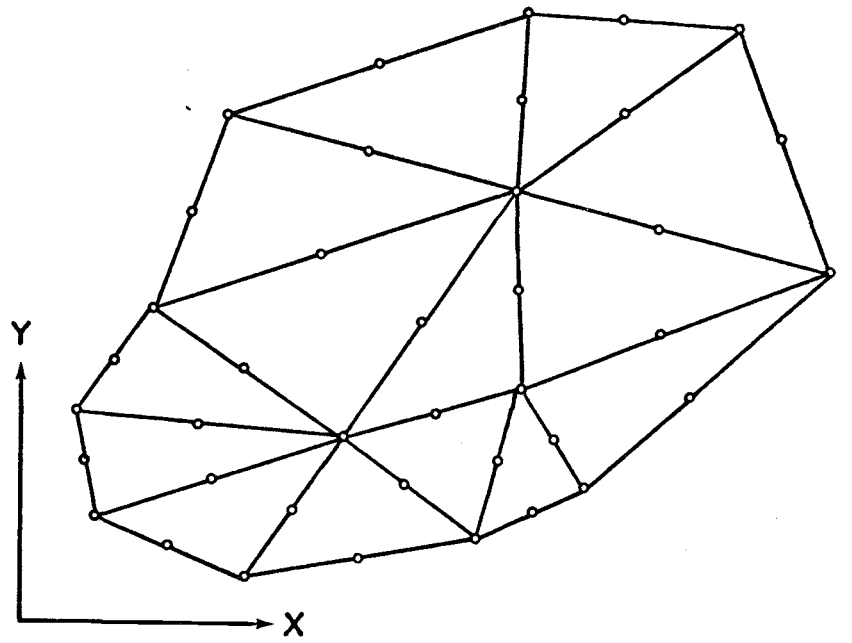

A

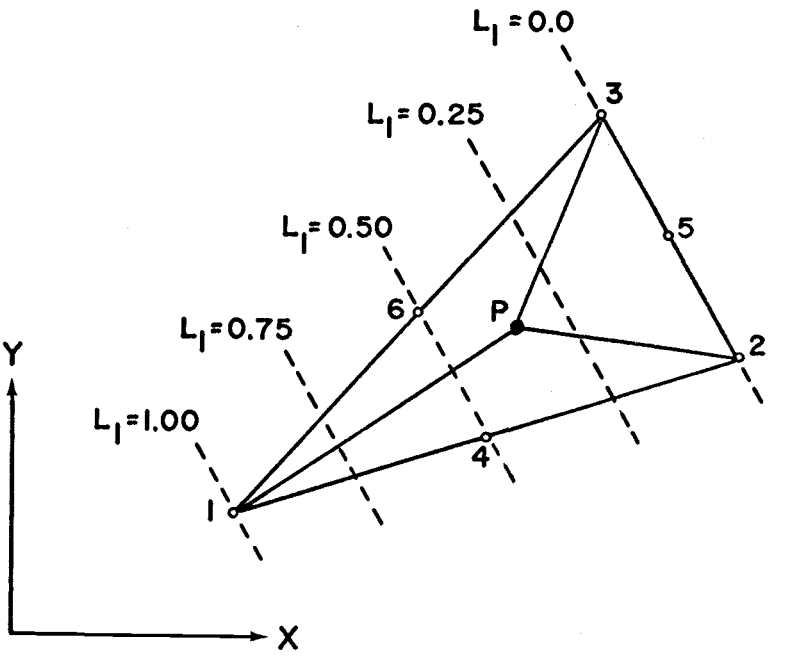

B

Figure 4.1. The finite element in space. (A). A domain discretized using quadratic, triangular, finite-element triangules. (B). Element notation. The position of point P is expresses in terms of area coordinates, e.g. L_1. Vertex and mid-side nodes are identified by numbers as shown.

Substitution for the local corrdinates gives:

$$L_1 = (a_1 + b_1x + c_1y)/2A, \tag{4.2.7}$$

$$L_2 = (a_2 + b_2x + c_2y)/2A, \tag{4.2.8}$$

$$L_3 = (a_3 + b_3x + c_3y)/2A, \tag{4.2.9}$$

where

$$A = \frac{1}{2} \det \begin{vmatrix} 1 & x_1 & y_1 \\ 1 & x_2 & y_2 \\ 1 & x_3 & y_3 \end{vmatrix} \tag{4.2.10}$$

and

$$a_1 = x_2y_3 - x_3y_2 \tag{4.2.11}$$

$$b_1 = y_2 - y_3 \tag{4.2.12}$$

$$c_1 = x_3 - x_2 \tag{4.2.13}$$

Succinctly, the area coordinates may be written as:

$$L_i = (a_i + b_ix + c_iy)/2A \tag{4.2.14}$$

4.3. Shape Functions

A function's value within any element is determined by interpolation using its values at points lying on the elements boundaries. It is natural to expect the accuracy of such an interpolation to increase with the number of nodes per element (Pinder and Gray, 1975). The number of nodes along any element edge determines the order of the shape function or basis set which is then used for interpolation. Figure 4.2. shows the basic triangular element used in this study, having three nodes per edge, which requires a quadratic interpolating polynomial or so-called "shape function". Zienkiewicz (1971) has shown that the proper shape function for quadratic element is:

$$N_i = L_i \left[2\, L_i - 1\right] \quad \text{for corner nodes} \tag{4.3.1}$$

and

$$N_{iJ} = 4\, L_iL_J \text{ for mid-section nodes} \tag{4.3.2}$$

where $L_{i,J}$ gives the area coordinates of a point relative to corner nodes adjacent to a mid-section point.

These shape functions may then be used in conjunction with the nodal concentrations to approximate the concentration at a point within the element. The concentration is given by:

$$\hat{C} = \sum_{i=1}^{3} L_i \left[2L_i - 1 \right] C_i + 4L_{Ji}L_{Ki} \overline{C}_i \qquad (4.3.3)$$

where

i denotes the ith corner node of an element,

J,K denote the remaining corner elements,

and $\overline{C}_i$ is the concentration of the mid-section node opposite the ith corner node.

4.4. The Galerkin Method of Weighted Residuals

4.4.1. Concept

Assuming that a function C exists which satisfies the given boundary value problem over the domain of interest, let the governing function be:

$$L\{C\} = 0 \qquad (4.4.1)$$

with boundary conditions:

$$B\{\Phi\} = 0. \qquad (4.4.2)$$

If a trial solution which satisfies the boundary conditions is assumed of the form

$$\{\hat{C}\} \simeq \left[N\right] \{C\}, \qquad (4.4.3)$$

[N] being the matrix of nodal shape functions, and $\{\hat{C}\}$ is the set of approximately-known values, then in general:

$$L\{\hat{C}\} \simeq L\{\left[N\right] \{C\}\} = R \neq 0. \qquad (4.4.4)$$

The best solution is one which minimizes the residual R over the complete domain. Although the point collocation and subdomain collocation minimization methods are applicable under certain conditions, the Galerkin method of weighted residuals has the greatest utility.

The Galerkin method is formulated by requiring the summation of weighted residuals over the entire domain to vanish when the nodal

weighting factors are the nodal shape factors, as discussed in the preceeding section, i.e.,

$$\int_V N_i \{R\}\, dV = \int_V N_i\, L([N]\ \{C\})\, dV = 0 \qquad (4.4.5)$$

4.5.2. Formulation

The terms involving second derivatives in the advection-dispersion equation (Eq. 3.2.1) would require continuity of the first derivatives at all element interfaces. To avoid being required to solve for the unknown first derivatives, integration by parts may be applied, resulting in a reduction of the order of differentiation. Assuming that at least locally the dispersion coefficients do not vary significantly in time or space, the modified Galerkin statement of this problem at any node becomes

$$\int_V N_i \left(\left[u \frac{\partial c}{\partial x} + v \frac{\partial c}{\partial y} + w \frac{\partial c}{\partial z} \right] + \left[D \frac{\partial N_i}{\partial x} \frac{\partial c}{\partial x} + D \frac{\partial N_i}{\partial y} \frac{\partial c}{\partial y} + D \frac{\partial N_i}{\partial z} \frac{\partial c}{\partial z} \right] + N_i \left[\frac{\partial c}{\partial t} - S \right] \right) dV - \int_S N_i\, D \frac{\partial c}{\partial x}\, dydz - \int_S N_i\, D \frac{\partial c}{\partial y}\, \partial x \partial z - \int_S N_i D \frac{\partial c}{\partial z}\, \partial x \partial y = 0 \qquad (4.4.6)$$

or

$$\int_V \left[N_i (\vec{v} \cdot \nabla c) + \nabla N_i \cdot (D \nabla c) + N_i \left(\frac{\partial c}{\partial t} - S \right) \right] dV - \int_S N_i (D \nabla c) \cdot \vec{n}\, dS = 0$$

where $\vec{n}$ is the normal to the surface of domain V.

Integrating over depth and assuming that terms involving vertical gradients may be neglected gives, for locally constant dispersion coefficients, Eq. 4.4.6 becomes:

$$\int_A \left(N_i \left[u \frac{\partial c}{\partial x} + v \frac{\partial c}{\partial y} \right] + \left[D_x \frac{\partial N_i}{\partial x} \frac{\partial c}{\partial x} + D_y \frac{\partial N_i}{\partial y} \frac{\partial c}{\partial y} \right] + N_i \left[\frac{\partial c}{\partial t} - S \right] \right) dxdy - \int_L N_i \left[D_x \frac{\partial c}{\partial x} \cdot n_x + D_y \frac{\partial c}{\partial y} \cdot n_y \right] dL = 0, \qquad (4.4.7$$

where L is the horizontal length of the domain boundary and n_x, n_y are the direction cosines of the normal boundary surface.

Observing that, for the finite element method, the suspended sediment concentration may be expressed as:

$$c = \sum_{\alpha=1}^{6} N_\alpha c_\alpha \quad , \alpha = 1, 2, \ldots , 6$$

then for each node the above Galerkin equation becomes

$$\left[\int_A \sum_{\alpha=1}^{6} \left(\left[N_i \left(u \frac{\partial N_\alpha}{\partial x} + v \frac{\partial N_\alpha}{\partial y}\right) + D_x \frac{\partial N_i}{\partial x}\frac{\partial N_\alpha}{\partial x} + D_y \frac{\partial N_i}{\partial y}\frac{\partial N_\alpha}{\partial y} \right] c_\alpha + \left[N_i N_\alpha\right]\frac{\partial c_\alpha}{\partial t} - N_i S \right) dxdy - \int_L \left(N_i \left[D_x \frac{\partial N_\alpha}{\partial x} \cdot n_x + D_y \frac{\partial N_\alpha}{\partial y} \cdot n_y \right] \cdot dL \right) c_\alpha \right] = 0 \qquad (4.4.8)$$

Or more succinctly,

$$(k_{i\alpha})c_\alpha + (t_{i\alpha})\frac{\partial c_\alpha}{\partial t} + (f_i) + (b_{i\alpha})c_\alpha = 0, \quad i=1, 2 \ldots 6, \quad \alpha=1, 2 \ldots 6 \qquad (4.4.9)$$

where

$$(k_{i\alpha}) = \int_A \left(N_i \left[u \frac{\partial N_\alpha}{\partial x} + v \frac{\partial N_\alpha}{\partial y} \right] + D_x \frac{\partial N_i}{\partial x}\frac{\partial N_\alpha}{\partial x} + D_y \frac{\partial N_i}{\partial y}\frac{\partial N_\alpha}{\partial y} \right) dxdy, \qquad (4.4.10)$$

$$(t_{i\alpha}) = \int_A N_i N_\alpha \, dxdy, \qquad (4.4.11)$$

$$(f_i) = -\int_A N_i S \, dxdy, \qquad (4.4.12)$$

and $$(b_{i\alpha}) = -\int_L N_i \left[D_x \frac{\partial N_\alpha}{\partial x} \cdot n_x + D_y \frac{\partial N_\alpha}{\partial y} \cdot n_y \right] dL. \qquad (4.4.13)$$

The complete matrices or vectors are commonly referred to as

$[k]$ = element coefficient, steady-state coefficient or "stiffness" matrix

$[t]$ = temporal or "mass" matrix

$\{f\}$ = element source or sink vector

$[b]$ = boundary or element load matrix

4.4.3. Procedure

Equation 4.4.9 is evaluated over the area of each element with the boundary integral term [b] {c} being included only for elements on the domain boundary. The coefficients of the nodal unknowns are arranged to form the 6x6 element coefficient matrix (the derivation of which is given in Appendix A). If one or more of the nodal unknowns are stipulated as boundary conditions, the row and column corresponding to that unknown are removed and the element load matrix is modified appropriately.

The element coefficient matrices and element load matrices are next assembled to form the system coefficient matrix and system load matrix. These matrices will be square and banded, but will not in general be symmetric, thereby increasing computer storage requirements over those of the alternative Rayleigh-Ritz method. If there are n nodes and boundary conditions are imposed at m of these nodes, then (n-m) equations will result, forming the system equation

$$\left[K\right]\{c\} + \left[T\right]\frac{\partial\{c\}}{\partial t} + \{F\} + \left[B\right]\{c\} = 0 \qquad (4.4.14)$$

Gaussian elimination is used to solve the set of equations for the node point concentrations.

4.4.4. The Finite Element In Time

Under steady-state conditions, the temporal terms in Eq. 4.4.14 vanish and the system equation 4.4.14 becomes

$$\left[K\right]\{c\} + \{F\} + \left[B\right]\{c\} = 0 \qquad (4.4.15)$$

which, upon evaluation of the system matrices, may be solved using standard matrix solution techniques. For transient problems, time is descritized into units Δt and Eq. 4.4.14 is solved stepwise.

The time-varying equation 4.4.14 may be solved using either a finite difference or finite element marching scheme. Pinder and Grey (1975) state that neither approach appears to have any significant

advantage. Conforming to Araithurai's (1974) development, the finite element scheme as used here is equivalent to a two-point finite difference approach.

The finite element in time may be throught of as a vertical prism extending upwards in time from the triangular spacial element forming its base as in Figure 4.2. The following development is according to Araithurai (1974). The temporal shape functions η_t are defined as

$$\eta_0 = \frac{\Delta t - t}{\Delta t}, \tag{4.4.16}$$

and $$\eta_1 = \frac{t}{\Delta t}, \tag{4.4.17}$$

where t = time in the interval Δt. Hence, by analogy to the spatial descritization technique, we have for the first time element

$$\{c\} = \left[\eta_0, \eta_1\right] \begin{Bmatrix} \{c_0\} \\ \{c_1\} \end{Bmatrix}, \tag{4.4.18}$$

where $\{c_0\}$ and $\{c_1\}$ indicate the system concentration vectors at time levels zero and one, respectively. Now,

$$\frac{\partial\{c\}}{\partial t} = \left[\frac{\partial \eta_0}{\partial t}, \frac{\partial \eta_1}{\partial t}\right] \begin{Bmatrix} \{c_0\} \\ \{c_1\} \end{Bmatrix} = \frac{1}{\Delta t} \left[-1, 1\right] \begin{Bmatrix} \{c_0\} \\ \{c_1\} \end{Bmatrix}. \tag{4.4.19}$$

Applying the Galerkin weighted-residual method to the governing system equation, after substituting the above quantities gives

$$\int_0^{\Delta t} \frac{t}{\Delta t} \left(\left[\bar{K}\right]\left[\eta_0, \eta_1\right] \begin{Bmatrix} \{c_0\} \\ \{c_1\} \end{Bmatrix} + \left[T\right]\left[\frac{\partial \eta_0}{\partial t}, \frac{\partial \eta_1}{\partial t}\right] \begin{Bmatrix} \{c_0\} \\ \{c_1\} \end{Bmatrix} + \{\bar{F}\} \right) dt = 0 \tag{4.4.20}$$

where overbars indicate average values for the time increment. Integration yields the two-point recurrence relation

$$\frac{2}{3}\left(\left[\bar{K}\right] + \frac{\left[T\right]}{\Delta t} \right) \{c\}^{n+1} = \left[\frac{\left[T\right]}{\Delta t} - \frac{\left[\bar{K}\right]}{3} \right] \{c\}^n + \{\bar{F}\} \tag{4.4.21}$$

This is a set of simultaneous equations which may be solved for the new nodal concentrations. Array $\left[\bar{K}\right]$ is constructed from the element geometry, node point velocities and diffusion coefficients as given in Appendix A.

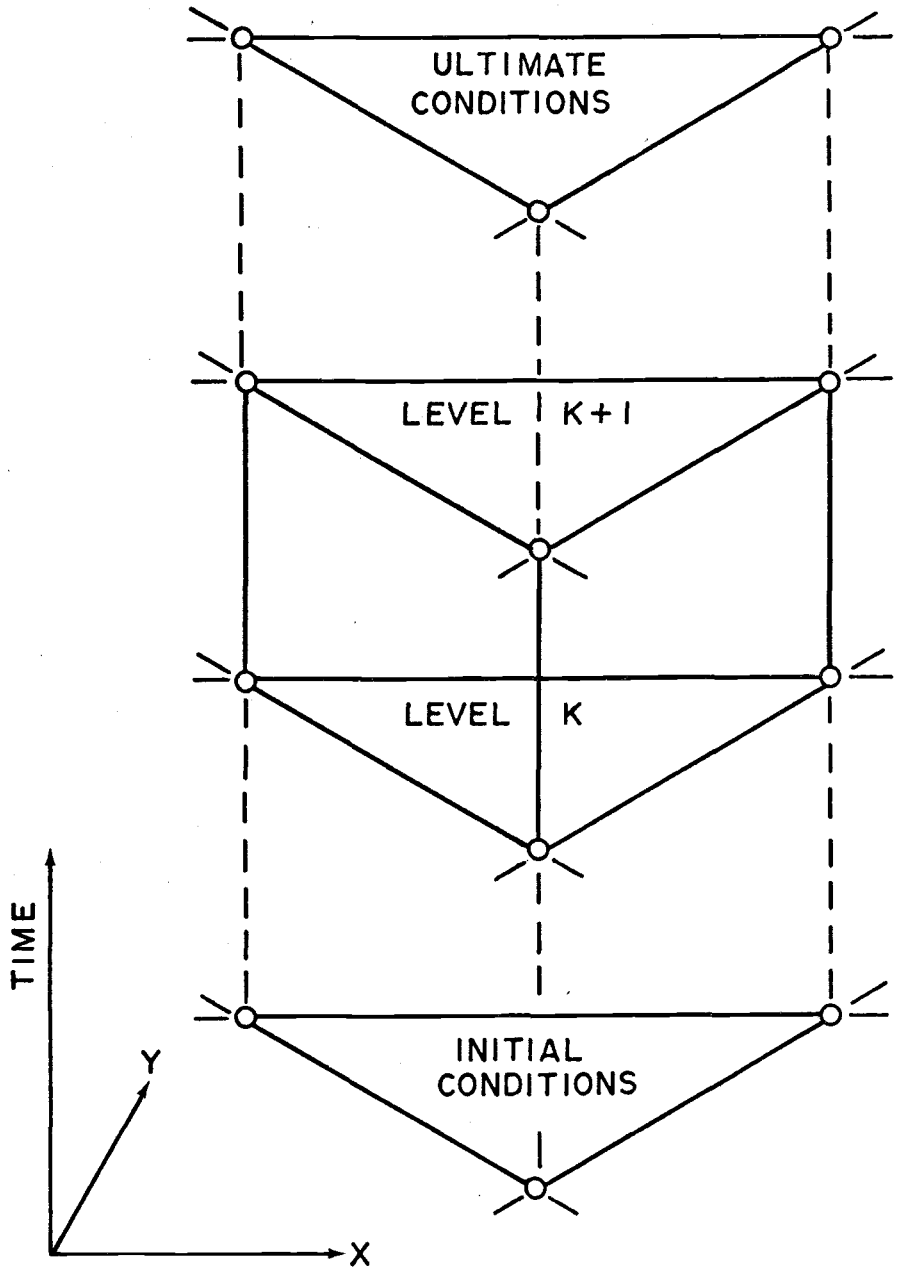

Figure 4.2. The finite element in time.

The temporal matrix [T] and source-sink vector {F} are determined as follows. Consider the integration of Eq. 4.4.11 and 4.4.12 for each element. Since, as pointed out by Zienkiewicz (1971)

$$\int_A L_1^a L_2^b L_3^c \, dxdy = \frac{a!\, b!\, c!}{(a+b+c+2)!} 2A, \tag{4.4.22}$$

the above integrals yield for each element

$$\{f\} = -\frac{AS}{3} \begin{bmatrix} 0 \\ 1 \\ 0 \\ 1 \\ 0 \\ 1 \end{bmatrix}, \tag{4.4.23}$$

and

$$[t] = \frac{A}{180} \begin{bmatrix} 6 & -1 & -1 & -4 & 0 & 0 \\ -1 & 6 & -1 & 0 & -4 & 0 \\ -1 & -1 & 6 & 0 & 0 & -4 \\ -4 & 0 & 0 & 32 & 16 & 16 \\ 0 & -4 & 0 & 16 & 32 & 16 \\ 0 & 0 & -4 & 16 & 16 & 32 \end{bmatrix}, \tag{4.4.24}$$

where the rows are ordered by corner nodes 1, 2, 3 and then by mid-side nodes, 4, 5, 6.

Equation 4.4.23 uses time-averaged values for source or sink effects, S. For the transient problem, the right-hand side of Eq. 4.4.21 contains the temporal element coefficient matrix and the right hand side contains the temporal element load vector.

4.5. Convergence and Stability of the Sedimentation Solution

Araithurai and Krone (1976) have demonstrated that the present model formulation will converge rapidly to the exact solutions for the one-dimensional, transient, heat conduction problem and for the steady-state one-dimensional advection-diffusion problem. For exact agreement in the steady-state case, a minimum of four quadratic spatial elements was necessary. These authors expressed concern that instabilities might result when Peclet numbers, uL/D, become either too large (improbable for the current study) or too small. For recirculating flows, the latter case may be of import as velocity decreases towards the basin

interior. Roundoff errors resulting from the subtractions of small numbers and their subsequent manipulation in iteratively solving the advection-dispersion equation may produce instabilities or, more likely, simply cause convergence to an answer having a greater absolute error than might otherwise be achieved. Since the advection-dispersion equation does not have a closed form solution, Araithurai and Krone (1976) compared computed and observed sediment accumulations in flume flows. Good agreement was noted and it was concluded that the model reasonably predicts sedimentation characteristics in steady, straight open-channel flows. It was suggested that the model would be similarly effective in two-dimensional, recirculating flows.

Leimkuhler, et al. (1975) in a finite element solution of the advection-dispersion problem for a point source in Massachusetts Bay found that instabilities may be generated if the minimum element grid size, ℓ, is not small enough for a given dispersion coefficient, D, and velocity, u. Their requirement for stability is

$$\frac{\ell u}{D} \gtrsim 2 \tag{4.5.1}$$

For cases which violated this requirement, the solution converged but unreal results, such as negative sediment concentration were realized. These authors noted that solution stability required:

$$\min \left[\Delta t \leq \frac{\ell^2}{10D} , \Delta t \leq \frac{\ell}{10u}\right] \tag{4.5.2}$$

To determine the stability of the Araithurai-Krone (1976) model as applied to recirculating flow conditions, the time step, Δt, was reduced until the convergence at each node occurred smoothly and any further decrease would not result in a significant improvement in convergence. A time step of one-half hour was optimal for a minimum element length of about 17 m and proved to be satisfactory for all other cases which had equal or longer elements. It was interesting to note that any attempt to change Δt during the computations resulted in oscillations in the solution which would slowly damp out. Such behavior required that a constant Δt be adopted.

4.6. The Rayleigh-Ritz Variational Method

The sediment advection-diffusion equation with any associated boundary conditions define the transport problem. When applied to a grid of nodes, a set of simultaneous equations results which may be solved by a number of techniques. An alternative way of posing this problem utilizes the calculus of variations (Zienkiewicz, 1971). The Euler theorem states that if the integral:

$$X(u) = \iiint_V f(x, y, z, \phi, \frac{\partial\phi}{\partial x}, \frac{\partial\phi}{\partial y}; \frac{\partial\phi}{\partial z}) \, dxdydz, \qquad (4.6.1)$$

is to be minimized over a rounded region V, then the necessary and sufficient condition for this minimum to be achieved is that the unknown function $\phi(x,y,z)$ satisfy the following differential equation

$$\frac{\partial}{\partial x}\left\{\frac{\partial f}{\partial(\partial\phi/\partial x)}\right\} + \frac{\partial}{\partial y}\left\{\frac{\partial f}{\partial(\partial\phi/\partial y)}\right\} + \frac{\partial}{\partial z}\left\{\frac{\partial f}{\partial(\partial\phi/\partial z)}\right\} - \frac{\partial f}{\partial\phi} = 0 \quad (4.6.2)$$

The advection-diffusion equation is nonself-adjoint and hence, does not have a corresponding variational functional. It may however, be transformed to a symmetric form through the use of the reducing factor, e^{β}, where

$$\beta = \left(\frac{ux}{D_x} + \frac{vy}{D_y}\right) \qquad (4.6.3)$$

The variational functional may then be formulated as the integral over all element subdomains of (Prakash, 1977):

$$\phi = \iint_{D_{ne}} \exp(\beta)\left[\frac{D_x}{y}\left(\frac{\partial c}{\partial x}\right)^2 + \frac{D_y}{y}\left(\frac{\partial c}{\partial y}\right)^2 - c\left(S - \frac{\partial c}{\partial t}\right)\right] dxdy \quad (4.6.4)$$

Introducing the shape functions, Eq. 4.3.1 and 4.3.2, and minimizing the functional, ϕ, with respect to nodal concentrations, c_i, over the element subdomain gives

$$\left[\frac{\partial\phi}{\partial c_i}\right]^m = \iint_{D_{ne}}\Bigg[D_x\left(\frac{\partial N_i}{\partial x}c_i + \frac{\partial N_J}{\partial x}c_J + \ldots\right)\frac{\partial N_i}{\partial x} + D_y\left(\frac{\partial N_i}{\partial y}c_i + \frac{\partial N_J}{\partial y}c_J + \ldots\right)\cdot\frac{\partial N_i}{\partial y} - \left\{S - \left(N_i\frac{\partial c_i}{\partial t} + N_J\frac{\partial c_J}{\partial t} + \ldots\right)\right\} N_i\Bigg] e^{\beta}\, dxdy \qquad (4.6.5)$$

Or:

$$\{\frac{\partial \phi}{\partial c}\}^m = [T]\{\frac{\partial c}{\partial t}\}^m + [K]\ \{c\}^m + \{F\}^m = 0 \qquad (4.6.6)$$

where

$$T_{iJ} = \iint_{D_{ne}} N_J N_i\ e^{\beta}\ dxdy\ , \qquad (4.6.7)$$

$$K_{iJ} = \iint_{D_{ne}} (D_x \frac{\partial N_i}{\partial x} \frac{\partial N_J}{\partial x} + D_y \frac{\partial N_i}{\partial y} \frac{\partial N_J}{\partial y})\ e^{\beta}\ dxdy\ , \qquad (4.6.8)$$

$$F_i = \iint_{D_{ne}} N_i \{S\}\ e^{\beta}\ dxdy\ , \qquad (4.6.9)$$

where

i,J... = element nodal numbers,

and m = element number.

Evaluating the above integrals and assembling all of the elemental matrices yields the system equation:

$$[TL]\ \{\frac{\partial c}{\partial t}\} + [KL]\{c\} + [F] = 0. \qquad (4.6.10)$$

With this formulation the matrices [T], [K], [TL], and [KL] are symmetric. On the other hand, Eq. 4.4.7 when assembled in the system equation does not yield symmetric matrices.

The use of the variational approach could greatly reduce computer storage requirements and computation time in comparison to adopting the Galerkin method. One limitation of the variational approach to nonself-adjoint problems is that significant computer round-off errors may occur for high Peclet number flows. The Peclet number, uL/D, indicates the relative importance of advection and dispersion, but also occurs in the reducing factor, Eq. 4.6.3. Remotely-located nodes may have a Peclet number of sufficient magnitude to cause computer overflow due to the e^{β} factor in Eq. 4.6.4, and 4.6.7 to 4.6.9. If local velocity and the dispersion coefficient are related, as for example in Eq. 3.5.4, 3.5.5, etc., then velocity changes in the numerator should be partially compensated for by changes in the denominator. Thus, only nodes at extreme distances from the origin could experience

exponential round-off errors. Hence, the Rayleigh-Ritz formulation would appear to be an attractive alternative to the Galerkin method used in this study.

4.7 Summary

In this chapter, the finite-element method for the solution of boundary-value problems was introduced and one variant, the Galerkin method of weighted residuals, was discussed in detail. The Galerkin formulation and solution of the two-dimensional, horizontal, sediment-transport equation was presented in detail following Araithurai (1974). An alternative and potentially more efficient formulation employing the Rayleigh-Ritz method was also presented for future reference.

V. RESULTS AND RECOMMENDATIONS

Chapter I introduced the fundamental considerations regarding circulation and sedimentation in a rectangular basin joined to a waterway and a number of case studies were designated to illustrate the functional dependence of those processes on basin geometry and environmental parameters. Chapters II, III, and IV discussed in detail the numerical solution techniques employed in this study. This chapter presents the computational results and gives some recommendations regarding their use in the marina design process. Finally, suggestions are made regarding the extension of the work presented herein.

5.1 Velocity Field

Streamer plots of the velocity field for each case of Section 1.3 (see Table 1-1 and Figure 1.5) are displayed in Figures 5.1 to 5.21 with streamlines of relative velocity, $\sqrt{u^2+v^2}/u_o$. The proportion of basin area contained within each streamline is presented in Figures 5.22 and 5.25. Horizontal velocity profiles on transects parallel to the coordinate axes and passing approximately through the center of the primary circulation gyre are shown in Figures 5.26 to 5.29. In some of Figures 5.26 to 5.29, curves for the upstream entrance cases have been omitted since the velocity fields for corresponding upstream and downstream entrance cases are essentially negative mirror images which differ in magnitude by less than one percent, downstream entrance cases having the higher values. As in Abbott (1977), this difference is attributed to the opposition of basin velocity and momentum dispersion processes acting across the upstream entrance boundary in contrast to their superposition for downstream entrances.

Interior velocities are functions of entrance velocity and basin configuration. For a given basin configuration, experience has shown that the normalized velocity fields, u/u_o, v/v_o, and $\sqrt{u^2+v^2}/u_o$, are independent of u_o for the range of velocities considered. Hence, Figures 5.1 to 5.30 apply not only to cases with equal basin Reynolds

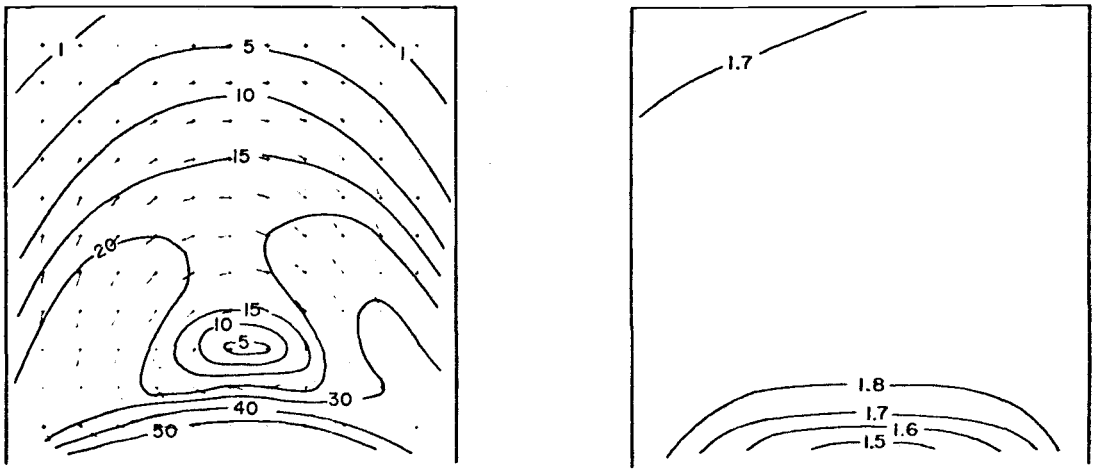

(A) (B)

Figure 5.1. Case 02X4. (A). Velocity field. Isopleths indicate the local velocity in percent of the entrance velocity, u_o. (B). Sedimentation rate field. Isopleths give the non-dimensional sedimentation rate $(S/u_oC_o)\times10^7$.

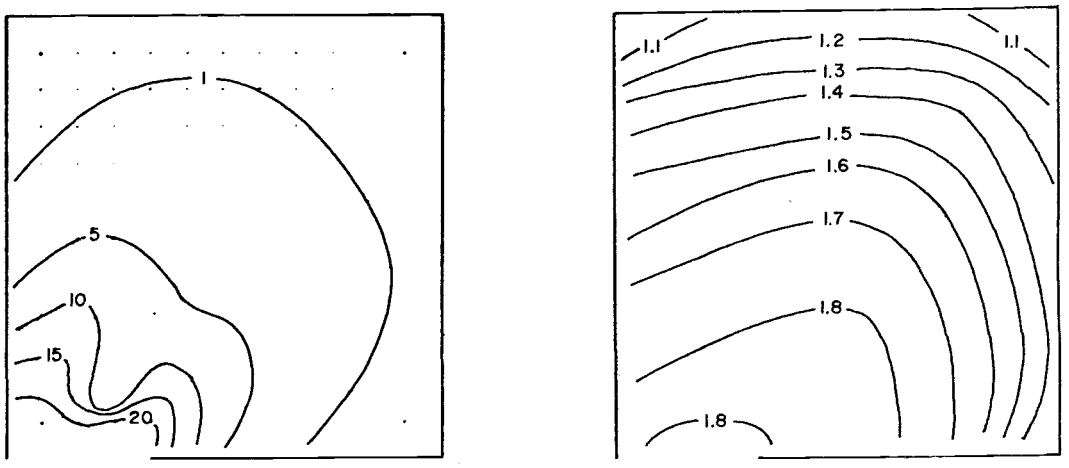

(A) (B)

Figure 5.2. Case U2X2. (A). Velocity field. Isopleths indicate the local velocity in percent of the entrance velocity, u_o. (B). Sedimentation rate field. Isopleths give the non-dimensional sedimentation rate $(S/u_oC_o)\times10^7$.

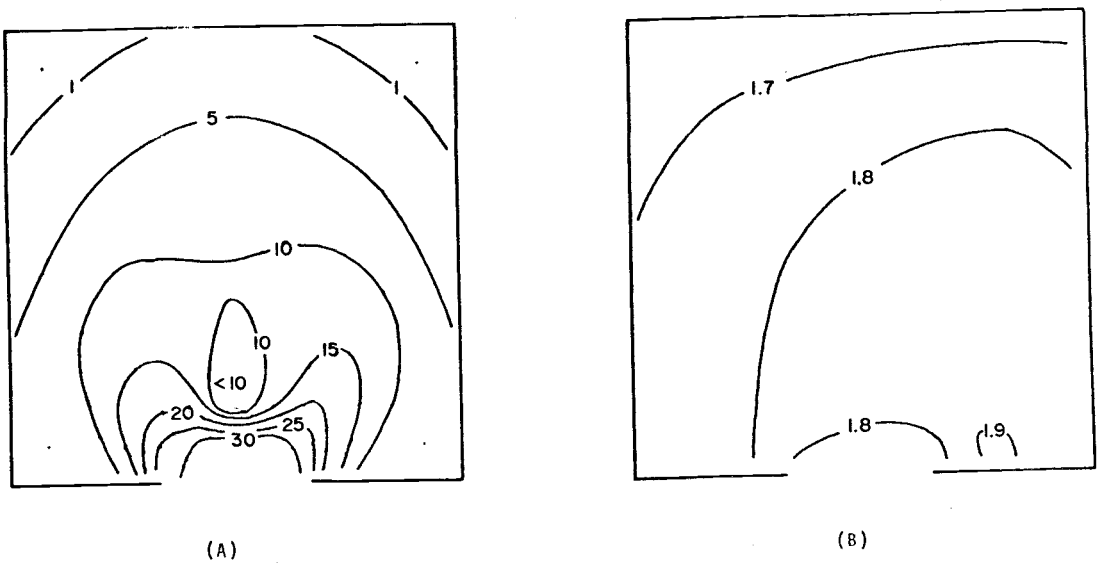

Figure 5.3. Case C2X2. (A). Velocity field. Isopleths indicate the local velocity in percent of the entrance velocity, u_0. (B). Sedimentation rate field. Isopleths give the non-dimensional sedimentation rate $(S/u_0C_0)\times10^7$.

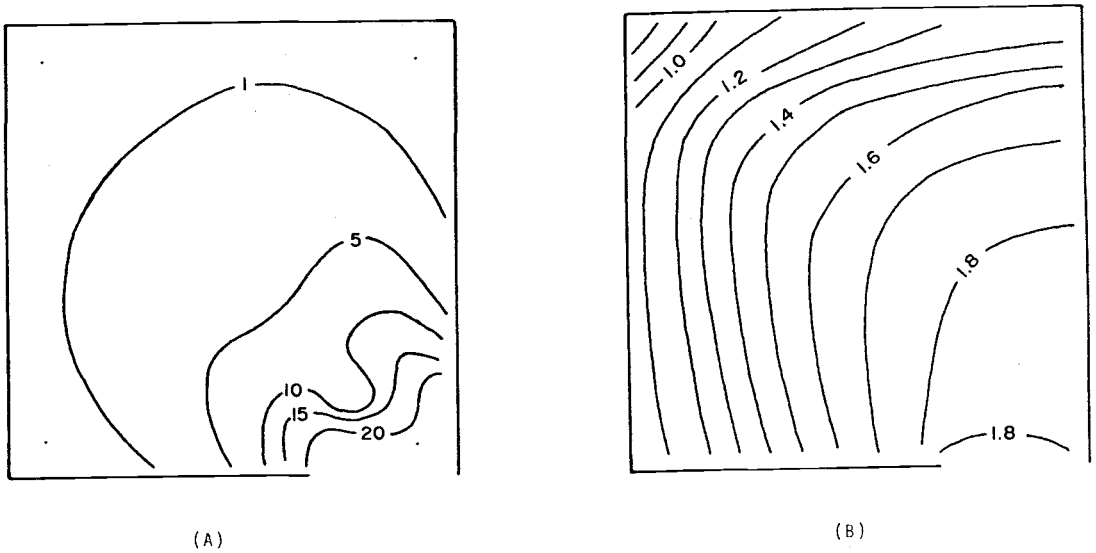

Figure 5.4. Case D2X2. (A). Velocity field. Isopleths indicate the local velocity in percent of the entrance velocity, u_0. (B). Sedimentation rate field. Isopleths give the non-dimensional sedimentation rate $(S/u_0C_0)\times10^7$.

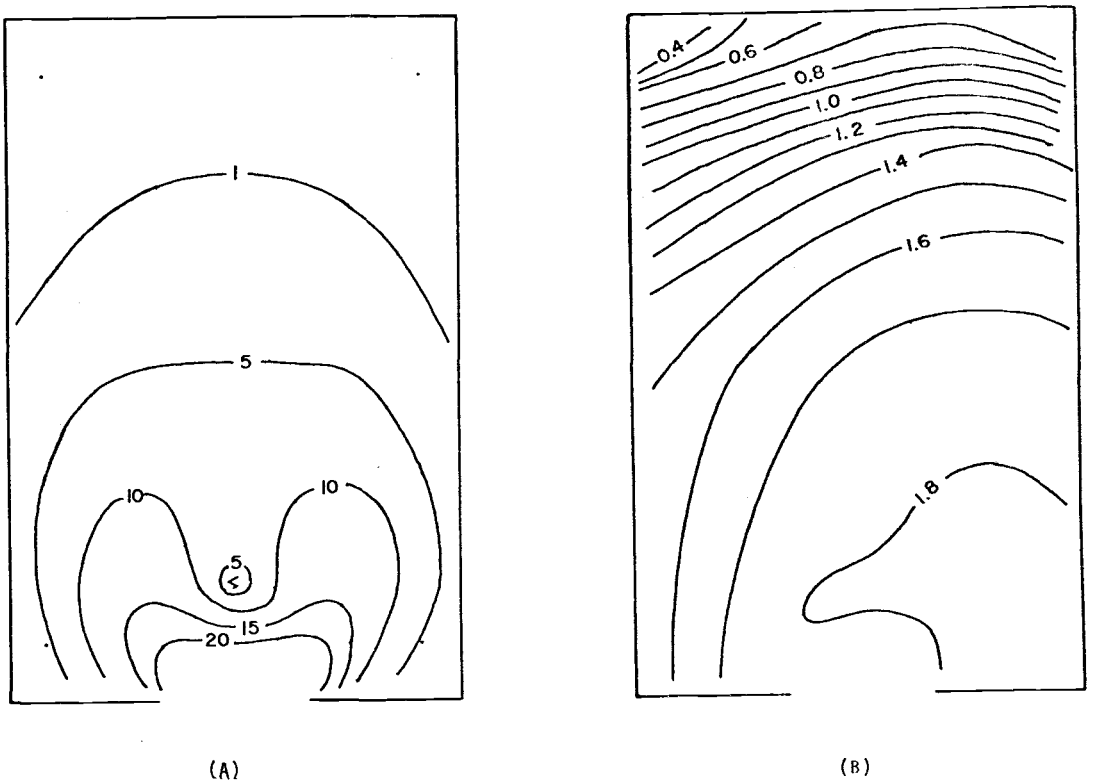

Figure 5.5. Case C2X3. (A). Velocity field. Isopleths indicate the local velocity in percent of the entrance velocity, u_o. (B). Sedimentation rate field. Isopleths give the non-dimensional sedimentation rate $(S/u_oC_o)x10^7$.

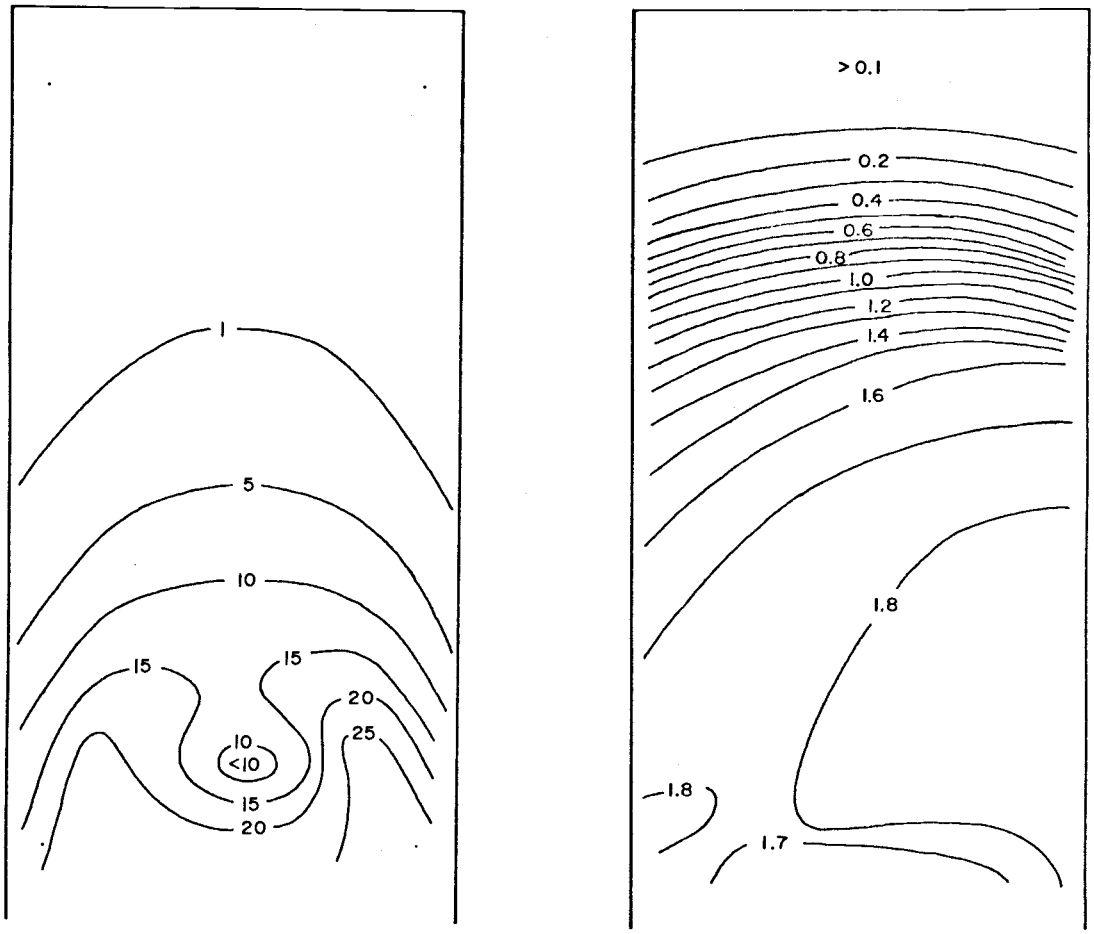

Figure 5.6. Case 02X4. (A). Velocity field. Isopleths indicate the local velocity in percent of the entrance velocity, u_o. (B). Sedimentation rate field. Isopleths give the non-dimensional sedimentation rate $(S/u_oC_o)x10^7$.

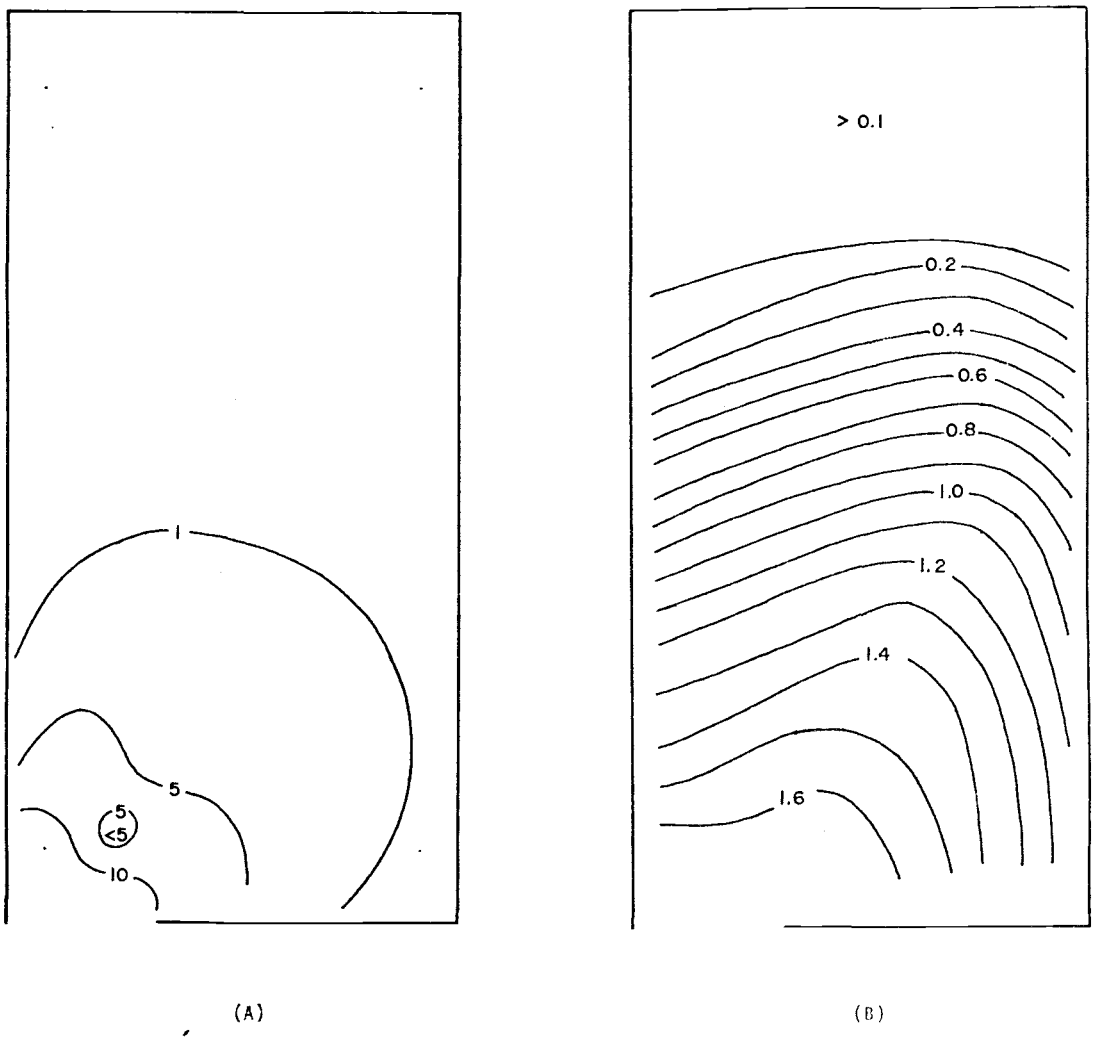

Figure 5.7. Case U2X4. (A). Velocity field. Isopleths indicate the local velocity in percent of the entrance velocity, u_o. (B). Sedimentation rate field. Isopleths give the non-dimensional sedimentation rate $(S/u_o C_o)x10^7$.

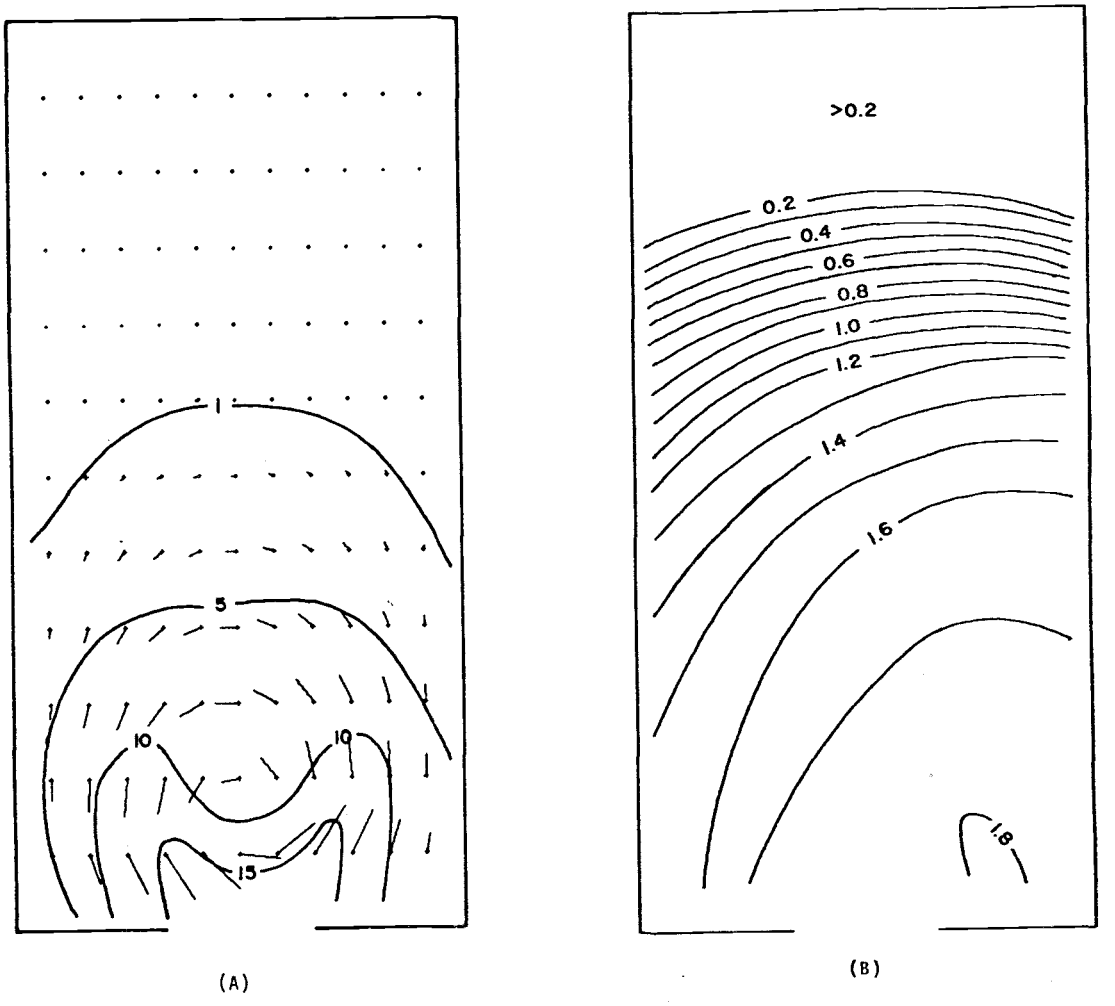

Figure 5.8. Case C2X4. (A). Velocity field. Isopleths indicate the local velocity in percent of the entrance velocity, u_o. (B). Sedimentation rate field. Isopleths give the non-dimensional sedimentation rate $(S/u_oC_o)x10^7$.

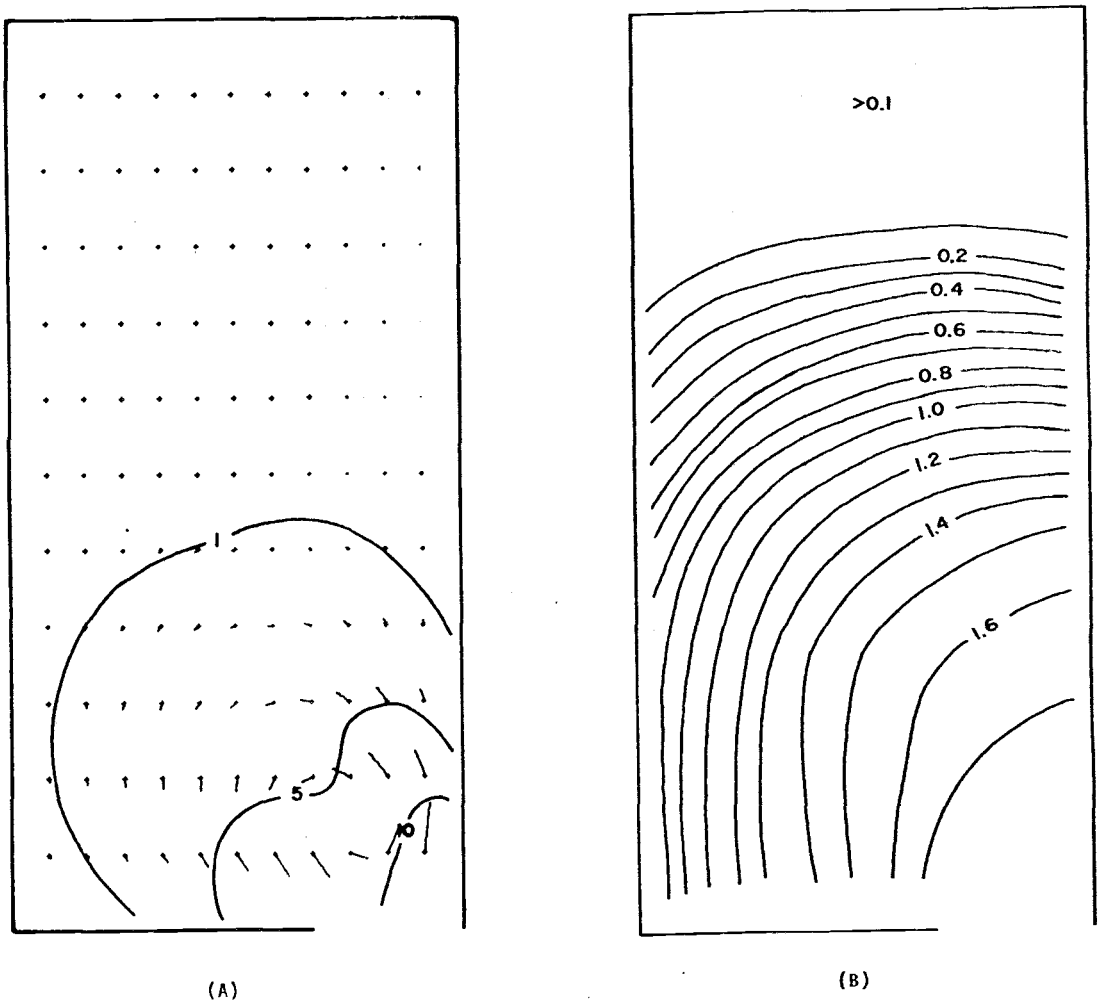

Figure 5.9. Case D2X4. (A). Velocity field. Isopleths indicate tne local velocity in percent of the entrance velocity, u_o. (B). Sedimentation rate field. Isopleths give the non-dimensional sedimentation rate $(S/u_oC_o)x10^7$.

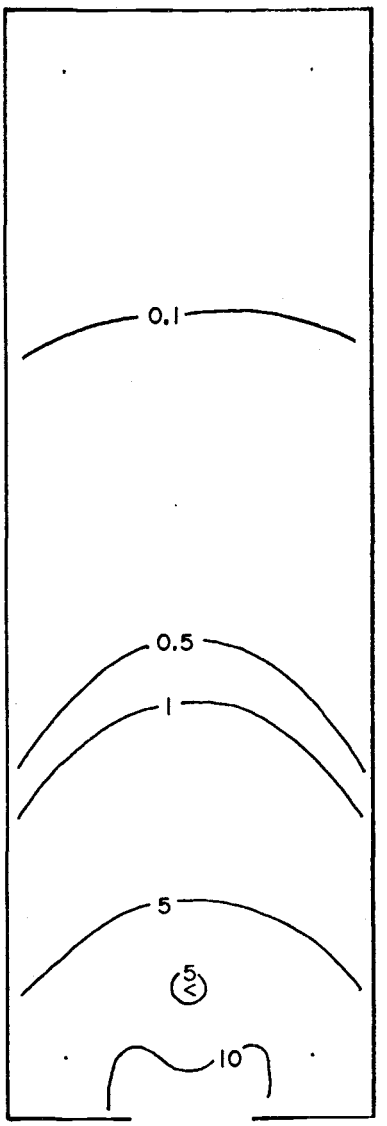

Figure 5.10. Case C2X6. (A). Velocity field. Isopleths indicate the local velocity in percent of the entrance velocity, u_0. (B). Sedimentation rate field. Isopleths give the non-dimensional sedimentation rate $(S/u_0C_0)x10^7$.

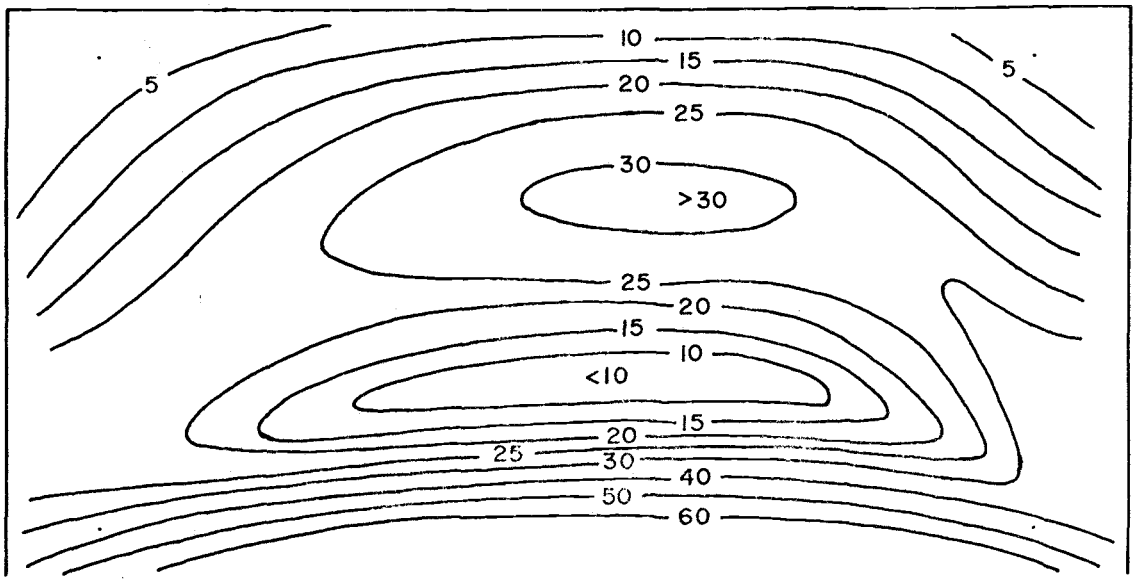

(A)

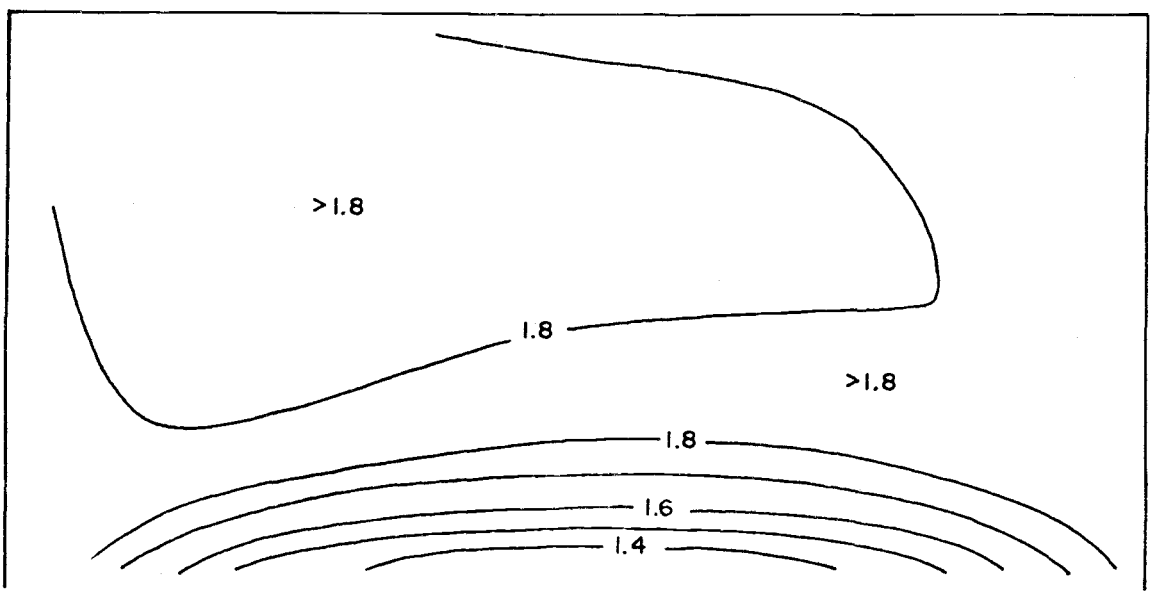

(B)

Figure 5.11. Case 04X2. (A). Velocity field. Isopleths give the local velocity in percent of the entrance velocity, u_0. (B). Sedimentation rate field. Isopleths give the non-dimensional sedimentation rate $(S/u_0C_0)\times10^7$.

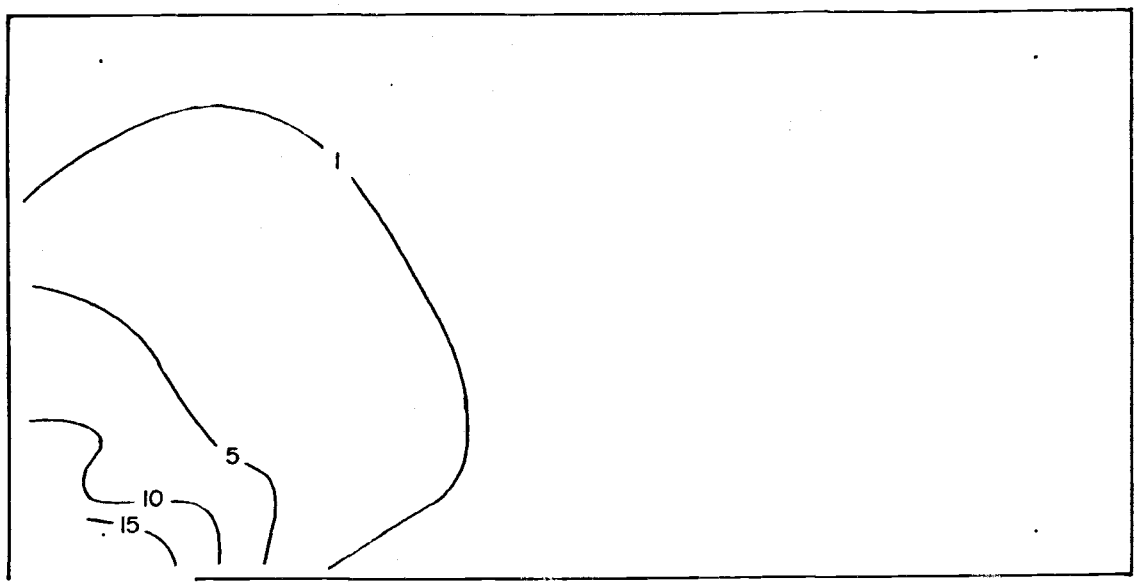

(A)

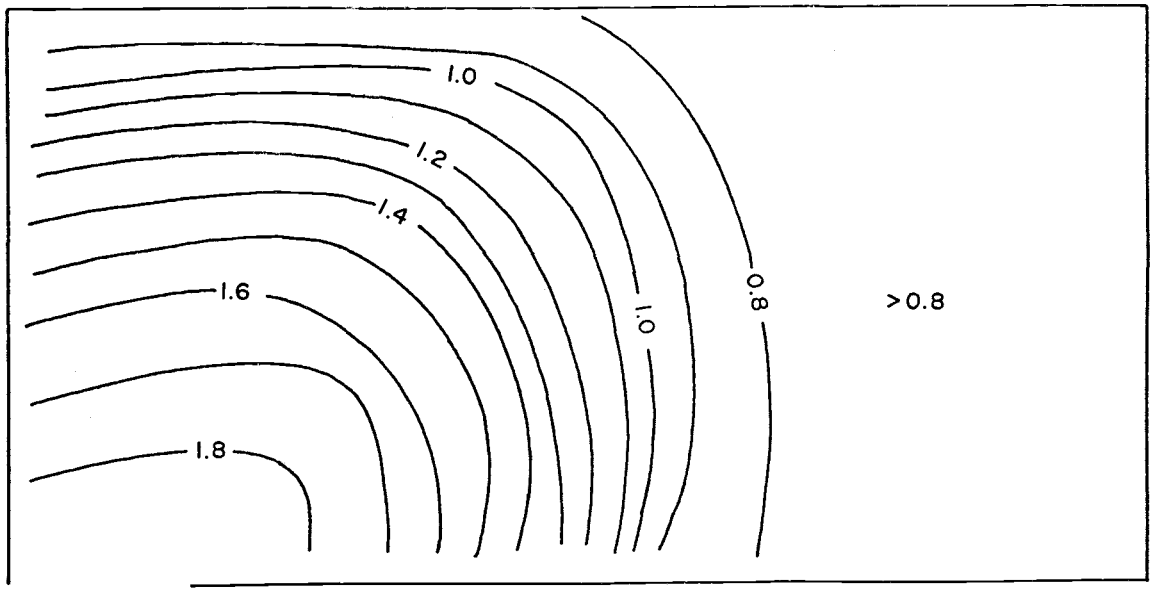

(B)

Figure 5.12. Case U4X2. (A). Velocity field. Isopleths give the local velocity in percent of the entrance velocity, u_o. (B). Sedimentation rate field. Isopleths give the non-dimensional sedimentation rate $(S/u_oC_o)x10^7$.

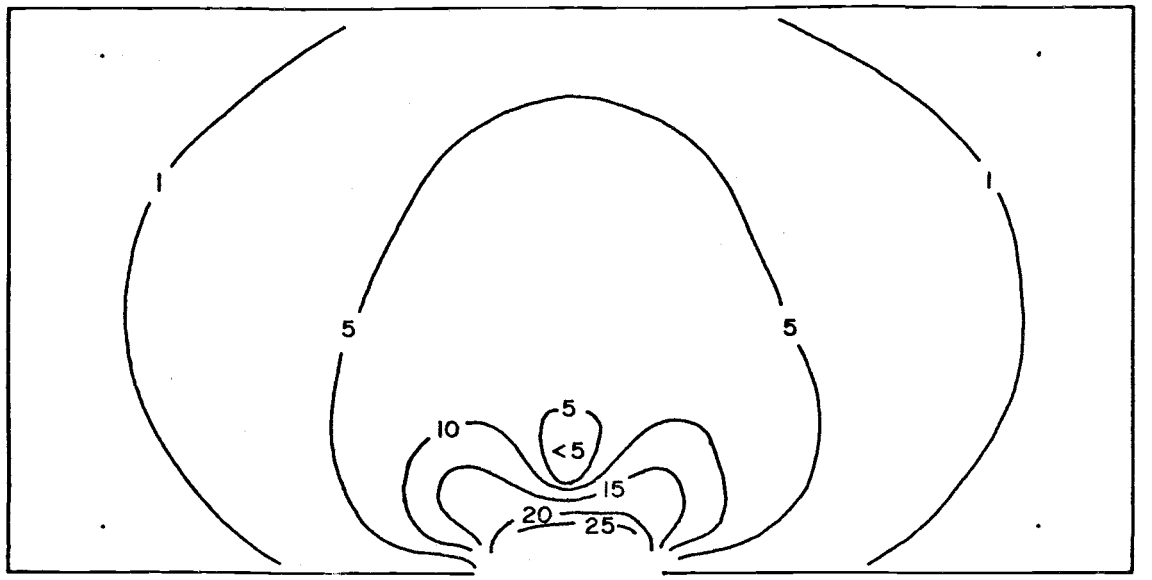

(A)

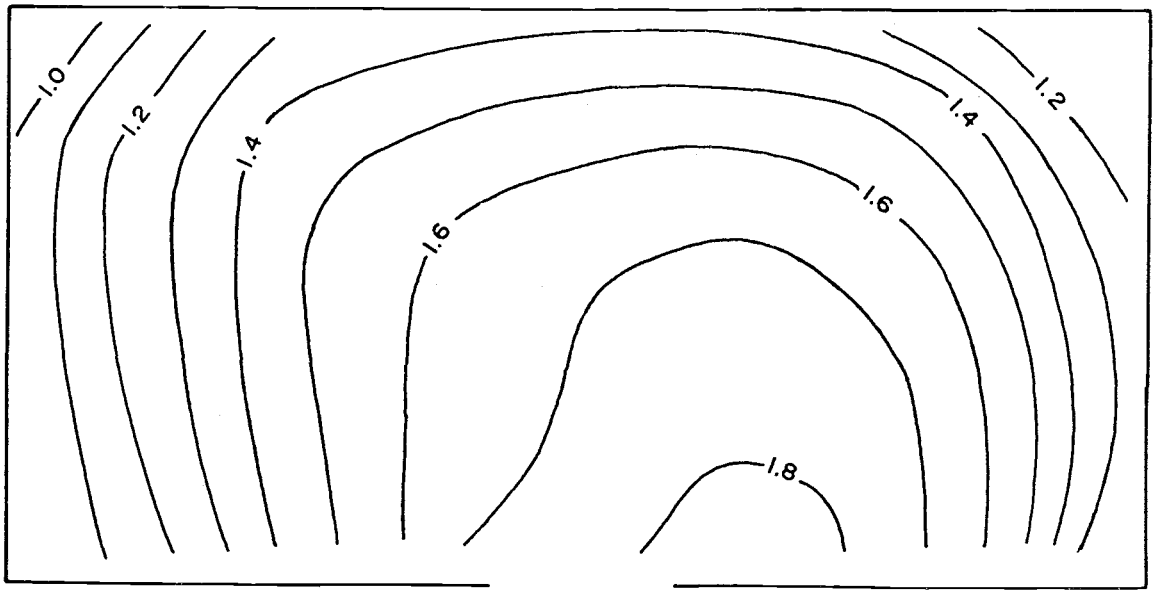

(B)

Figure 5.13. Case C4X2. (A). Velocity field. Isopleths give the local velocity in percent of the entrance velocity, u_o. (B). Sedimentation rate field. Isopleths give the non-dimensional sedimentation rate $(S/u_oC_o)x10^7$.

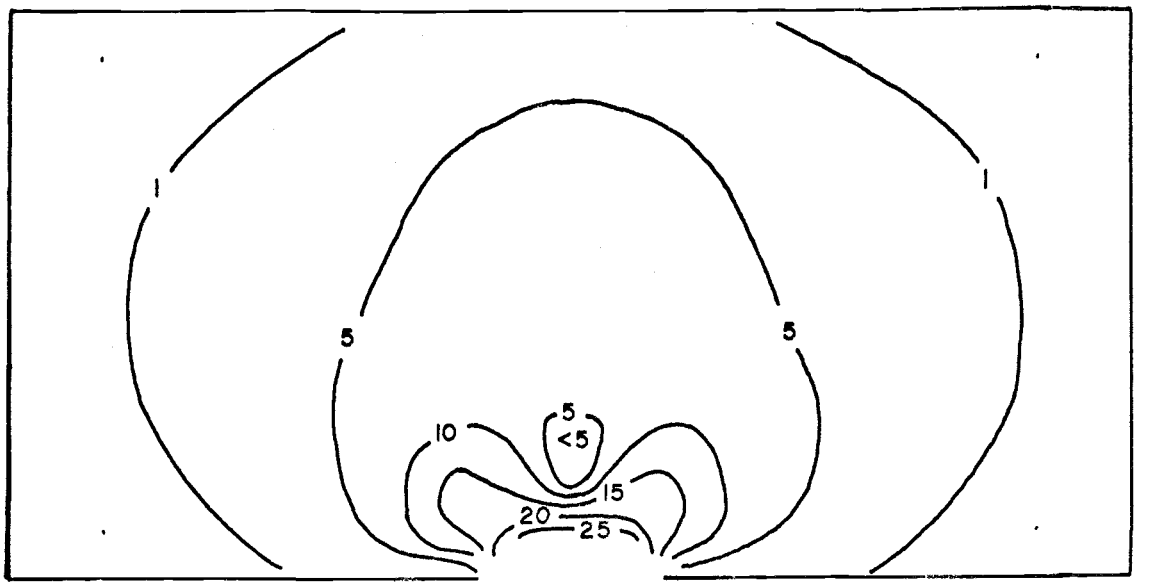

(A)

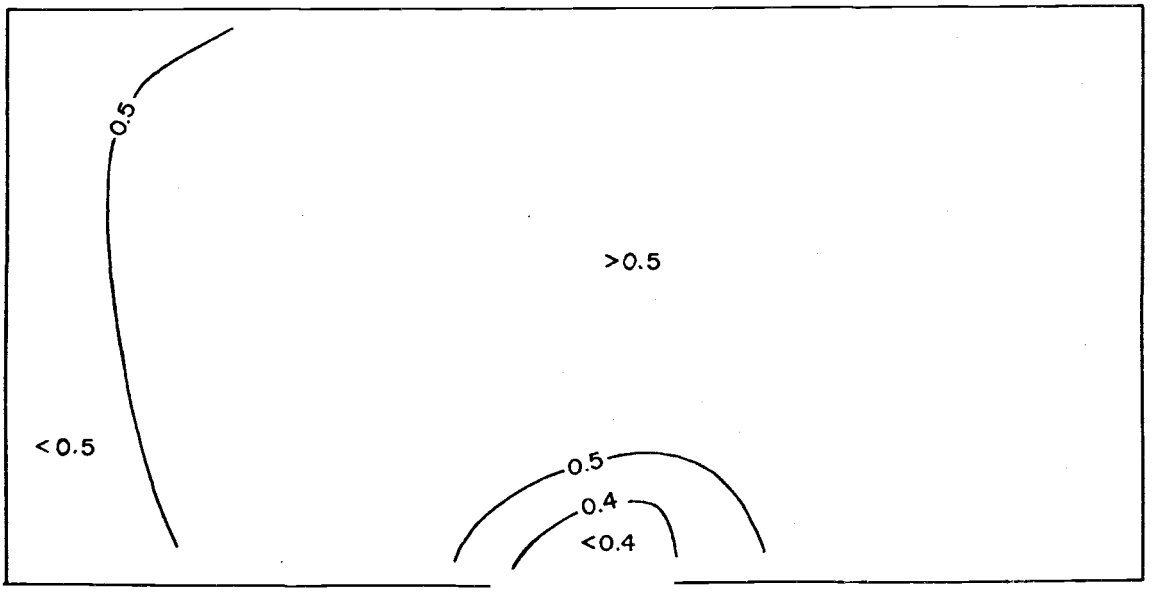

(B)

Figure 5.14. Case C4X2V50. (A). Velocity field. Isopleths give the local velocity in percent of the entrance velocity, u_o. (B). Sedimentation rate field. Isopleths give the non-dimensional sedimentation rate $(S/u_oC_o)x10^7$.

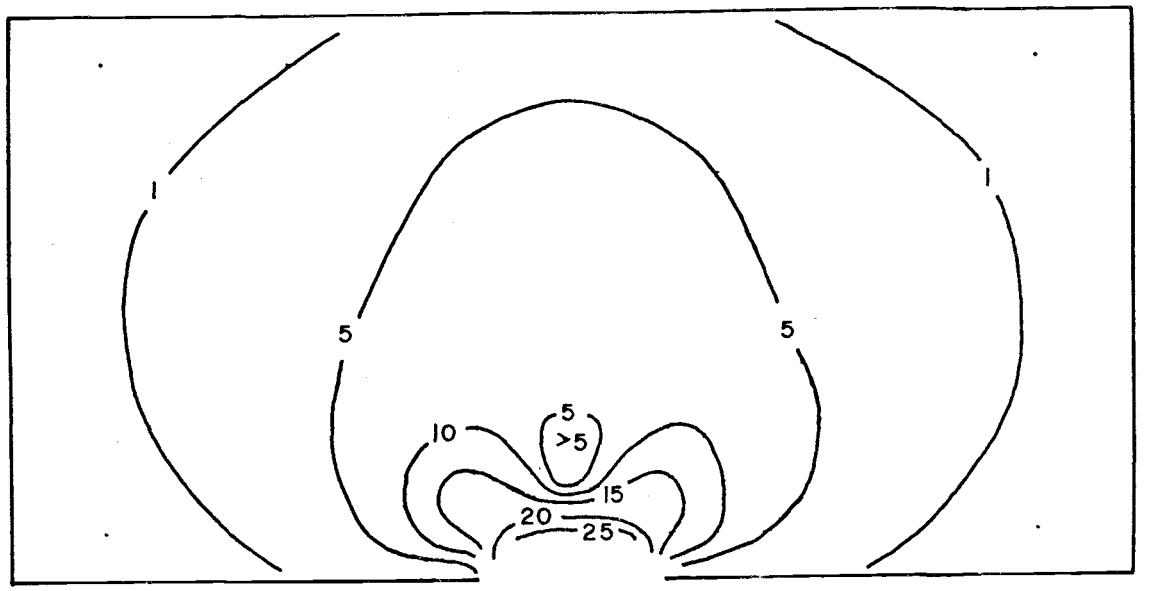

(A)

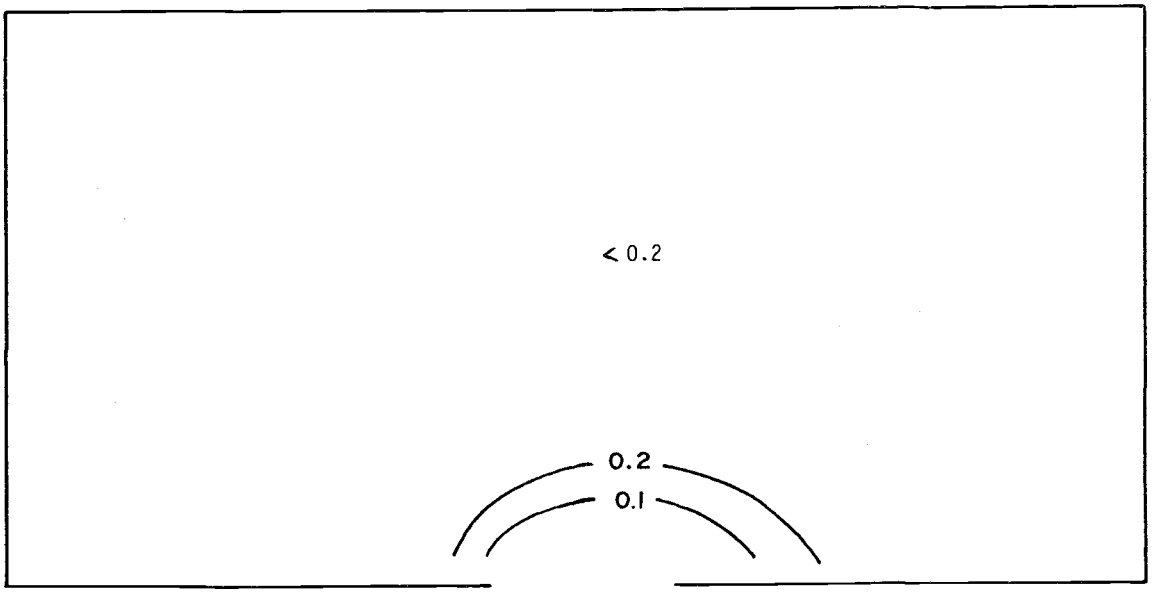

(B)

Figure 5.15. Case C4X2V100. (A). Velocity field. Isopleths give the local velocity in percent of the entrance velocity, u_0. (B). Sedimentation rate field. Isopleths give the non-dimensional sedimentation rates $(S/u_0C_0)\times10^7$.

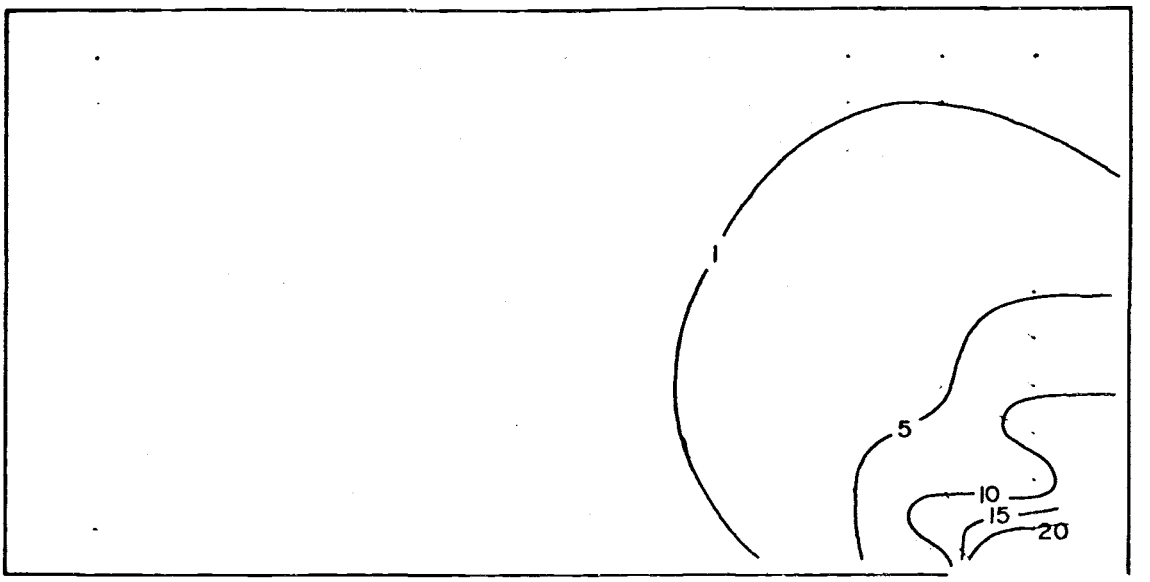

(A)

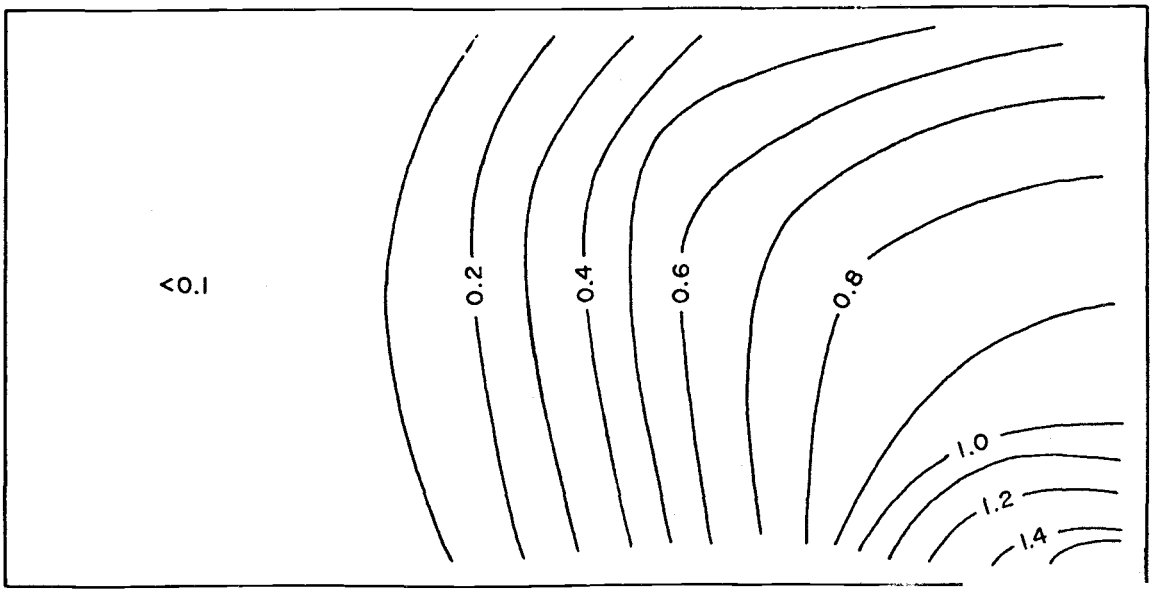

(B)

Figure 5.16. Case D4X2. (A). Velocity field. Isopleths give the local velocity in percent of the entrance velocity, u_o. (B). Sedimentation rate field. Isopleths give the non-dimensional sedimentation rates $(S/u_oC_o)\times10^7$.

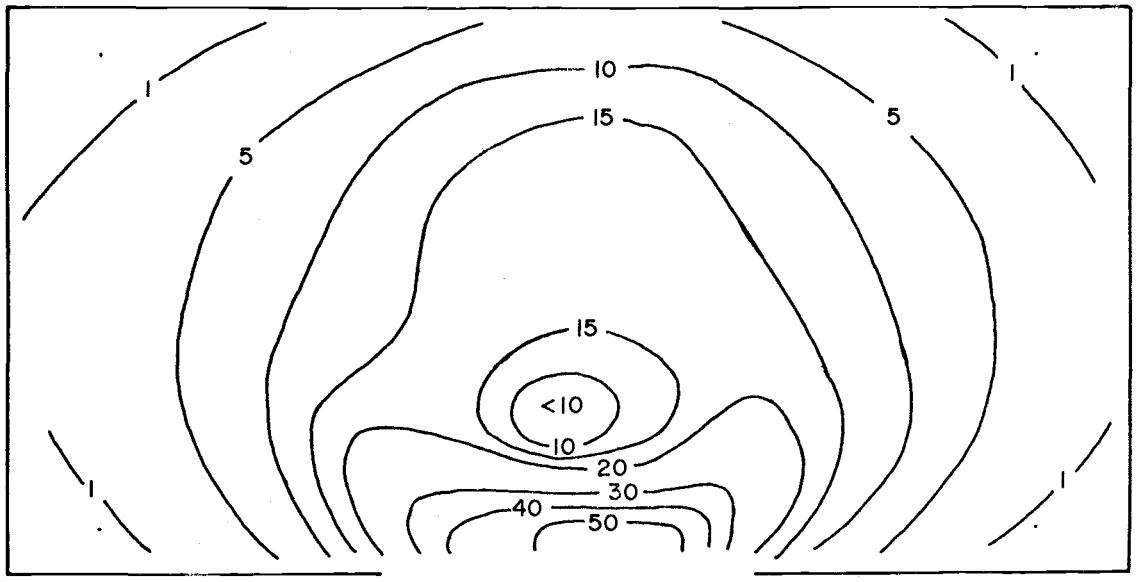

(A)

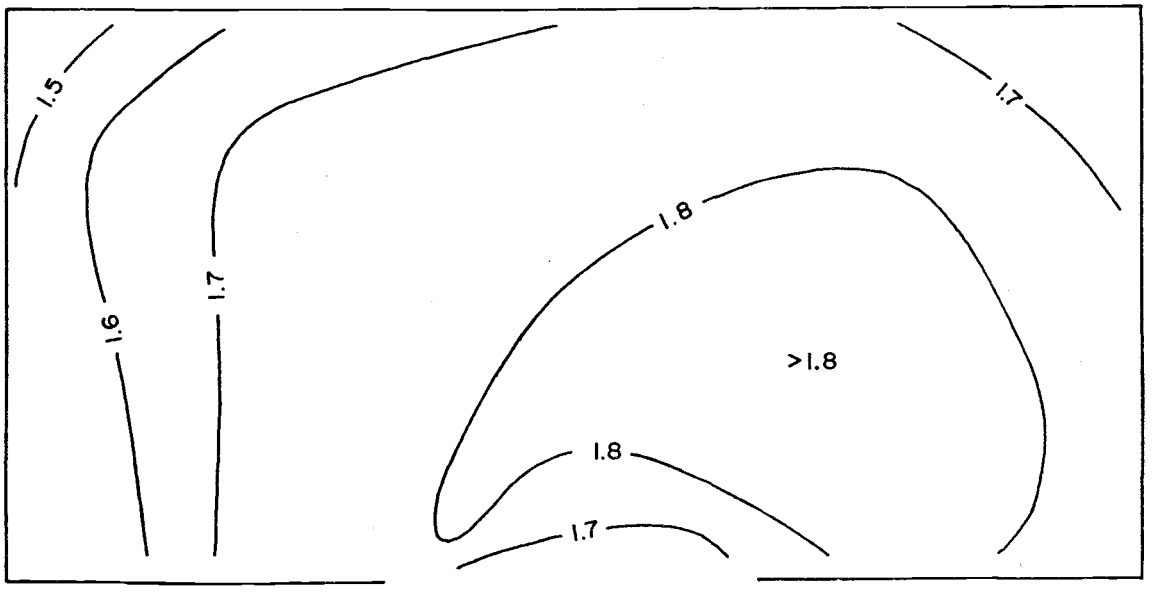

(B)

Figure 5.17. Case CE4X2. (A). Velocity field. Isopleths give the local velocity in percent of the entrance velocity, u_o. (B). Sedimentation rate field. Isopleths give the non-dimensional sedimentation rates $(S/u_oC_o)x10^7$.

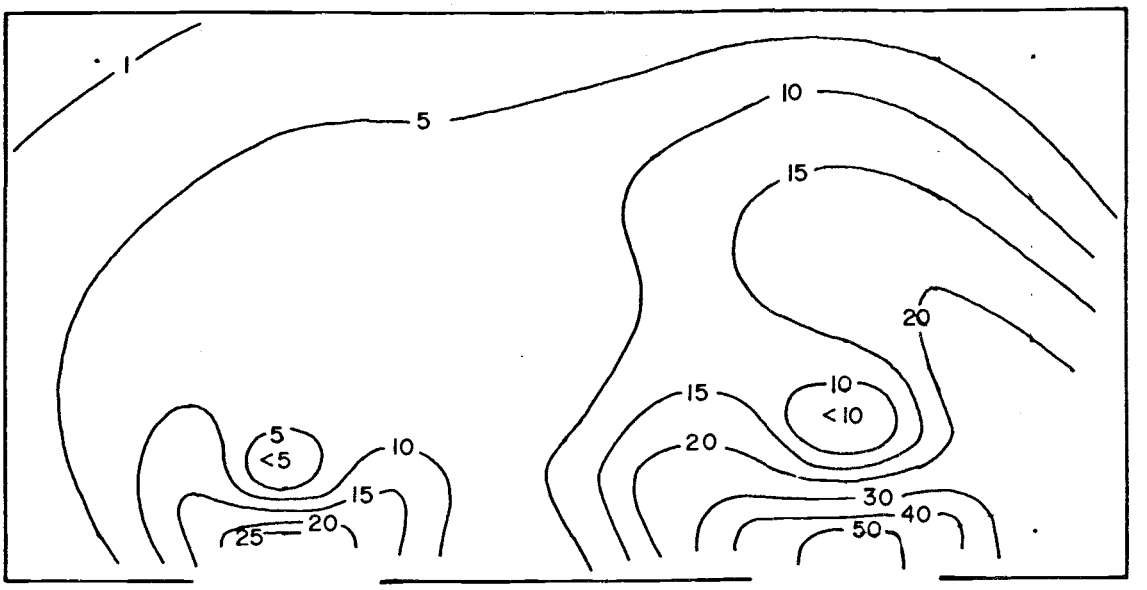

(A)

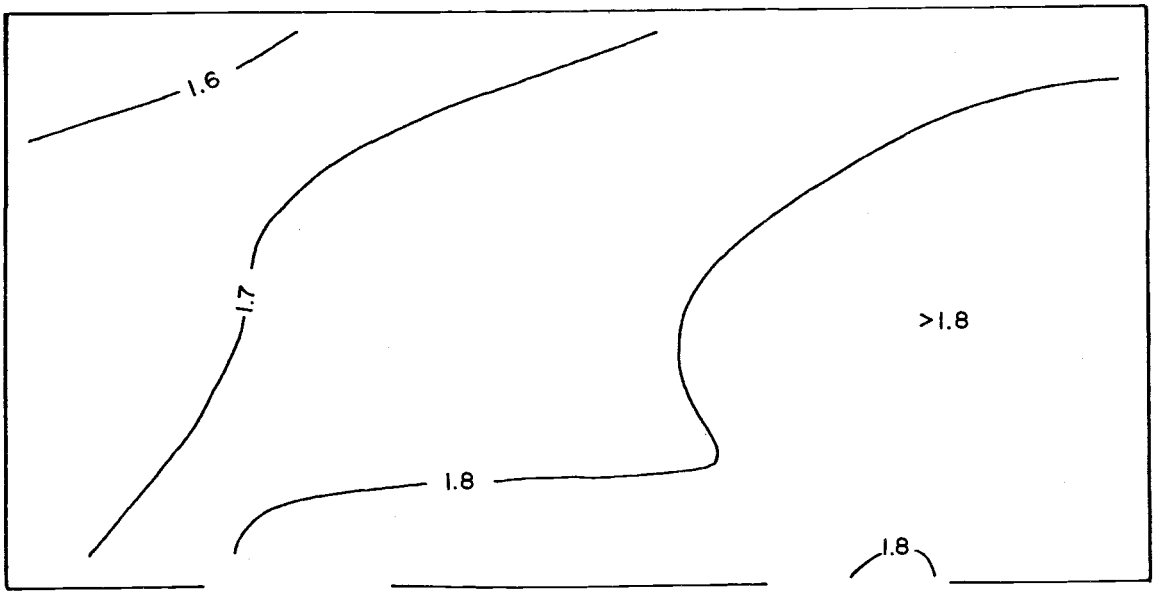

(B)

Figure 5.18. Case UD4X2. (A). Velocity field. Isopleths give the local velocity in percent of the entrance velocity, u_o. (B). Sedimentation rate field. Isopleths give the non-dimensional sedimentation rates $(S/u_oC_o)\times10^7$.

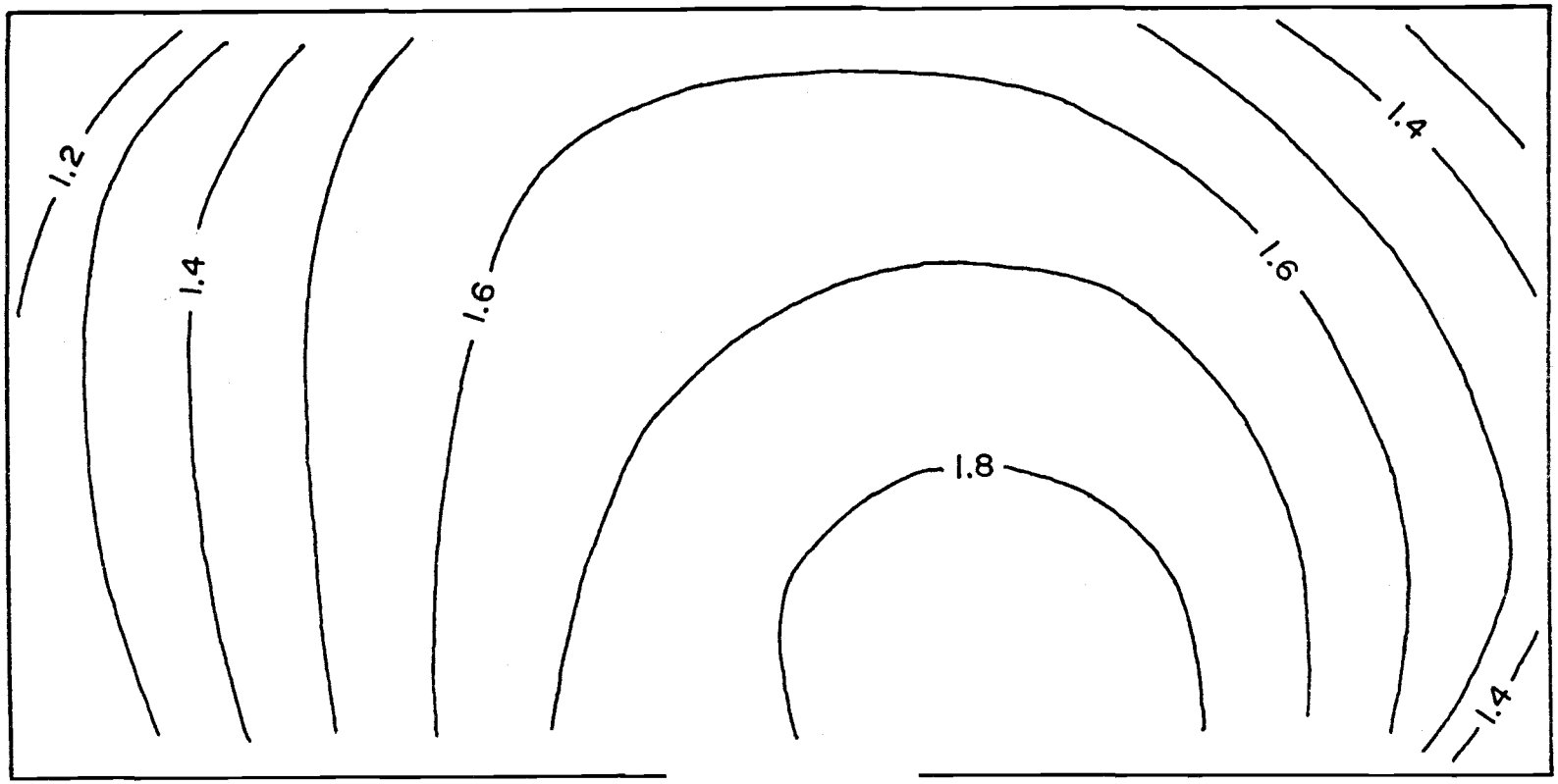

Figure 5.19. Case C4X2D100. Sedimentation rate field. Isopleths give the non-dimensional sedimentaiton rates $(S/u_oC_o)x10^7$.

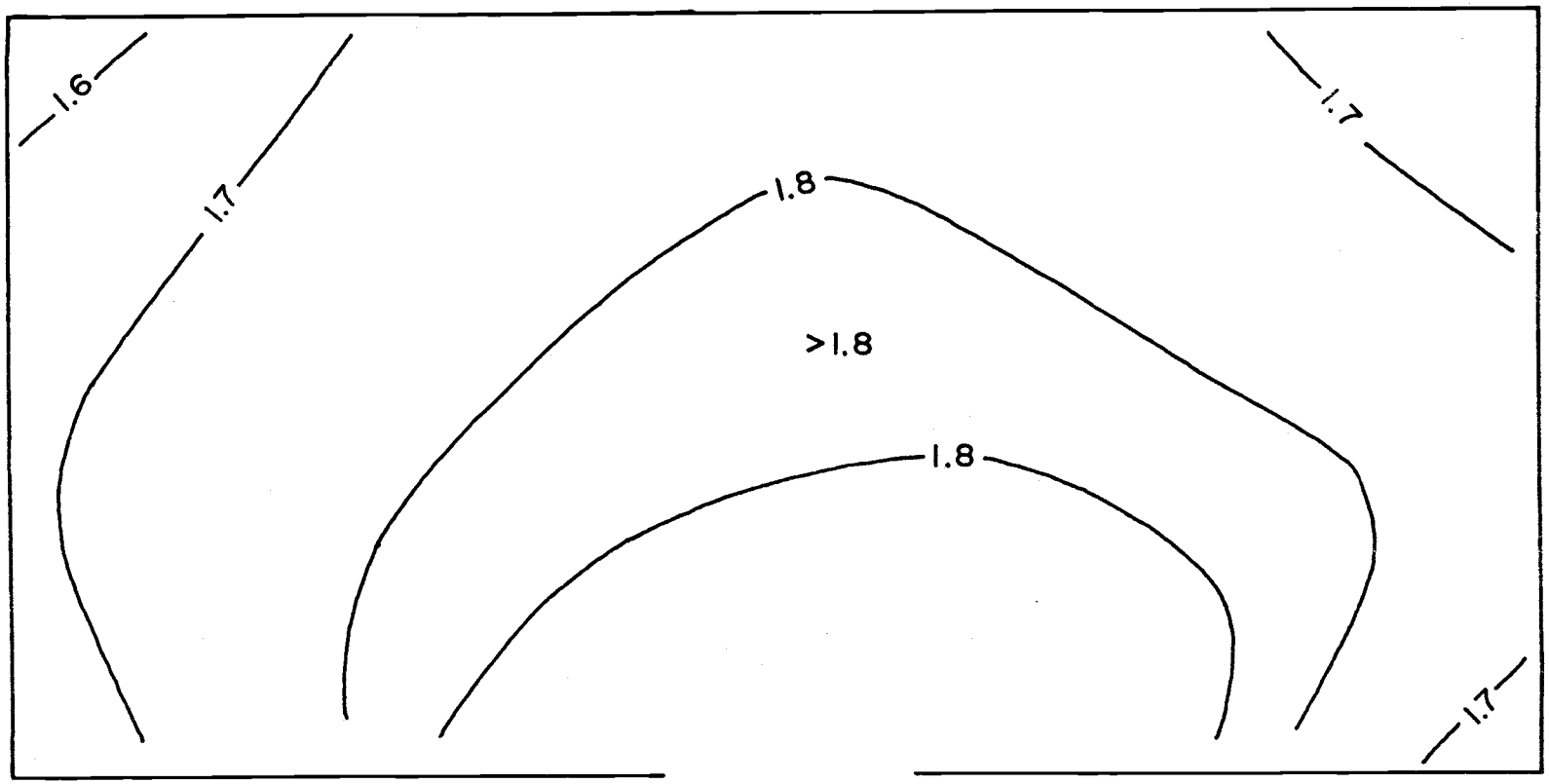

Figure 5.20. CAse C4X2D1000. Sedimentation rate field. Isopleths give the non-dimensional sedimentation rates $(S/u_oC_o)x10^7$.

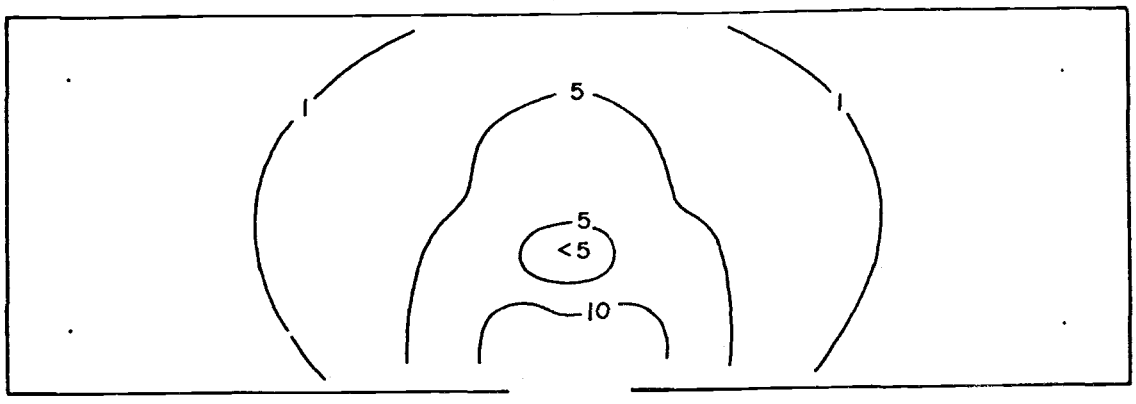

(A)

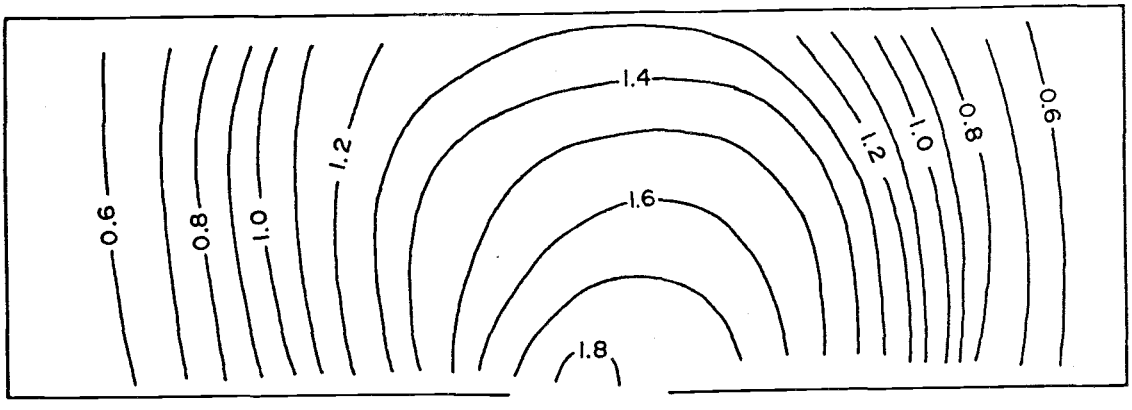

(B)

Figure 5.21. Case C6X2. (A). Velocity field. Isopleths give the local velocity in percent of the entrance velocity, u_o. (B). Sedimentation rate field. Isopleths give the non-dimensional sedimentation rates $(S/u_oC_o)\times10^7$.

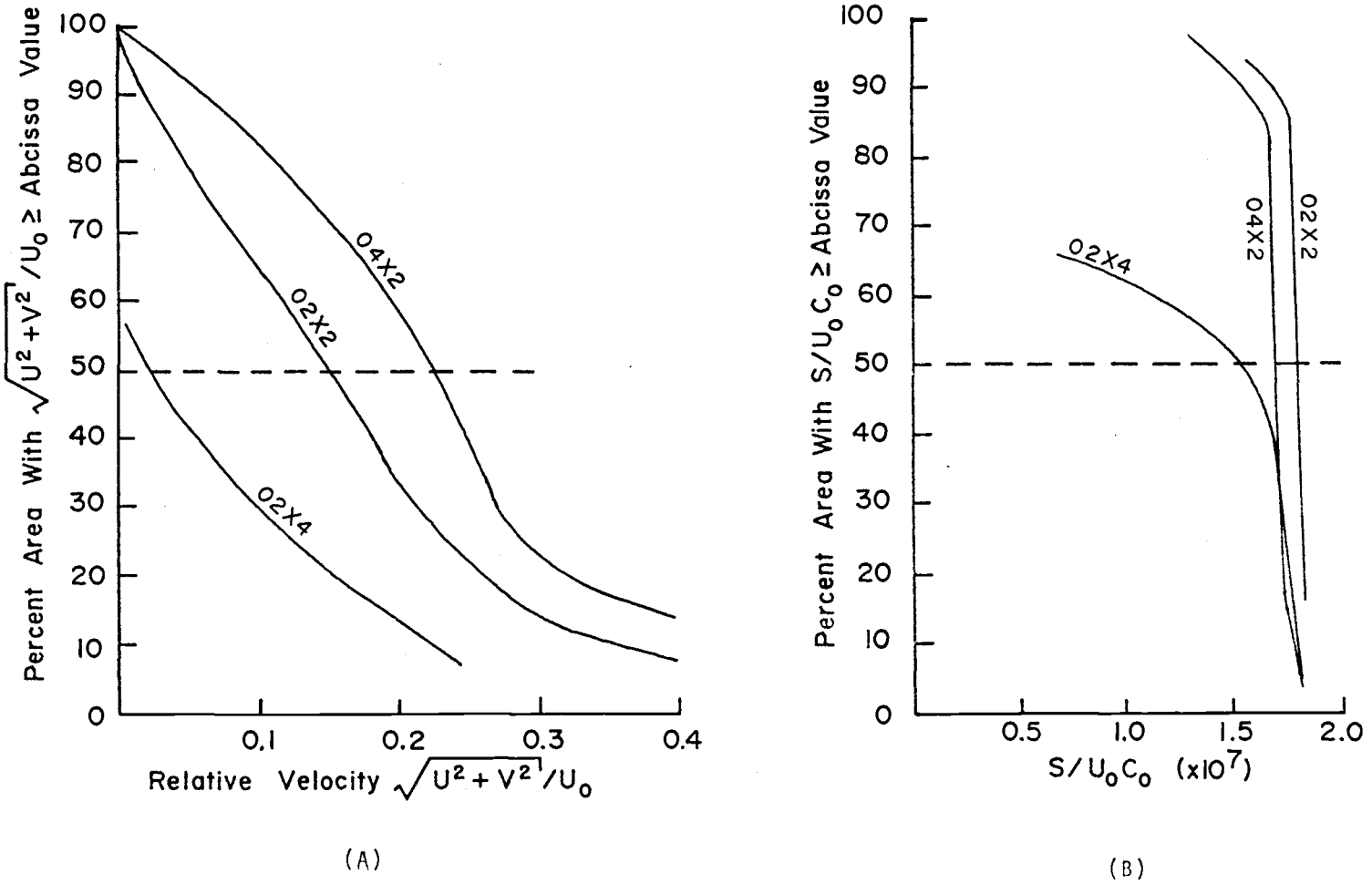

Figure 5.22. Percent of basin area having (A) relative velocities or (B) non-dimensionalized sedimentation rates greater than the value indicated on the abscissa. (For basins with an unconstricted entrance.)

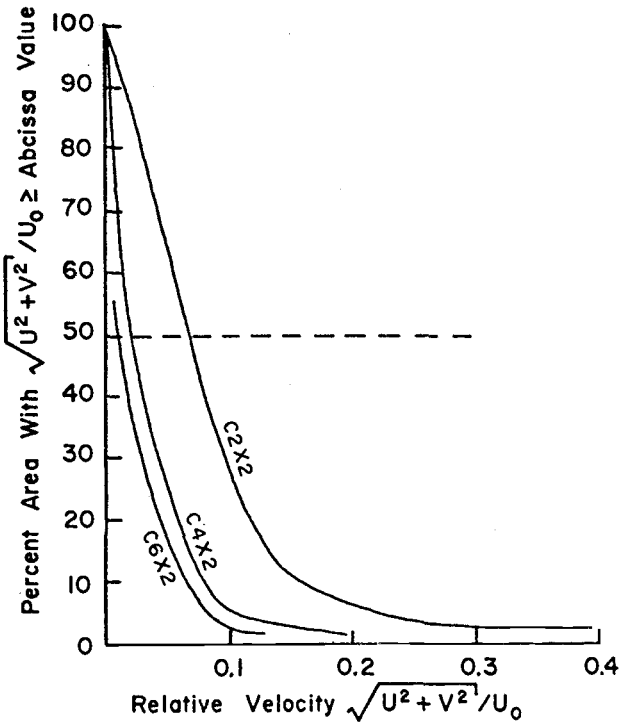

(A)

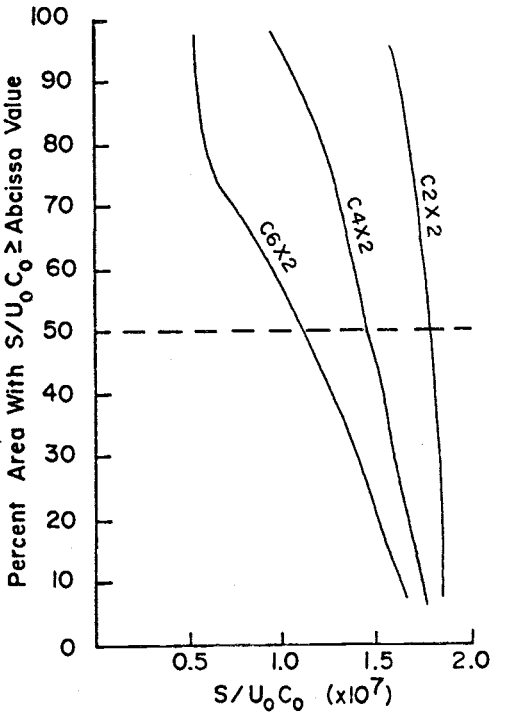

(B)

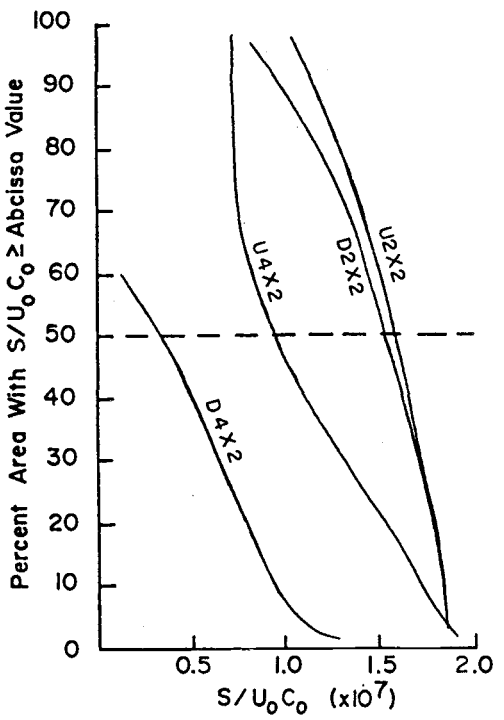

(C)

Figure 5.23. Effects of varying basin length on the percent of basin area with (A) relative velocities or (B and C) non-dimensionalized sedimentation rates greater than the value indicated on the abscissa. (For basins with constricted entrances).

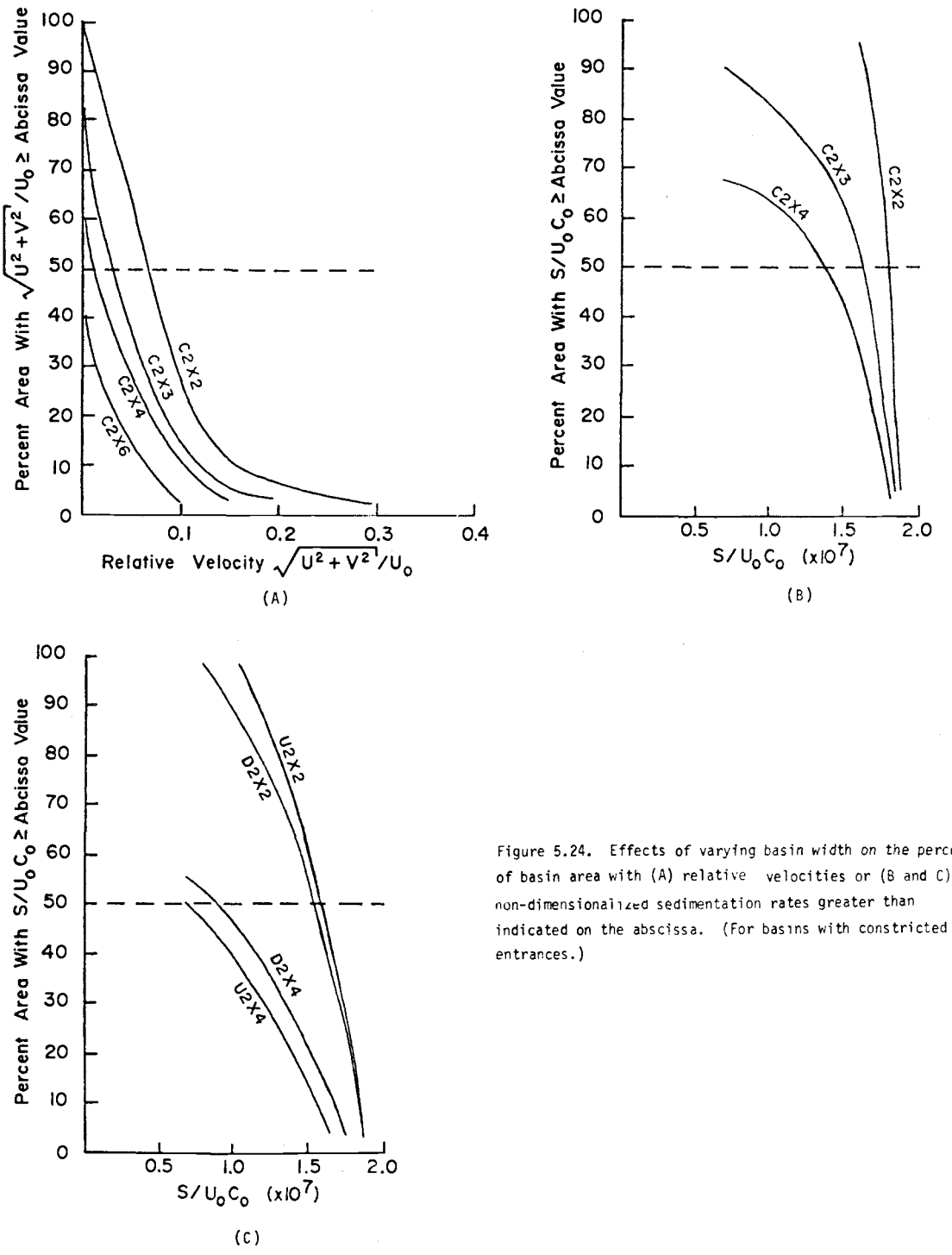

Figure 5.24. Effects of varying basin width on the percent of basin area with (A) relative velocities or (B and C) non-dimensionalized sedimentation rates greater than indicated on the abscissa. (For basins with constricted entrances.)

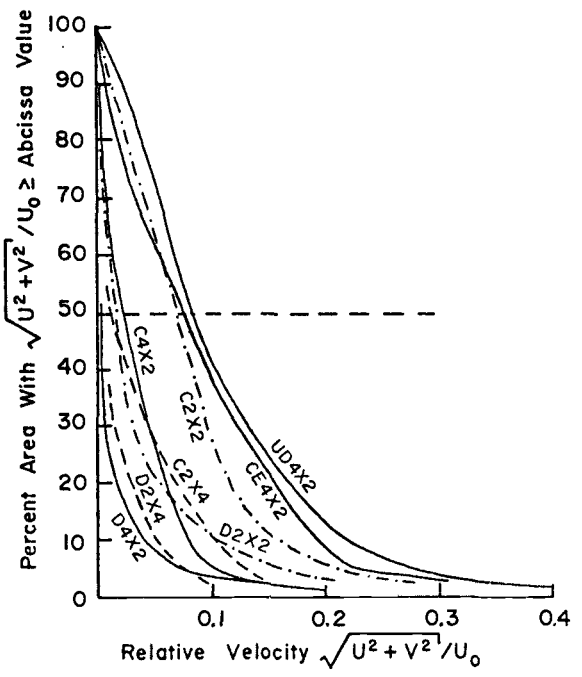

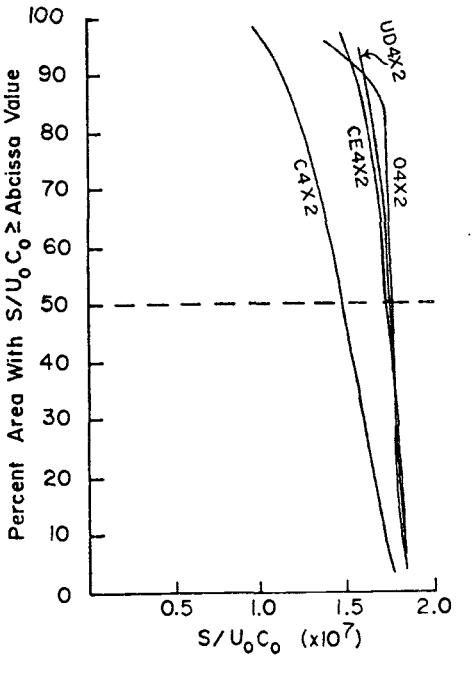

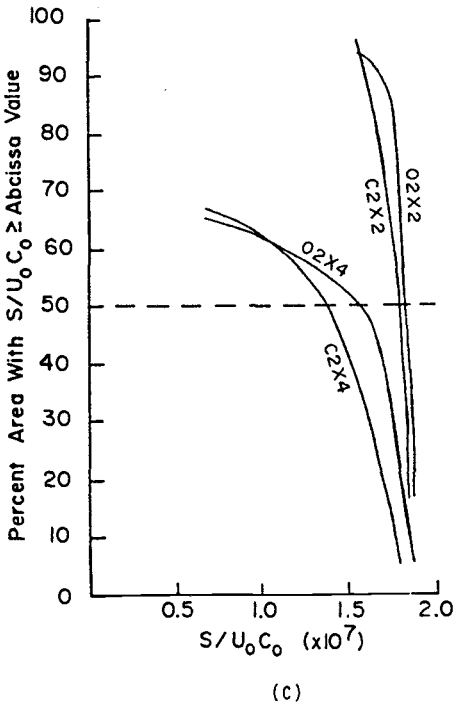

Figure 5.25. Effects of varying entrance width or location on the percent of basin area with (A) relative velocities or (B and C) non-dimensional sedimentation rates greater than indicated on the abscissa.

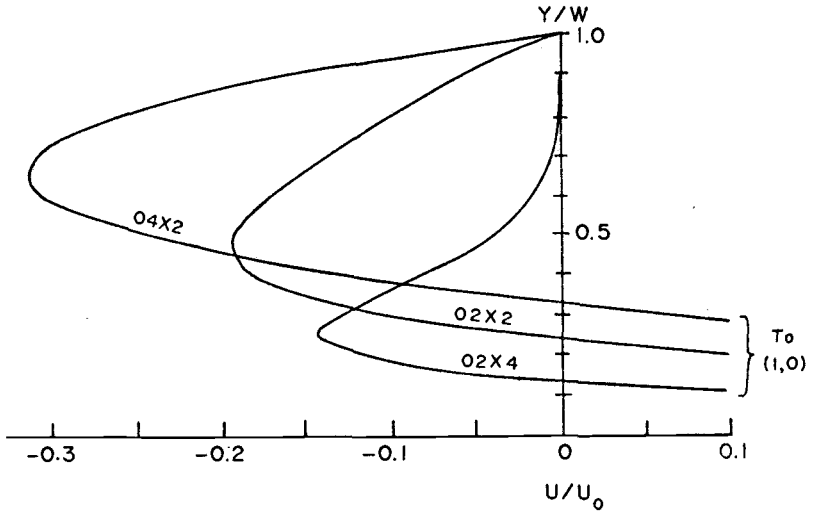

(A)

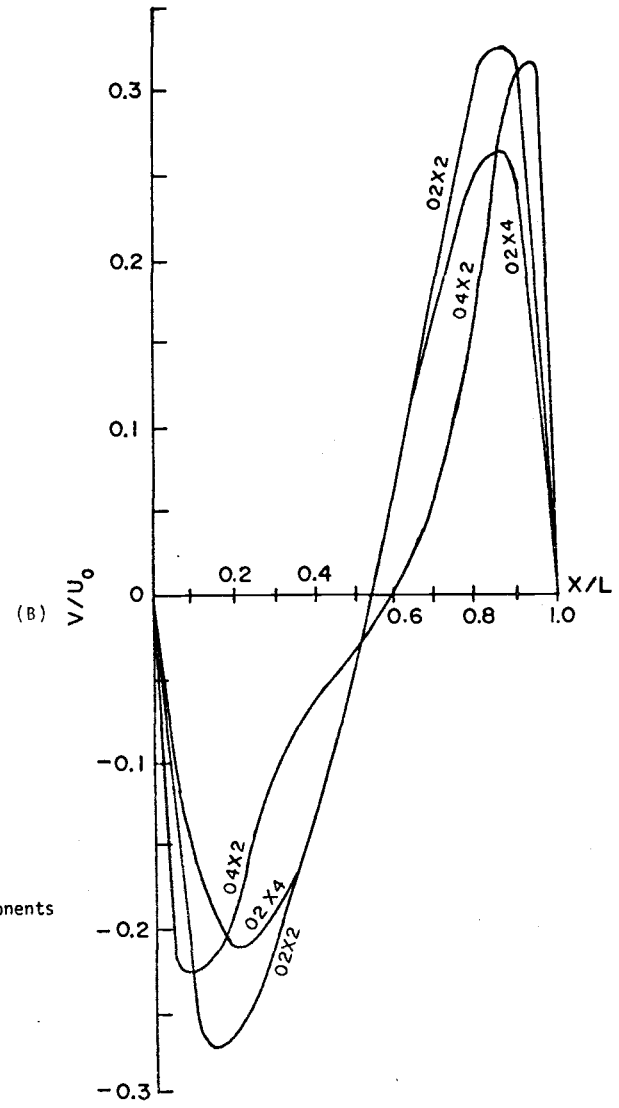

(B)

Figure 5.26. Effects of varying basin length and width on the relative velocity components (A) u/u_0 and (B) v/u_0. (For unconstricted entrance cases.)

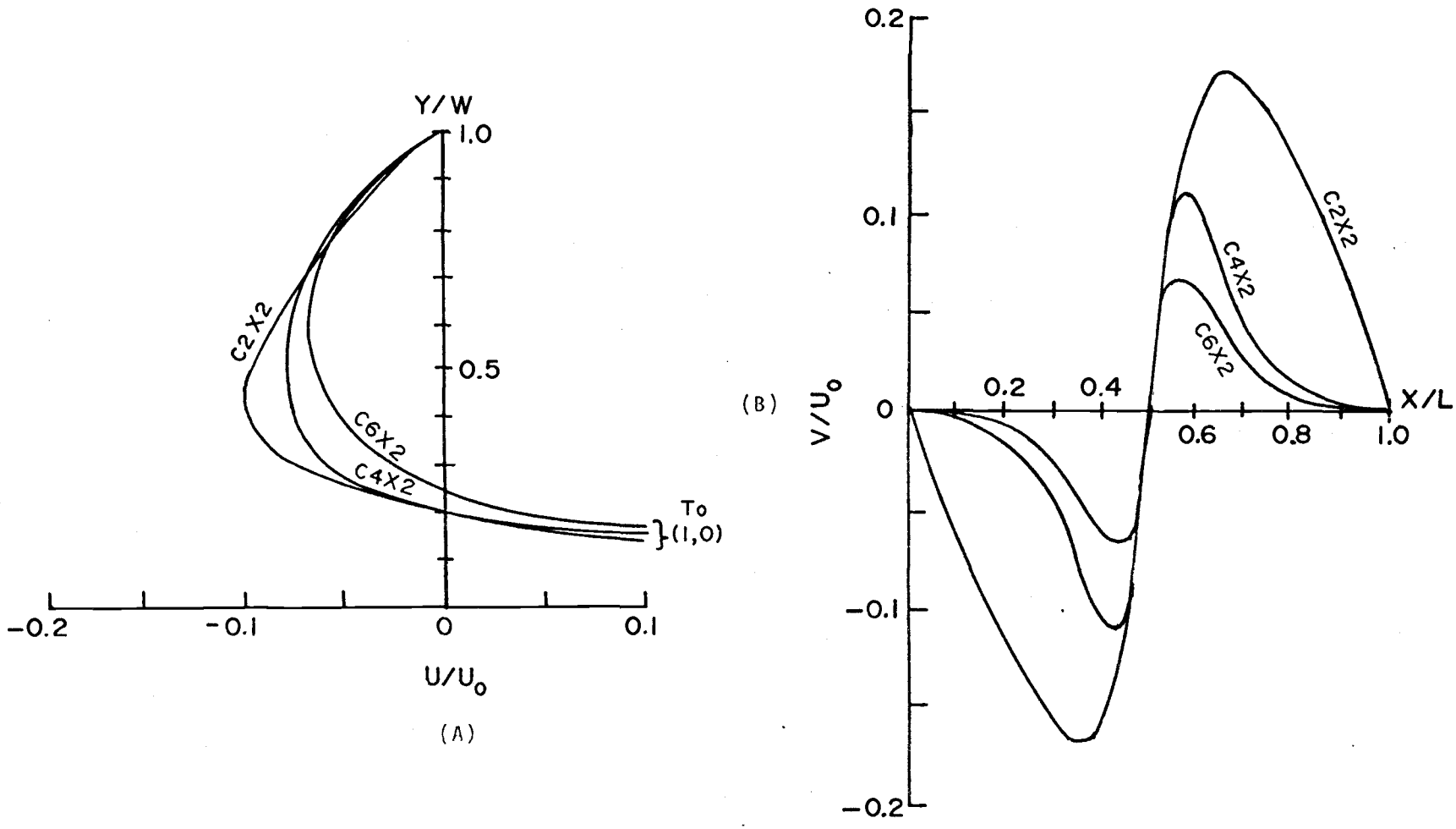

Figure 5.27. Effects of varying basin length on the relative velocity components (A) u/u_0 and (B) v/u_0. (For constricted entrance cases.)

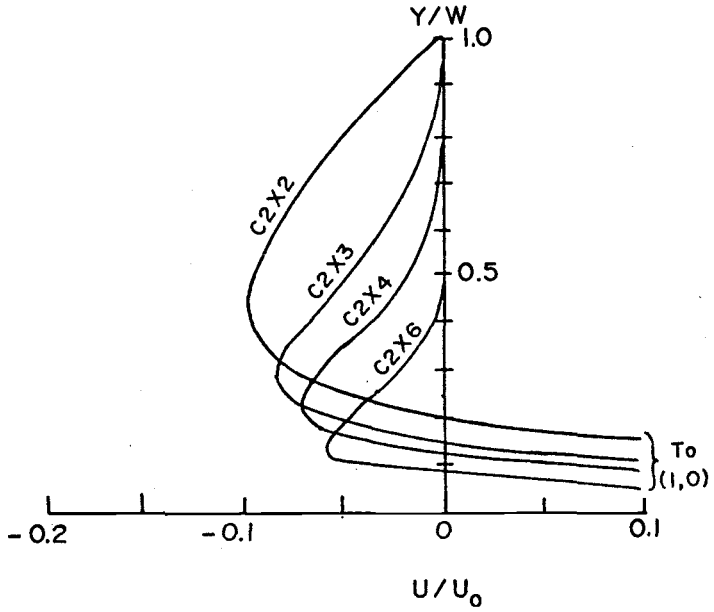

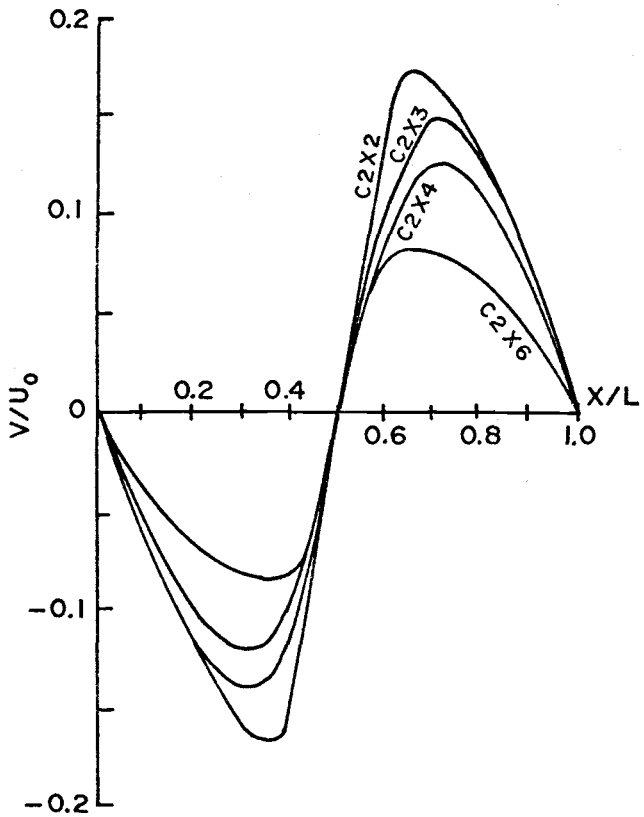

Figure 5.28. Effects of varying basin width on the relative velocity components (A) u/u_0 and (B) v/u_0.

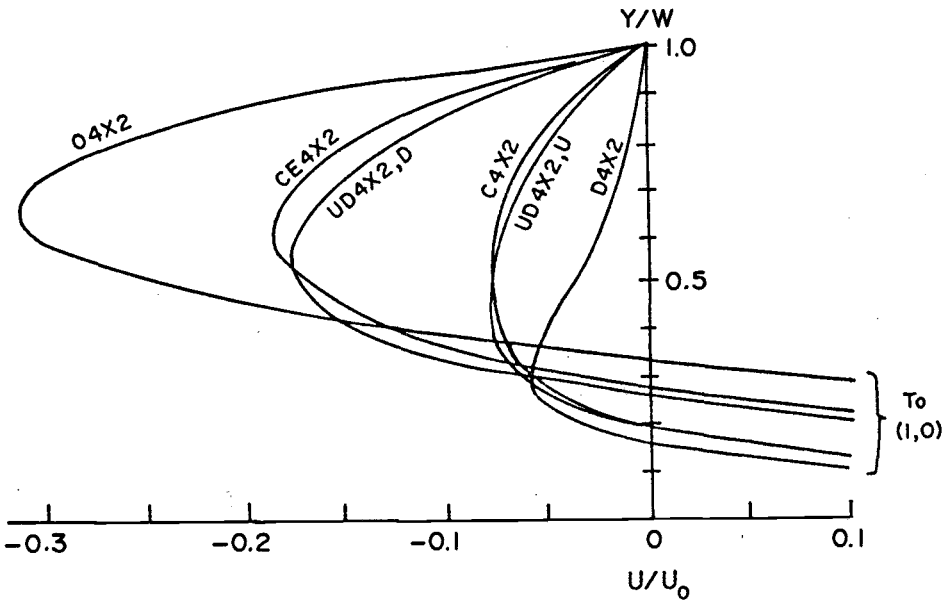

(A)

(B)

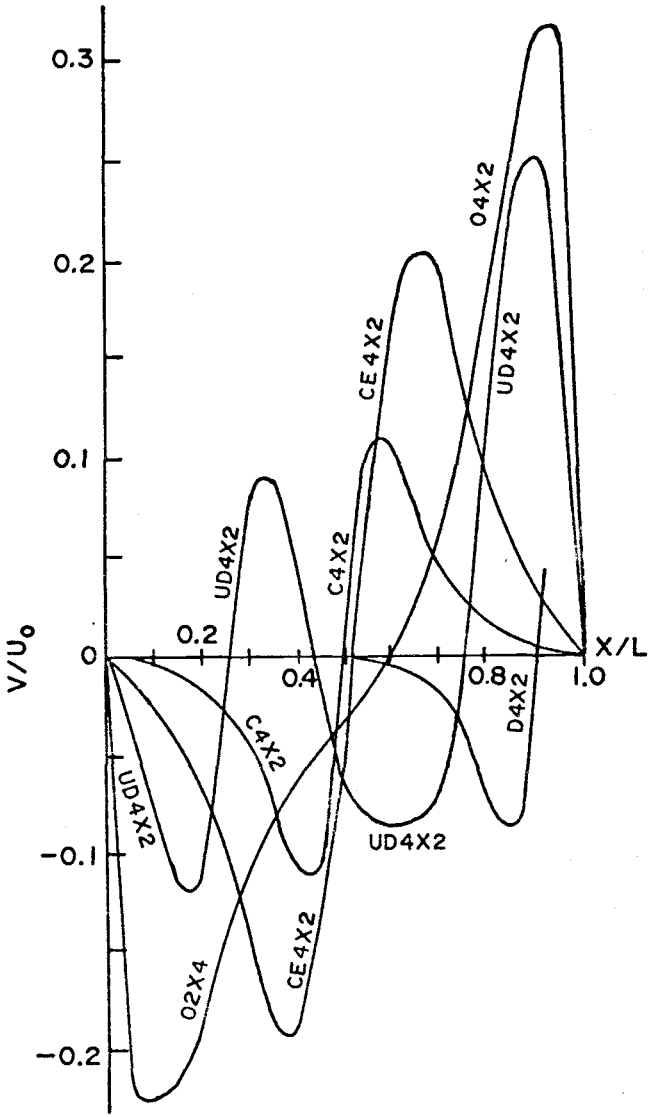

Figure 5.29. Effects of varying entrance width and location on the relative velocity components (A) u/u_0 and (B) v/u_0.

numbers, $u_o L/D$, but also for any reasonable velocity for which the flow is turbulent.

Each velocity field may be divided into entrance and interior zones. The former lies between the entrance and the center of the primary gyre and is characterized by strong velocity gradients and fluid shear (Figures 5.1 to 5.21 and 5.24 to 5.29). This zone occupies from 5 to 10% of the basin plan area, the larger percentage being associated with basins without entrance constrictions (Figures 5.22 to 5.25). The interior zone occupies the remainder of the basin and contains the basin's response to entrance zone velocity and shear fields.

For cases with length-to-width (L/W) ratios between approximately 0.5 and 2.0, the flow pattern consists of a single gyre as observed for turbulent flow conditions in laboratory experiments by Westrich (1975) and Nece, et al. (1976) and in computer simulations by Abbott (1977). For $0.5 > L/W > 2.0$, a secondary gyre develops in the interior with opposite rotation, but with greatly reduced velocities. If the basin is further elongated, the secondary eddy grows, but the size of the primary eddy and the position of the centers of rotation do not change greatly. Such behavior is similar to that described by Weiss and Florsheim (1965) for solutions to the Navier-Stokes equations with low Reynolds number. It also conforms to Westrich's (1975) laboratory observations of secondary gyre formation in turbulent flows where basin L/W is 0.3 or less. As pointed out by Westrich (1975) and others, such secondary cells are sluggish--velocities in the cases herein considered are on the order of 0.01% of the entrance velocity--and greatly increase the residence time for a given water mass. In so doing, the probability of sedimentation increases for suspended particles. To avoid such semi-stagnant bodies of water and the associated nearly-complete deposition of suspended sediments entering the basin, a basin aspect (L/W) ratio between approximately 0.3 and 2.0 is to be preferred. Improved circulation due to tidal flushing and currents flowing through the entrance (entrance jet effects) may extend these limits somewhat.

Table 5-1 lists the cases according to decreasing average basin velocity, $\bar{v}/u_o$, from Figures 5.22 to 5.25, which acts perpendicular to transects paralleling the coordinate axes and passing approximately through the center of the primary gyre. Table 5-2 lists velocity data for basins with aspect ratios of 0.5, 1.0, and 2.0 as fractions of the values in the corresponding unconstricted entrance cases. For a given basin aspect ratio (L/W) and entrance boundary velocity, highest mean or peak velocities are naturally associated with basins with open (unconstricted) entrances and, for such entrances, increase as either basin length increases or width decreases (cases O4X2, O2X2, O2X4; Figures 5.22, 5.26, 5.29). Since case O2X4 has much lower velocities than several cases with constricted entrances--e.g. C2X3, C2X2, CE4X2--suggests the undesirability of basins with small L/W ratios, e.g. less than say 0.5 to 0.3.

For constricted entrances, velocities increase as either basin length or width decreases (Figures 5.23, 24, 27, 28, 29) and are highest for centralized entrances. Thus, the basin length has the opposite effect for constricted entrance cases that it has for unconstricted entrance cases. Figure 5.30 illustrates the dependence of mean and interior peak velocities on basin width and length. Case C2X2 is taken as a standard for comparison since it has the highest mean velocity for all cases with similar entrance width. Mean basin velocity is more sensitive to changes in basin aspect (L/W) than either peak interior velocity and is more sensitive to basin width than to length. Entrance location plays an especially important role in determining the mean, vertically-averaged velocity, $\bar{v}$, as seen in Figure 5.30. For both upstream and downstream entrances, the mean velocity is some 77% lower than for a central entrance and decreases about 83% as either basin width or length doubles (Table 5-1 and Figure 5.25). For centralized entrances, $\bar{v}$ decreases some 67% as basin length doubles and 83% as basin width doubles (Figures 5.23 and 5.24). For an optimum basin-averaged recirculating velocity, then, it is preferable to use a central entrance and a basin aspect approaching unity, basin length perhaps exceeding width.

TABLE 5-1. Magnitudes of the relative mean basin velocities, $\bar{v}/u_o$, and peak interior velocities u_m/u_o and v_m/u_o ordered according to decreasing $\bar{v}/u_o$.

Case	$\lvert\bar{v}/u_o\rvert$	$\lvert u_m/u_o\rvert$	$\lvert v_m/u_o\rvert$*
04X2	.230	.317	0.271
02X2	.153	.196	0.300
UD4X2	.087	.081(U)	0.120
		.178(D)	0.255
CE4X2	.078	.187	0.199
C2X2	.070	.098	0.170
C2X3	.035	.084	0.148
02X4	.023	.143	0.239
C4X2	.023	.079	0.110
D2X2	.016	.097	0.128
U2X2	.016	.092	0.115
C2X4	.013	.074	0.122
C6X2	.010	.068	0.065
D2X4	.003	.045	0.050
U2X4	.003	.040	0.045
D4X2	.003	.060	0.086
U4X2	.003	.055	0.082
C2X6	.002	.060	0.084

* From Figures 5.22 to 5.25. For central entrance cases, the average of the upstream and downstream maxima is taken. For eccentric entrance cases, the value of the maximum farthest from the entrance is taken.

TABLE 5-2. Interior mean and peak velocities expressed as fractions of the values for the unconstricted entrance cases.

Case	$\bar{v}/\bar{v}(o)$	$u_m/u_m(o)$	$v_m/v_m(o)$*
O2X2	1.00	1.00	1.00
C2X2	0.46	0.50	0.57
U2X2	0.10	0.47	0.35
D2X2	0.10	0.50	0.47
O2X4	1.00	1.00	1.00
C2X4	0.57	0.52	0.50
U2X4	0.13	0.28	0.17
D2X4	0.13	0.32	0.24
O4X2	1.00	1.00	1.00
UD4X2(U)	0.38	0.26	0.53
(D)	0.38	0.56	0.80
CE4X2	0.34	0.59	0.76
C4X2	0.10	0.25	0.42
U4X2	0.01	0.17	0.26
D4X2	0.01	0.19	0.28

* From Figures 5.22 to 5.25. For central entrance cases, the average of the upstream and downstream maxima is taken. For eccentric entrance cases, the value of the maximum farthest from the entrance is taken.

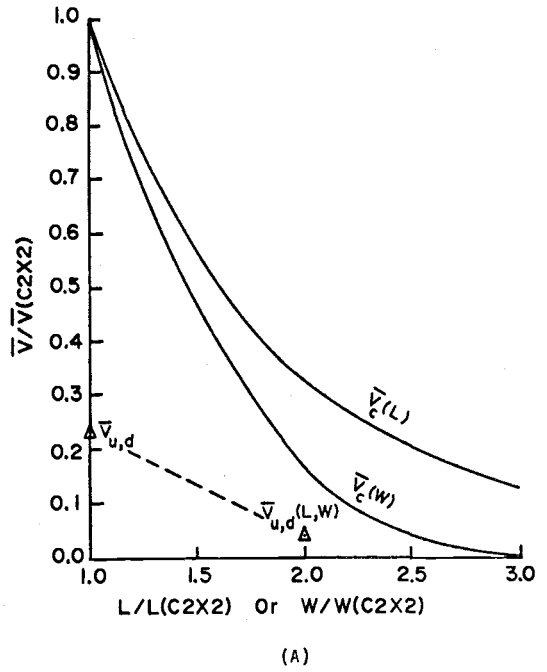

(A)

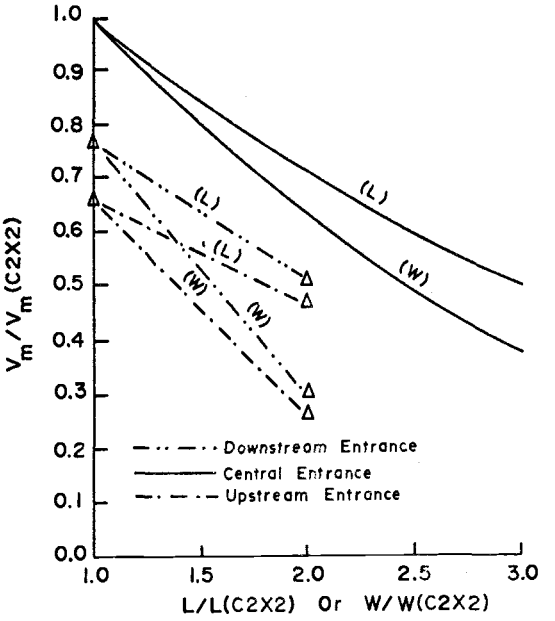

(B)

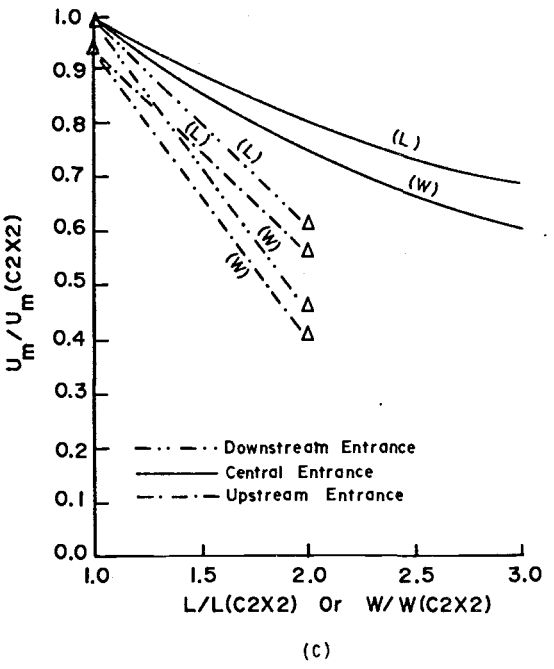

(C)

Figure 5.30. Effects of varying basin length or width on (A) the relative average velocity, $\bar{v}/\bar{v}$(C2X2), (B) the relative maximum velocity v_m/v_m(C2X2), and (C) the relative maximum velocity u_m/u_m(C2X2).

Maximum interior velocities likewise decrease as either basin width or length increase; increases in width were observed to have the greater effect (Figure 5.30). The parameters u_m and v_m are less sensitive to basin aspect ratio than is the mean velocity. Doubling basin length for centralized entrances produces a 19% and 28% decrease respectively, in u_m and v_m relative to case C2X2, but a 67% decrease in $\overline{v}$. Doubling the basin width causes decreases of 25, 37, and 83% respectively, in u_m, v_m, and $\overline{v}$.

Changes in basin aspect (L/W) more strongly affect u_m and v_m for basins with eccentric entrances. Compared to either case U2X2 or D2X2, doubling the basin length in cases U4X2 and D4X2 reduced u_m 40% and v_m 30%, approximately, substantially more than for centralized entrances. Doubling the basin width in cases U2X4 and D2X4 produces a 56 and 61% decrease in u_m and v_m. Compared to the corresponding central entrance cases, the elongated basins (aspect ratio of 2.0) with eccentric entrances have 27 and 23% lower u_m and v_m. Wide basins (aspect ratio of 0.5) have 42 and 61% lower values, respectively. The lower contrasts in u_m and v_m between central and eccentric entrance cases occurs for a square basin, 5 and 29%, respectively. Thus, as for the mean basin velocity, interior velocities are maximized through the use of a centralized entrance and a square planform. Should design criteria require other than a square planform or central entrance, an elongated basin ($L/W > 1$) is preferable to a wide basin since interior velocities will be least affected. Whether the entrance location is upstream or downstream of the center of the breakwater appears to have little effect on u_m and v_m.

Considering Table 5-2, it is apparent that internal velocities are directly proportional to the relative entrance width, W_e/L, and vary with the basin aspect ratio, L/W. Compared to open-entrance values, reducing W_e/L to 0.3 reduces $\overline{v}/\overline{v}(o)$ 43, 54, and 66%, respectively, for central-entrance cases C2X4, C2X2, and CE4X2 but 87% for upstream and downstream entrance cases. Here the parenthetic (o) denotes the unconstricted entrance value. Further constricting W_e/L to 0.15 in cases C4X2, D4X2, and U4X2 reduces $\overline{v}/\overline{v}(o)$ an additional

27 and 12% for central and eccentric entrances for a total reduction of 90 and 99%, respectively. Momentum transfer across the entrance is thus inhibited by entrance constriction with damping effects being five to ten times stronger for eccentric entrances than for central entrances. The closure effect varies non-linearly with entrance width and for a given W_e/L ratio the efficiency of momentum transfer increases with increasing L/W for both central and eccentric entrances. Such tendencies again suggest that central entrances are to be preferred in the marina design process and that the widest possible entrance width be used. Although the mean velocity for wide basins ($L/W < 1$) is lease affected by entrance closure, it must be remembered that the effects considered in this paragraph are computed relative to the respective open entrance cases. Whereas the relative effect of entrance closure increases as the basin aspect ratio (L/W) increases, the actual basin-averaged velocities increase with increasing L/W for a given relative entrance width (W_e/L).

The behavior of the relative peak interior velocities, $u_m/u_m(o)$ and $v_m/v_m(o)$, with varying W_e/L and L/W is more complex than that of the mean velocity. Decreasing W_e/L to 0.3 reduces $v_m/v_m(o)$ as much as 53, 47, and 35%, respectively, for cases C2X4, C2X2, and CE4X2. Further narrowing the entrance to W_e/L of 0.14 in case C4X2 reduces $v_m/v_m(o)$ a total of 65%. Hence, for a central entrance and a given entrance-width/basin length ratio, $v_m/v_m(o)$ increases with increasing L/W, a trend similar to that observed for $\overline{v}/\overline{v}(o)$. Such behavior reflects the increasingly effective transfer of momentum across the entrance as the absolute entrance width increases with increasing basin length or, alternatively, the confinement of the recirculating flow as the basin width decreases. For eccentric entrance cases with equal W_e/L ratio $v_m/v_m(o)$ increases as L/W approaches unity. The magnitude of $u_m/u_m(o)$ for central entrances is only slightly affected by varying basin aspect ratio. For eccentric entrances, however, it increases markedly as L/W increases; the reasons for this behavior are the same as discussed above for $v_m/v_m(o)$.

Interestingly, increasing the entrance width in the same proportion as basin length produces a mean basin velocity in case CE4X2 similar to that of a shorter basin (e.g. case C2X2) but with significantly improved circulation over much of the basin (Figure 5.25). Increasing entrance width (cases C2X2, C2X4, O2X4) cannot, however, compensate for the effects of increased basin width and would result in increasingly less efficient basin flushing. Thus, a square or elongated basin planform with a maximized relative entrance width (W_e/L) should be preferred over wider planforms in the design process.

Basins with extensive areas isolated from entrance influences have an exponentially decreasing u/u_o-versus-y/W curve in the interior (e.g. C2X4, D4X2, Figures 5.27, 5.28). Basins with smaller aspect ratios have a quasi-parabolic curve of u/u_o versus y/W (C2X2, C4X2). The parabolic curves of u/u_o versus y/W may be interpreted as indicating the confinement of the circulation gyre by finite boundaries. As the boundaries recede from the entrance (C2X2, C2X4, D2X2) the gyre expands until a balance is achieved between the centrifugal force and internal pressure gradients. As illustrated in Figure 5.28, the inland extension of the basin produces a change in the form of the velocity-versus-distance curve from parabolic to exponential. Local and basin-averaged velocities simultaneously decrease. For optimum local and basin-averaged circulation then, a "confined" vortex flow with a parabolic velocity profile such as in Figure 5.28 is to be preferred.

The parabolic curves are similar to those of Burggraf (1966) for low Reynolds number flows (see Figure 2.2). Whereas Burggraf observed the development of an inviscid core as the Reynolds number (u_oL/ν) increased, no such phenomenon was observed in this present study. This difference is due to Burggraf's use of the Navier-Stokes equations versus the use herein of the Reynolds equations of motion. In the Navier-Stokes equation, the terms involving molecular viscosity become insignificant compared to terms involving the velocity as velocity gradients increase, resulting in the development of the inviscid core. In contrast, the definition of the dispersion

coefficients used here (Eqs. 3.5.4 and 3.5.5) in the Reynolds equations involve the local velocity which prevents the "viscous-like" effects from being overshadowed by the convective terms as velocity increases. With such a velocity-dependent definition of the dispersion coefficient, the inviscid state will not be reached and the inviscid core will not form. Physically, the core development is prevented by the increasingly effective and non-uniform flux of momentum throughout the water body.

For the cases considered in this study, the center of the primary gyre moves inward and downstream as momentum exchange improves between basin and exterior waters (e.g. cases C4X2, CE4X2, O4X2 in Table 5-3). For constricted entrances sufficiently far removed from the walls, the x coordinates of the center, x_0, is near that of the entrance midpoint, but increases slightly (less than 10%) as the entrance width increases and the gyre center moves slightly downstream (C4X2, CE4X2, O4X2). For upstream and downstream entrances, x_0 corresponds to about 70% of the entrance width away from the nearest boundary, slightly higher values possibly occurring as basin width increases or lower values as length increases. The relative y coordinate, $y_0/y_0(0)$, increases nonlinearly with W_e/L and y_0 increases as either basin width or length increases (Figure 5.31). Higher values occur for central entrances than for noncentral ones, but y_0 responds similarly for either entrance type as basin width or length changes.

For unconstricted entrance cases, y_0 is more sensitive to changes in basin length than to changes in width. Interestingly, the reverse is true for basins with constricted entrances. As either basin or entrance width increases, y_0 approaches a limiting value, 52 m approximately--(C2X2, C2X3, C2X4, C2X6, CE2X4, O2X4) which is about 25% greater than that predicted by Weiss and Florsheim (1965) for low Reynolds number solutions to the Navier-Stokes equations. The effect of varying levels of flow turbulence, i.e. varying eddy viscosity coefficient or eddy Reynolds numbers (u_0L/A_h), was not investigated in this study. It seems reasonable to conclude, however, that increasing turbulence would shift the center of rotation inward, the exact amount

TABLE 5-3

Location of Center of Circulation Gyre

Case	$(x_o-x_{eu})/W_e$*	x_o(m)	y_o(m)
04X2	.60	240	67
02X2	.54	108	48
02X4	.54	108	52
C6X2	.50	300	50
CE4X2	.52	208	55
C4X2	.50	200	40
C2X2	.50	100	38
C2X3	.50	100	44
C2X4	.50	100	52
C2X6	.50	100	52
U,D4X2	.60, .40	40, 360	32
U,D2X2	.69, .40	46, 160	30
U,D2X4	.75, .25	50, 150	44
UD4X2	.56, .50	104, 176, 300	40, 52

*x_{eu} = x-coordinate of upstream end of entrance

W_e = entrance width

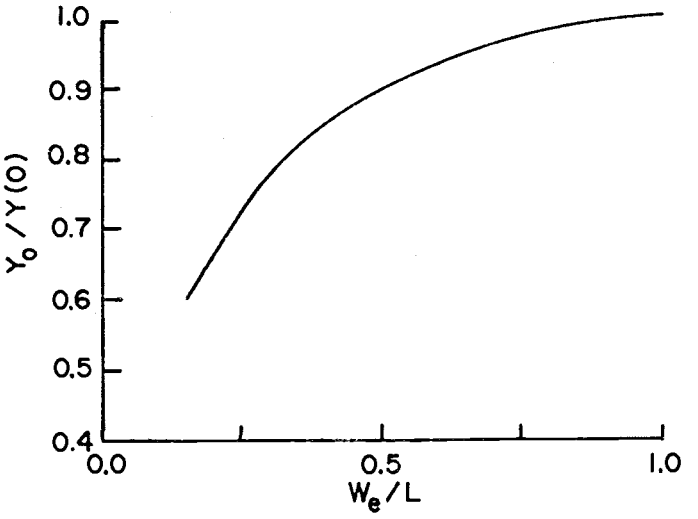

(A)

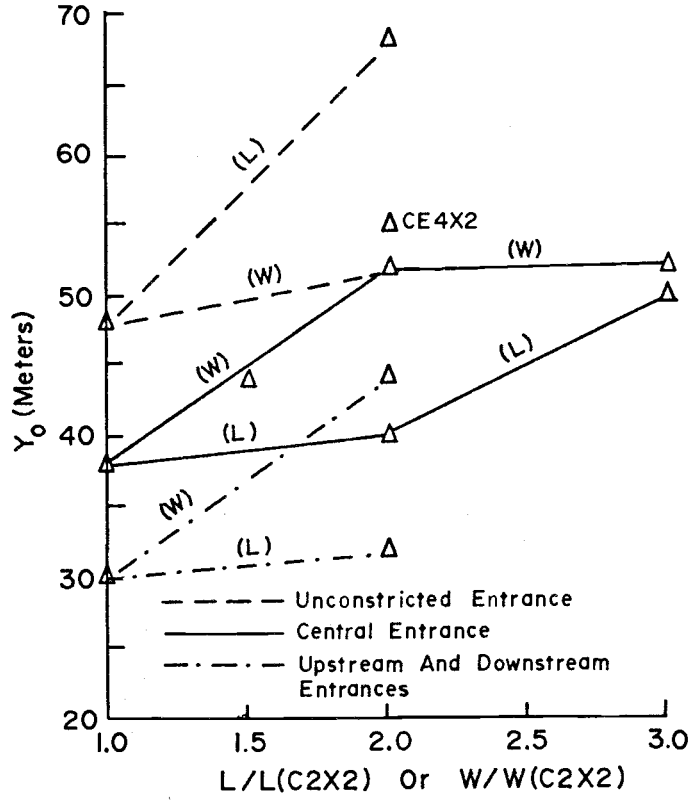

(B)

Figure 5.31. The y coordinate of the primary vortex center. (A) Effects of varying W_e/L on $y_o/y(0)$ where y(0) denotes the y_o value of the corresponding open or unconstricted entrance case. (B) Effects of varying relative basin length or width on y_o.

being determined by basin width and the entrance width/basin length ratio that in part determines the rate of influx of momentum to the basin.

Since for the range of velocities considered the curves and plots of relative velocities are identical for a given basin, the location of the gyre center is independent of entrance velocity. This conclusion conflicts with Burggraf's (1966) observation for unconstricted entrance cases of first downstream and then inward migration of the center as the boundary velocity increases. Evidently, either the limited closure of the entrance prohibits such migration or, more likely, the coarse finite-difference grid and limited variation of the parameters prevented the detection of such movement. Indeed, the discussion of the previous paragraphs assumes that the relatively small differences in y_o and x_o measured from Figures 5.26 to 5.29 are real, although in many cases they are only slightly greater than the uncertainty due to grid size.

The relative and absolute distances between the center of the primary gyre and the maximum interior velocities acting across transects passing approximately through the gyre center and parallel to the coordinate axes are shown diagramatically in Figure 2.1 and listed for various cases in Table 5.4. The distances r_x and r_x/L are indicators of the efficiency of the momentum transfer process from external to basin waters and r_y/W appears to be a function of the interaction between the inner shore boundary and circulating fluid. The distance r_x is a measure of the momentum transfer efficiency since it is independent of changes in basin length for a given entrance width, but increases markedly as the relative entrance width, W_e/L, increases for constricted entrance cases or as basin length increases for unconstricted entrance cases. As basin width is increased and the inward-directed momentum is distributed within a larger body of water, both r_x and r_x/L increase to a maximum for case C2X4 and decrease as the basin is widened further. The maximum in r_x/L coincides with the incipient development of the secondary gyre in the basin interior. Thus, r_x/L appears to be an easily-measured parameter for laboratory

TABLE 5-4. Relative and absolute distances from center of rotation to maximum velocities acting perpendicular to transects parallel to the coordinate axes and passing through the center of rotation.

Case	r_x/L	r_y/W	r_x (m)	r_y (m)
C6X2	.05	.35	33	69
O4X2	.34	.33	136	66
CE4X2	.15	.33	60	66
C4X2	.08	.33	32	66
O2X2	.36	.23	75	46
C2X2	.15	.24	30	48
C2X3	.16	.15	32	45
O2X4	.32	.12	64	48
C2X4	.19	.11	38	44
C2X6	.12	.05	29	31

L/W Increases ↑

and field studies that grossly characterizes both the efficiency of momentum exchange across the entrance and circulation efficiency within the basin. Design configurations that maximize r_x/L should have optimal momentum exchange characteristics and a minimum of circulation cells.

The distances r_y or r_y/W are insensitive to changes in relative entrance width and so are not indicators of the entrance momentum-exchange efficiency. However, both parameters increase strongly as basin width decreases or basin length increases which suggests a strong interaction between basin boundaries and gyre characteristics. As basin width decreases for a given length, the conservation of angular momentum within the basin requires either higher velocities at a given point or an increased radius of gyration or curvature for the maximum velocity, e.g. v_m and u_m, hence the increase in r_y/L as basin width decreases. That r_y/W increases as basin length increases expresses the relaxation of the confining pressure of upstream and downstream shore boundaries. This parameter does not appear to be affected by the development of secondary circulation cells and therefore is not as useful as r_x/L for design purposes.

The parameters r_x and r_y may, however, prove most useful in estimating the "rolling dispersion" of Engelund (1974) and Abbott (1977):

$$D_r = \frac{C^3}{18} \left(\frac{d}{r}\right)^2 vd \qquad (3.5.8)$$

where

C = the non-dimensional Chezy number v/u_*,

v = vertically-averaged horizontal velocity,

d = depth,

r = radius of flow curvature.

For example, using the following values from case C2X2,

$\bar{v} \cong 0.2\ u_o = 3\times10^{-2}$ m/s

r = 0.36 L = 72 m

d = 4.5 m

$C = 3\times10^{-2}/0.12\times10^{-2} = 25$

yields $D_r = 0.46\ m^2/s$. In this present study, the momentum dispersion coefficient was assumed to be constant,

$$D = 60\ u_* d$$

where u_* is the value corresponding to the entrance velocity, u_o. For most cases, the momentum dispersion coefficient used was $1.47\ m^2/s$ which enhanced momentum dispersal and increased local velocities in the basin interior relative to those that would have been obtained using a spacially-varying dispersion coefficient. The magnitude of the effect is not expected to be great since trial computations showed the vertically-averaged velocity field to be relatively insensitive to changes in the dispersion coefficient. Further investigation into the properties and effects of spacially-varying dispersion in recirculating flows could prove valuable to both the scientific and industrial communities.

Cases C4X2, CE4X2, and UD4X2 illustrate the effects of multiple entrances. Cases CE4X2 and UD4X2 have twice the entrance width of case C4X2, but in case UD4X2 there are two equally-wide entrances (Figure 5.18). The area/velocity distributions and mean basin velocities for cases UD4X2 and CE4X2 are similar (Figure 5.25). Case UD4X2, however, significantly reduces the area with very low velocities. In Figure 5.29, the curve for case UD4X2 is nearly identical to that of case CE4X2 (Figure 5.27), suggesting that v/u_o is more sensitive to entrance number and location than is u/u_o. The center of circulation for the upstream entrance gyre is displaced downstream slightly compared to that of case C4X2 which has an equally wide entrance. The relative location of the center for the downstream entrance gyre of case UD4X2, however, is more similar to that of case CE4X2 which has twice the entrance width. The decrease in the relative area with low velocities and the apparent increase in efficiency of the downstream entrance suggest that multiple small entrances may be used to provide adequate protection and improve basin circulation where a single large entrance would be unsatisfactory.

As discussed previously, maximum basin-averaged velocities are associated with a square basin and central entrance and any deviation

in basin aspect (L/W) ratio should favor the selection of a longer basin for increased circulation to maintain water quality and reduced sedimentation. Nece, et al. (1976) in physical model studies of tidal circulation in basins of varying aspect ratio concluded that optimal flushing was achieved using a square planform with a downstream entrance. They did not investigate the effects of centrally located entrances, however, only entrances at the extreme upstream or downstream ends of the breakwater. Again, the square planform optimizes fluid circulation, but whether this optimization requires different positioning of the entrance for shear-generated and tidally-induced circulation components remains to be verified.

Cases C2X6 and C6X2 are the only cases found to violate Noble's (1976) guidelines for acceptable basin-flushing characteristics. In both cases mentioned, the internal velocities were extremely low and secondary circulation cells were present (Figures 5.23 and 5.24). Average sedimentation rates were also low as a consequence of the near-complete sedimentation of suspended sediments near the entrance and the vast area of sluggishly-moving water (Figures 5.10 and 5.21). Noble's guidelines were derived from statistical regression studies of the sediment chemistry of 13 Oregon marinas. Since this present study does not consider tidal effect on flushing and circulation, Noble's guidelines are not directly applicable here. However, as pointed out by Vollmers (1976), the flushing characteristics of a basin are strongly related to the strength of the circulation gyre, which suggests that Noble's criteria can be used jointly with these results to alert the designer to potential flushing problems.

5.2 Sedimentation Field

Figures 5.1 through 5.21 present the velocity and sedimentation rate fields for each of the cases considered. Maximum sedimentation rates occur at the centers of the circulation gyres and along the breakwater or land boundary downstream of the entrance, as described

by Vollmers (1976). The higher sedimentation rates at the gyre center are the consequence of the dispersion of suspended sediments towards the center of circulation where the velocities are low. In the prototype situation, secondary currents generated by curvature of the flow could also contribute to such accumulation of sediments. High rates of sedimentation along the downstream boundary are the consequence of the unique location of the sediment source, the basin entrance. Currents flowing parallel to the entrance transport sediment dispersed across the entrance boundary around the basin. Since the velocity field is depth-averaged, there is no component other than that of turbulent dispersion capable of transporting the sediment towards the basin center. Consequently, much of the suspended sediment would settle out along the downstream boundary.

In most cases, the entrance zone has the lowest sedimentation rates for the entire basin, which is a consequence of higher bed shear near the entrance. The low sedimentation rates are most obvious for basins with unconstricted entrances or high boundary velocities but tend to increase as either entrance width or entrance boundary velocity decrease. For the cases that do not exhibit lower-than-average sedimentation rates near the entrance, it is reasonable to assume that the coarseness of the finite element grid and the computation of a single average sedimentation rate for each element, rather than for each nodal point did not permit the resolution of the low-sedimentation areas.

For most cases, the isopleths of sedimentation rate are approximately symmetric about the entrance. For case UD4X2, however, the isopleths run diagonally across the basin and the maximum sedimentation rate occurs in the downstream corner (Figure 5.18).

The sedimentation field is relatively sensitive to the transverse dispersion coefficient which, during this simulation study was varied by two orders of magnitude to gage its effect on sediment dispersal. Since there is no flux of water permitted perpendicular to the entrance boundary, only turbulent diffusion can effect the exchange of suspended sediment between the basin and exterior waters. This coefficient is a

direct measure of the effectiveness of the dispersal process. In Figure 5.32, it is seen that the average basin sedimentation rate increases approximately 10% for each order of increase in the magnitude of the transverse dispersion coefficient relative to case C4X2. The distribution of the isopleths of sedimentation rates are not greatly affected by increasing D_t but for case C4X2D1000 in which D_t is 1000 times greater than used in most other studies, the higher sedimentation rates occur in an annular semi-circle centered on the entrance rather than in an area downstream of the entrance (Figure 5.20).

As discussed in the previous section, estimates of the spatially-constant, transverse, momentum-dispersion coefficient used in this study are somewhat higher than is indicated using Engelund's (1974) "rolling dispersion" formula (Eq. 3.5.8). The transverse sediment dispersion coefficient used in this present study is given as explained in Section 3.5 by:

$$D_t = 0.23\, u_* d \tag{3.5.5}$$

where

$$u_* \cong \frac{\sqrt{u^2+v^2}}{22} \tag{3.5.14}$$

Using Engelund's definition (Eq. 3.5.8) and the data from case C2X2 as in the previous section, D_r is 0.46 m^2/s versus 0.0014 m^2/s from Eqs. 3.5.5 and 3.5.14. Eqs. 3.5.5 and 3.5.14 were derived for steady or quasi-steady, unidirectional and straight flow conditions whereas Engelund's (1974) formuli attempt to account for the effects of channel curvature in steady, unidirectional flows. Future investigators as well as designers who use the material presented in this present paper are advised to consider the effects of higher transverse dispersion through the use of Figure 5.32, part D.

As mentioned in Section 3.2, Westrich (1977) has suggested that two-dimensional, vertically-integrated transport models such as used in this present study may not accurately reproduce the transportive effects of secondary currents generated by curved flow. Although this

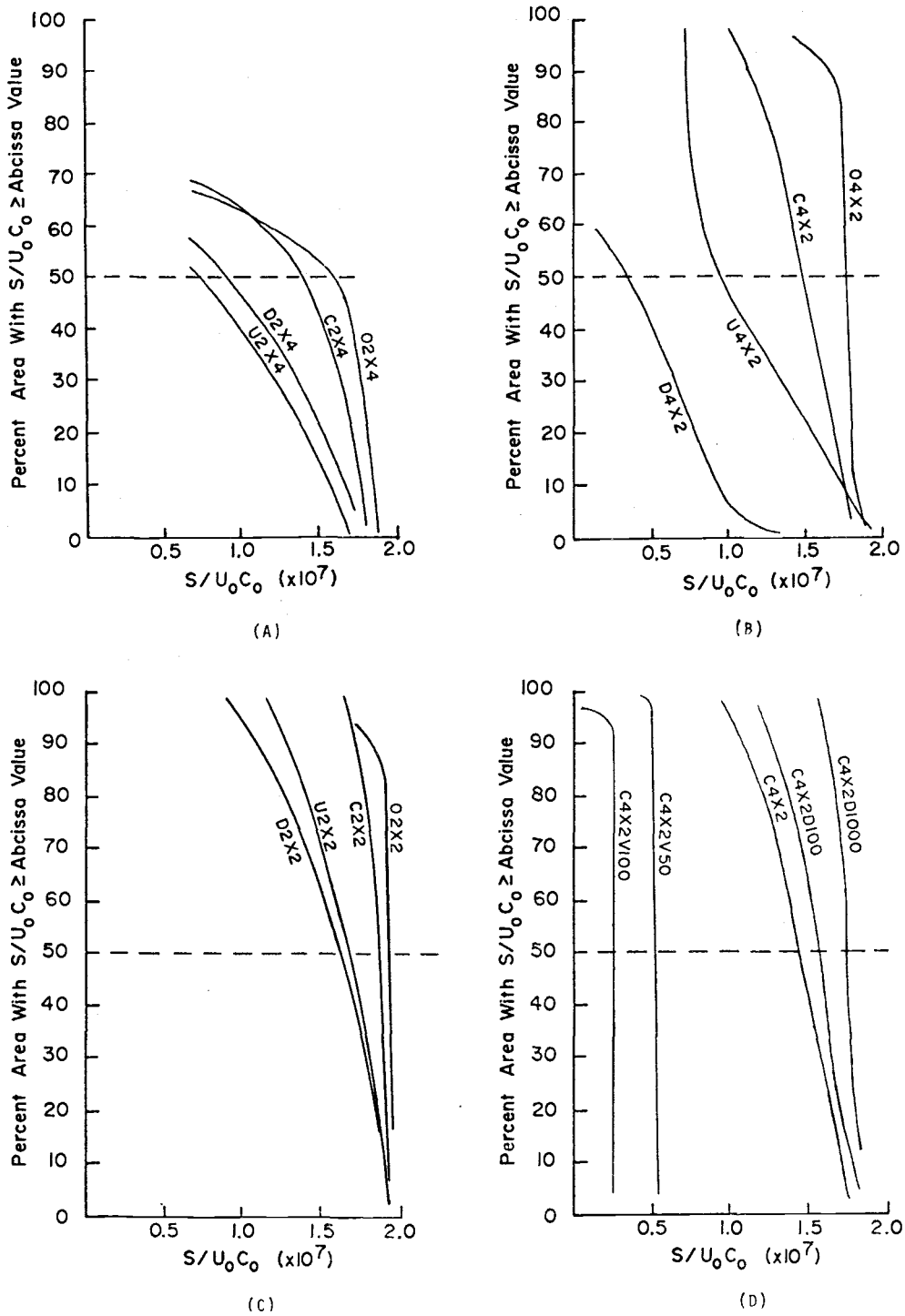

Figure 5.32. Percent of basin area with non-dimensional sedimentation rates (S/u_0C_0) greater than abscissa value. Effects associated with varying entrance width and location for basin aspect ratios (L/W) of (A) 0.5, (B) 2.0 and (C) 1.0. (D) Effects of varying entrance boundary velocity, u_0, or the magnitude of the transverse dispersion coefficient.

present study does not resolve this point, it does demonstrate that the computed sedimentation field is sensitive to the transverse dispersion coefficient. It appears reasonable to assume that the effects of secondary currents can be accounted for (at least in part) through the manipulation of the magnitudes of both longitudinal and transverse dispersion coefficients. Future laboratory and field investigations might be directed towards considering this possibility.

Figures 5.22 to 5.25 and 5.32 and Table 5-5 summarize the effects of basin length, basin width, entrance width, entrance number or location, entrance boundary velocity, and transverse dispersion on the distribution of sedimentation rates. The ordinate of each graph is the proportion of basin area (in Figures 5.1 to 5.22) having sedimentation rates equal to or greater than the value on the abscissa. Sedimentation rates decrease with decreasing suspended sediment concentration, decreasing transverse dispersion, and with increasing entrance boundary velocity, basin length or width. It also decreases with decreasing entrance width, as the basin aspect ratio deviates from unity and as the entrance location is farther displaced from the center of the breakwater.

Figure 5.32 presents the area/sedimentation rate curves for basins with aspect ratios of 0.5, 1.0, and 2.0 and similar entrance width, boundary velocities, and suspended sediment concentrations. Basin-averaged sedimentation rates decrease as the entrance is constricted but maximum rates are approximately the same in most cases. Interestingly, for basins with aspect ratios (L/W) of one or greater, an entrance positioned at the extreme downstream end of the breakwater produces a minimum sedimentation rate for the basin as a whole. For wider basins, an entrance at the upstream end of the breakwater will minimize this rate (Figure 5.24). Apparently, the slightly more intense circulation characteristic of downstream entrances transports the sediment into the basin interior more efficiently for aspect ratios of unity or greater as basin width increases. For basin aspect ratios less than unity, more efficient distribution occurs with the upstream introduction of the sediments and their subsequent dispersal by basin

TABLE 5-5. Average basin sedimentation rates and percent reductions in that rate for various cases relative to the respective unconstricted and central entrance cases.

Case	$S/C_o u_o$ ($\times 10^7$)	$\frac{[(\overline{S/C_o u_o}) - (\overline{S/C_o u_o})_o]}{(\overline{S/C_o u_o})_o}$ %	$\frac{[(\overline{S/C_o u_o}) - (\overline{S/C_o u_o})_c]}{(S/C_o u_o)c}$ %
O2X2	1.87	0	+4
U2X2	1.60	-14	-11
C2X2	1.80	-4	0
D2X2	1.53	-17	-15
C2X3	1.63	--	0
O2X4	1.60	0	+14
U2X4	0.73	-55	-48
C2X4	1.40	-12	0
D2X4	0.90	-44	-36
O4X2	1.75	0	+19
U4X2	0.95	-46	-35
C4X2	1.47	-16	0
C4X2V50	0.52	-70	-65
C4X2V100	0.27	-85	-82
D4X2	0.35	-80	-76
CE4X2	1.73	-1	+18
UD4X2	1.75	0	+19
C4X2D100	1.61	-8	+10
C4X2D1000	1.79	+2	+22
C6X2	1.11	--	0

currents and dispersive processes. Naturally, in tidal waters the distinction between upstream and downstream loses meaning. Nevertheless, it seems reasonable to recommend that in tidal waters, a single entrance be oriented with respect to the ebb current since the discharging river water generally contains higher suspended-solids concentrations (especially during high runoff periods) than do flooding ocean waters. Hence, elongated ($L/W > 1$) basins would have an entrance in the "ocean-ward" half of the breakwater but a wide ($L/W < 1$) basin would have an entrance in the inland half of the breakwater. Since it was pointed out in the previous section that optimum circulation within the basin occurs for centrally-located entrances, a compromise between circulation and sedimentation could be rapidly reached by displacing the entrance position in the "upstream" or "downstream" directions, as prescribed above.

Increasing the entrance boundary velocity intensifies basin circulation and turbulent dispersion processes, which results in lower, more uniform sedimentation rates over the majority of the basin (Figure 3.32, part D); accordingly, the sedimentation in the entrance zone decreases (Figures 5.13, 5.14, 5.15). For very low u_o, trial computations indicated that maximum sedimentation rates occur in the downstream portion of a constricted entrance. As the velocity is increased, the maximum sedimentation site shifts downstream along the breakwater and sediments deposit well into the basin. For very small basins (0.2 m by 0.2 m) and high velocities (2 m/s), Araithurai and Krone (1976) also have shown that this zone moves into the interior of the basin. Thus, as the velocity increases, the deposition field associated with the currents flowing parallel to the entrance is spread over more of the basin. For sufficiently high velocities, the dispersion of sediments towards the center of the gyre and the low velocities there result in a maximum rate of sedimentation. That the rate of decrease in the mean basin sedimentation rate is higher for low velocities suggests that where temporally-varying flows are involved, it is

best to locate the marina entrance where stream or entrance velocities are high and the duration of low velocity or slack water is at a minimum.

Figure 5.22 demonstrates the effect of varying basin aspect ratio for basins without constricted entrances. Sedimentation rates decrease as the aspect ratio (L/W) deviates from unity, smallest rates occurring in the wider, smaller aspect-ratio, basins. The similarity of the curves 04X2 and 02X2 and their contrast with curve 02X4 suggest that for a given basin width, the sedimentation curves will be similar for varying lengths and that width has a more significant effect on basin sedimentation patterns, other conditions being equal. Doubling basin length decreases $\overline{S/C_o u_o}$ some 6% relative to case C2X2 whereas doubling the width produces a 14% decrease. The range of sedimentation rates for constricted entrances is similarly more strongly affected by increasing basin width. The lower sedimentation rates are associated with increasingly less efficient circulation over the basin as a whole and the increasing isolation of interior water from entrance effects as the basin becomes wider.

Variations in either basin width or length more strongly affect sedimentation in basins with eccentric entrances than in basins with centralized entrances (Figures 5.23 and 5.24). Doubling basin width or length decreases $\overline{S/C_o u_o}$ 20 to 30%, approximately, for central entrances. For upstream or downstream entrances, respectively, doubling the basin length lowers $\overline{S/C_o u_o}$ 40 or 78%, as opposed to a 54 or 42% reduction from doubling the width. Obviously, downstream entrance cases are more strongly affected by changes in basin length than are upstream entrance cases whereas changes in basin width equally affect both entrance cases. Increasing or decreasing the aspect ratio (L/W) from unity also increases the difference between the curves of $\overline{S/C_o u_o}$ for upstream and downstream entrances; increasing the aspect ratio has the greater effect. For the square basin, the difference between $\overline{S/C_o u_o}$ for upstream and downstream entrances is less than 4% but for aspect ratios of 0.5 and 2.0 relative sedimentation ratio differences of 20 and 60%, respectively, were noted.

Figure 5.25 illustrates the effect of varying entrance width and location on sedimentation and/or circulation for basins having constricted entrances. Interestingly, the sedimentation rate/area curves 04X2, CE4X2, and UD4X2, are very similar although the areal distributions in Figures 5.11, 5.17, and 5.18 are markedly different. That these curves are also different from case C4X2 suggests that, at least for elongated basins, such curves are independent of the relative entrance length W_e/L above some value, say between 0.15 and 0.30. In all cases, reducing W_e decreases the rate of sedimentation but basins with aspect ratios less than unity seem to be more sensitive to basin closure. For a centralized entrance with a width equal to one-third the basin length, the wide basin (aspect ratio of 0.5) exhibited a 16% reduction in $\overline{S/C_o u_o}$ relative to the unconstricted entrance case versus a reduction of less than 2% for the square or elongated basins. Sedimentation rates for eccentric entrance cases are up to five times more sensitive to entrance closure than for central entrances (Table 5-5 and Figure 5.4). Cases D2X4 and U2X4 have $\overline{S/C_o u_o}$ values 80 to 46% lower than case 02X4 or 30 to 64% lower than for a centralized entrance. Further constriction of the entrance appears to decrease this contrast in sensitivity since for a W_e/L ratio of 0.15, case C4X2 has a $\overline{S/C_o u_o}$ value which is 16% less than for 04X2 but U4X2 and D4X2 have values 36 and 76% lower than C4X2. Obviously, basin sedimentation rates can be decreased by narrowing the entrance of the marina. Unfortunately, circulation would also be inhibited if the marina entrance were narrowed and it must be recognized that a balance must be struck between minimizing sedimentation and providing adequate circulation and water quality.

5.3 Summary of Results

In summary, the following aspects may be noted and summarized schematically in Table 5-6 regarding circulation and sedimentation in a rectangular basin connected to a waterway:

TABLE 5-6. Matrix summary of effect that some geometric and environmental parameters have on the quality of circulation and sedimentation in a rectangular marina connected to a waterway.*

Circulation/Sedimentation

Condition	W increases	L increases	W_e increases	u_o increases	C_o increases	L/W increases	W_e/L increases	L/W ≠ 1	D_t increases	upstream entrance	central entrance	downstream entrance	open entrance
Unconstricted entrance	- / +	+ / +			+ /		/ -						
Upstream entrance	- / +	- / +				/ -	+ / -						
Central entrance	- / +	- / +	+ / -	+ / +	/ -	/ +	+ / -	+ / -	/ -				
Downstream entrance	- / +	- / +					/ -	+ / -					
L/W > 1										1/3	2/2	1/4	3/1
L/W = 1										1/3	2/2	1/4	3/1
L/W < 1										1/4	2/2	1/3	3/1

* + upper triangle indicates effect on circulation, lower triangle - the effect on sedimentation

\+ denotes increased circulation or decreased sedimentation relative to square basin case with an entrance as noted.

\- denotes decreased circulation or increased sedimentation.

Blanks indicate that the effect was not directly considered in this study

1, 2 ... is the order of preference (highest value most preferred) for entrance position given the basin aspect ratio (L/W) as noted.

1. The circulation and sedimentation fields can be divided into entrance and interior zones. The entrance zone is characterized by strong horizontal gradients in velocity and/or sedimentation rates.
2. For a single marina entrance, the velocity field within the basin consists of a single gyre for basin aspect ratios between 0.5 and 2.0. For other aspect ratios, multiple circulation cells develop and the basin-averaged velocity will be low. Although the basin-averaged sedimentation rate would also be low, Noble's (1976) guidelines suggest that undesireably low basin flushing conditions also would exist.
3. The vortex center migrates slightly downstream and inland as the basin width increases. Increasing the relative entrance width or increasing the basin length moves the center inland. Increasing basin length moves the center upstream.
4. The distance measured parallel to the breakwater between the vortex center and the maximum velocity vector, v_m, appears to be a measure of the angular momentum of the vortex and increases as the relative entrance width increases. The distance measured inland from the vortex center to the maximum velocity, u_m, appears to be a function of the inner boundary influence, increasing as the basin width increases for a given relative entrance width.
5. The distances r_x and r_y measured between the vortex center and the maximum velocity vectors u_m and v_m acting parallel to the basin sides can be used as first-order estimates for the radius of curvature in Engelund's (1974) equation estimating "rolling dispersion". The use of this equation to predict the transverse momentum dispersion coefficient produces values only one-third as large as the values used in this study. The effect of this difference is not expected to be great since trial computations showed the velocity field to be relatively insensitive to the changes in the momentum dispersion coefficient. The transverse sedimentation dispersion coefficient used in most of this study is only one-four-hundredth of the Engelund estimate.

The curves in Figure 5.33D should be used to correct the data in this study if Engelund's estimates are adopted.

6. The basin-averaged velocity and the shear-driven circulation are enhanced by increasing the relative entrance width, decreasing basin width or, for basins with constricted entrances, by decreasing basin length. For unconstricted entrance cases, increasing basin length enhances the vortex circulation. Basin aspect ratios (L/W) less than about 0.6 have undesireably poor circulation conditions and should be avoided.
7. Sedimentation rates vary directly with marina entrance width, the concentration of suspended sediment at the entrance boundary and the transverse dispersion coefficient. Sedimentation also varies inversely with the entrance boundary velocity, basin width, and basin length.
8. Optimum vortex circulation for basins with constricted entrances is achieved through the selection of a square planform with a central entrance. The basin aspect ratio of unity, however, yields the highest basin-averaged sedimentation rates for given boundary conditions. Clearly, since changes in basin length or width have opposite effects on these two parameters, a case-specific compromise is required.
9. Deviations from a square planform decrease both the average velocity and sedimentation rate. Increasing basin width has a substantially greater effect on both parameters than that from increasing basin length. Hence, any necessary deviation from a square planform should favor aspect ratios (L/W) greater than one.
10. For basins with aspect ratios greater than, or equal to unity, a downstream entrance produces the minimum basin-averaged sedimentation rate. For aspect ratios less than one, an upstream entrance yields the lowest average rate. The basin-averaged velocities for such aspect ratios are independent of whether the entrance is upstream or downstream of the basin but eccentric entrances produce a much weaker basin circulation than do centralized entrances.

11. Maximum sedimentation rates occur at the center of the primary circulation gyre or downstream of the marina entrance. As the entrance boundary velocity is increased, the zone of higher sedimentation rates is displaced downstream due to the advective effects. Increasing the transverse dispersion coefficient causes higher average sedimentation within the basin. Very strong transverse dispersion causes the higher rates to occur in a semi-annual ring centered on the entrance. For very high entrance velocity conditions, the high sedimentation zone corresponds to the center of the circulation gyre.
12. For a given basin width and entrance width/basin length ratio, increasing the basin length (and automatically the entrance width) improves the overall circulation of the basin without significantly altering the average basin velocity.
13. Significant decreases in the basin-averaged sedimentation rate do not occur for centrally-located entrances until the breakwater constitutes two-thirds or more of the basin length. Eccentric entrance cases are up to five times more sensitive to entrance closure, however.
14. Multiple entrances are to be preferred since they provide an improved velocity distribution within the basin than would result for a single, equivalently-wide entrance. Because the basin-averaged velocity is strongly dependent upon the total entrance width, rather than on its distribution, the use of multiple entrances does not significantly change the mean basin velocity over that of the equivalent single entrance. The average sedimentation rate varies directly with the total entrance width and is relatively insensitive to the distribution of that width.

5.4 Utilization of Study Results

The use of these results requires that some characteristic channel velocity and suspended sediment concentration be specified along with the basin plan area, entrance width, basin depth, etc. Figures 5.22 to 5.29 and 5.32 may then be entered and interpolated to yield first-order estimates of circulation and sedimentation in rectangular basins for various aspect ratios. Since the results represent equilibrium conditions for given boundary conditions, time-varying channel currents will need to be represented by average velocities, the averaging time interval being problem-dependent. For river floods, the velocity and sediment concentration may be averaged over the entire flood period or over some shorter period. For tidal flows, natural averaging periods are those of ebb and flood stages and the superposition and averaging of the two resulting sedimentation fields may be taken as an estimate of long-term sedimentation differences within the basin. An example in Appendix C illustrates this procedure.

5.5 Recommendations

This study has considered the phenomena of shear-driven vortex circulation and sedimentation in rectangular basins connected to a waterway. From the consideration of the dependence of these phenomena on basin and environmental parameters, the following design recommendations are tentatively given:

1. A basin aspect ratio greater than unity should be used to effect an optimum balance between basin-averaged sedimentation rates and velocities. In no case should the basin aspect ratio (L/W) be less than about 0.3 or greater than about 2.0 since undesirable secondary vortices form in the basin interior which adversely affect basin circulation.

2. Where single entrances are used, the entrance should be centrally positioned in the breakwater if the marina site lacks significant suspended sediment concentrations. Such an entrance position maximizes velocities within the basin.
3. Where sedimentation in the basin is expected to be a problem and a single entrance is to be used, the entrance should be displaced either upstream or downstream of the center of the breakwater, the amount depending on the concentration of suspended sediments and on the channel velocity. For basins with aspect ratios (L/W) greater than or equal to one, the entrance should be in the downstream half (for tidal waters, in the "ocean-ward" half) of the breakwater. For basin aspect ratios less than one the entrance should be in the upstream half (for tidal waters, in the inland half) of the breakwater. Such placement of a single entrance will allow a compromise to be struck between circulation and sedimentation rates in the basin.
4. Multiple entrances are desirable since they provide an opportunity to develop a through-flowing current. Moreover, the multiplicity appears to cause some entrances to act as if they are effectively wider, thereby improving basin circulation without significantly increasing basin sedimentation.
5. Entrance or basin configurations that produce a parabolic u/u_o-versus-y/W curve are preferable to those producing an exponentially decreasing curve since the former provides improved circulation over the entire basin.
6. The parameter r_x/L, where r_x is the distance between the vortex center and the maximum velocity, v_m, acting parallel to the upstream or downstream boundaries, is a convenient measure of the momentum transfer efficiency of the entrance configuration and of the circulation efficiency of the vortex. Maximizing r_x/L should minimize the number of

circulation cells present and maximize the momentum exchange between basin and exterior waters. Future laboratory and field studies or recirculating flows in rectangular basins should include the r_x/L parameter in their data acquisition and analysis phases.

7. First-order estimates of the gross characteristics of circulation and sedimentation in rectangular marinas can follow from the results of this study as illustrated in Appendix C. Tidal conditions can also be approximated if the tidal cycle is divided into flood and ebb stages for which average velocities and suspended sediment concentrations at the marina entrance are known. Since the analysis in this study did not consider tidal or density circulation effects, Noble's (1976) guidelines regarding marina flushing should be used jointly to warn of possible undesirable flushing conditions.
8. Future investigations of basin circulation should include tidal effects. A simple approach in extending the results of the studies presented here would be to superimpose the shear-induced velocity field onto either analytical or numerical solutions for jet flow directed into or out of the basin. More desirable would be the continued application of numerical or physical models such as those of Nece, et al. (1976) and Abbott (1977) which directly consider the effects of entrance configuration and changes in water depth. Whichever approach is adopted, field data should be used for calibration purposes. Future investigations of basin sedimentation should be conducted both in the field and laboratory to improve our understanding of dispersion in recirculating, shear-and tidally-driven flows. The effects of secondary currents could also be evaluated.
9. The use of the alternative Rayleigh-Ritz formulation in solving the sedimentation problem could result in the more efficient and economical use of computer memory

capacity. A three-dimensional or multi-layered, two-dimensional model could then be formulated which more accurately reproduces the circulation and sedimentation processes, including the effects of secondary currents.

BIBLIOGRAPHY

Abbott, M.B., "Marina Flushing and Circulation Tests", Danish Hydraulic Institute, Hoersholm, Denmark, April 1977.

_____and Rasmussen, C.H., "On the Numerical Modelling of Rapid Expansions and Contractions in Models that are Two-Dimensional in Plan", presented at the August 1977 IAHR Congress in Baden-Baden.

Abramowitz, M. and Stegun, I., Handbook of Mathematical Functions, Dover Publications, Inc., New York, N.Y., 1965.

Araithurai, C.R., "A Finite Element Model for Sediment Transport in Estuaries", thesis presented to the University of California, at Davis, Calif., in 1974, in partial fulfillment of the requirements for the degree of Doctor of Philosophy.

_____and Krone, R.B., "Finite Element Model for Cohesive Sediment Transport", Journal of the Hydraulics Division, ASCE, Vol. 102, No. HY3, pp. 323-338, 1976.

Batchelor, G.K., "On Steady Laminar Flow with Closed Streamlines at Large Reynolds Numbers", Journal of Fluid Mechanics, Vol. 1, pp. 177-190, 1956.

Boericke, R.R., and Hall, D.W., "Hydraulics and Thermal Dispersion in an Irregular Estuary", Journal of the Hydraulics Division, ASCE, Vol. 100, No. HY1, Proceedings Paper 10282, Jan. 1974, pp. 85-102.

Bowden, K.F., "Horizontal Mixing in the Sea Due to a Shearing Current", Journal of Fluid Mechanics, Vol. 21, part 2, pp. 83-95, 1965.

Burggraf, O.R., "Analytical and Numerical Studies of the Structure of Steady Separated Flows", Journal of Fluid Mechanics, Vol. 24, part 1, pp. 113-151, 1966.

Callaway, R.J., "Application of Some Numerical Models to Pacific Northwest Estuaries", Proceedings, 1971 Technical Conference in Estuaries of the Pacific Northwest, Oregon State University, Corvallis, Oregon, Engineering Experiment Station Circular No. 42, pp. 29-97, 1971.

Choi, B., "Pollution and Tidal Flushing Predictions for Oregon's Estuaries", thesis presented to the Oregon State University, Corvallis, Oregon, in 1975, in partial fulfillment of the requirements for the Master of Science Degree.

Elder, J.W., "The Dispersion of Marked Fluid in Turbulent Shear Flow", Journal of Fluid Mechanics, Vol. 5, pp. 541-560, 1959.

Engelund, F., "Flow and Bed Topography in Channel Bends", Journal of The Hydraulics Division, ASCE, Vol. 100, No. 11, Nov. 1974.

Fischer, H.B., "The Mechanics of Dispersion in Natural Streams", Journal of the Hydraulics Division, ASCE, Vol. 93, HY6, pp. 187, 216, Nov. 1967.

_____ "A Method for Predicting Pluutant Transport in Tidal Waters", Water Recearch Center Contribution No. 132, Hydraulic Engineering Laboratory, University of California, at Berkeley, Calif. 1970.

Frankel, S.P., "Convergence Rates of Iterative Treatments of Partial Differential Equations", Math Tables and Other Aids to Computation, Vol. 4, pp. 65-75, 1950.

Glover, R.E., "Dispersion of Dissolved or Suspended Materials in Flowing Streams", U.S. Geological Society Professional Paper 433-B, 1964.

Guymon, G.L., "A Finite Element Solution of the One-Dimensional Diffusion-Convection Equation", Water Resources Research, Vol. 6, No. 1, pp. 204-210.

Haag, F.G. and Bedford, K.W., "Transport Equation Stability and Estuary Modeling", Journal of the Hydraulics Division, ASCE, Vol. 97, No. HY12, pp. 2051-2066, Dec. 1971.

Hinwood, J.B. and Wallis, I.G., "Classification of Models of Tidal Waters", Journal of the Hydraulics Division, ASCE, Vol. 101, No. HY10, pp. 1315-1331, 1975.

_____ "Review of Models of Tidal Waters", Journal of the Hydraulics Division, ASCE, Vol. 101, No. HY11, pp. 1405-1421, Nov. 1975.

Holley, E.R., Harleman, D.R.F., and Fischer, H.B., "Dispersion in Homogeneous Estuary Flow", Journal of the Hydraulics Division, ASCE, Vol. 96, No. HY8, pp. 1691-1712, Aug. 1970.

Hoskins, C.M., "Sedimentation in St. Louis Bay, Mississippi", Water Resources Research Institute Report, Mississippi State University, State College, Miss., June 1971.

Hubbell, D.W., Glenn, J.L. and Stevens, Jr., H.H., "Studies of Sediment Transport in the Columbia River Estuary", Proceedings 1971 Technical Converence on Estuaries of the Pacific Northwest,

Circular No. 42, Engineering Experiment Station, Oregon State University, Corvallis, Oregon, pp. 190-226, 1971.

Klingeman, P.C. and Daufman, W.J., "Transport Radionuclides with Suspended Sediment in Estuarine Systems", Sanitary Engineering Research Laboratory Report No. 65-15, University of California, at Berkeley, Calif. 1965.

Krone, R.B., "Flume Studies of the Transport Sediment in Estuarial Shoaling Process", Technical Report, Hydraulic Engineering Laboratory, University of California, at Berkeley, Calif, 1962.

_____ "A Study of the Rhelogic Properties of Estuarial Sediments", Technical Report, Hudraulic Engineering Laboratory, University of California, at Berkeley, Calif. 1963.

_____ "A Field Study of Flocculation as a Factor in Estuarial Shoaling Processes", Technical Bulletin No. 19, Committee on Tidal Hydraulics, U.S. Army Corps of Engineers, June 1972.

Kruyt, H.R., Colloidal Science, Vol. 1. Elsevier Puglishing Co., Amsterdam, The Netherlands, 1952.

Leendertse, J.J., "A Water Quality Simulation Model for Well Mixed Estuaries and Coastal Seas. Vol. 1 - Principles of Computation," RM-6230-RC, Rand Corp., Santa Monica, Calif., 1970.

Leimkuler, W., et al., "Two Dimensional Finite Element Dispersion Model", Proceedings, Symposium on Modeling Techniques, Second Annual Symposium of the Waterways, Harbors and Coastal Engineering Division of the ASCE, held Sept. 3-5, 1975, San Francisco, Calif., pp. 1467-1486.

Masch, F.D., et al., "Numerical Model for the Simulation of Tidal Hydraulics in Shallow Irregular Estuaries", University of Texas, Hydraulics Engineering Laboratory Technical Report, HYD 12-7104, 1971.

Metha, A.J., and Partheniades, E., "An Investigation of the Depositional Properties of Flocculated Fine Sediments," Journal of Hydraulic Research, Vol. 13, No. 4, pp. 361-381, 1974.

Nece, R.E., R.A., Falconer, R.A., and Tsutsumi, T., "Platform Influence on Flushing and Circulation in Small Harbors", Proceedings of the Fifteenth Coastal Engineering Conference, pp. 3471-3486, Honolulu, Hawaii, July 11-17, 1976.

Nihoul, J.C.J., and Adam, Y., "Dispersion and Settling Around a Waste Disposal Point in a Shallow Sea", Journal of Hydraulic Research, Vol. 13, No. 2, pp. 171-186, 1975.

Noble, S., "Use of Sediments to Determine Marina Flushing," thesis presented to Oregon State University, at Corvallis, Oregon, in 1976, in partial fulfillment of the requirements for the degree of Masters.

O'Connor, B.A., and Zein, S., "Numerical Modeling of Suspended Sediment," Proceedings, Thirteenth Coastal Engineering Conference, held at Copenhagen, Denmark, pp. 1109-1128, 1974.

O'Connor, B.A., "Marine Hydraulics, Sediment Intrusion in a Tidal Lock," Proceedings, 16th IAHR Congress on Fundamental Tools to be Used in the Environmental Problems, held at Soa Paulo, Brazil, Vol. 3, Paper C35, pp. 301-8, 1975.

O'Connor, D.J., "Oxygen Balance of an Estuary," Journal of Sanitary Engineering Division, ASCE, Vol. 86, No. SA3, pp. 35-55, 1960.

Odd, N.V.M., and Owen, M.W., "A Two-Layer Model for Mud Transport in the Thames Estuary," Proceedings, Institution of Civil Engineers, London, England, Supplement (ix), Paper 7517S, 1972.

Okubo, A., "The Effect of Shear in an Oscillatory Current on Horizontal Diffusion from One Instantaneous Source," International Journal of Oceanography and Limnology, Vol. 14, No. 4, 1967, pp. 514-520.

Pan, F., and Acrivos, A., "Steady Flows in Rectangular Cavities," Journal of Fluid Mechanics, Vol. 28, part 4, pp. 643-655.

Pinder, G.F., and Gray, W.G., The Finite Element Method in Surface and Subsurface Hydrology, Elsevier Publishing Co., Amsterdam, The Netherlands, 1977.

Pollock, T.P., "A Two-Dimensional Random Walk Transport Model," Geophysical Fluid Dynamics Laboratory, Monash University, Clayton, Virginia, Australia, 1973.

Prakash, A., Discussion of "Finite Element Model for Cohesive Sediment Transport," by C.R. Araithurai and R.B. Krone, "Finite Element Model for Cohesive Sediment Transport", Journal of the Hydraulics Division, ASCE, Vol. 102, HY3, PP. 323-338.

Prandtl, L., "Motion of Fluids with Very Little Viscosity," Technical Memorandum No. 452, U.S. National Advisory Committee for Aeronautics, 1928.

Roach, P., Computational Fluid Dynamics, Hermosa Publishers, Albuquerque, N.M. 1976.

Singamsetti, S.R., "Diffusion of Sediment in a Submerged Jet," Journal of the Hydraulics Division, ASCE, Vol. 192, No. HY2, pp. 153-168, 1966.

Snyder, L.J., Spriggs, J.W., and Stweart, W.E., American Institute of Chemical Engineering, Vol. 10, p. 535, 1964.

Taylor, G., "The Dispersion of Matter in Turbulent Flow Through a Pipe," Sewage and Industrial Wastes, Vol. 25, No. 9, Sept. 1953, pp. 1065-1071.

Taylor, C., and Davis, J., "Finite Element Modelling of Flow and Dispersion in Estuaries," International Symposium of River Mechanics, International Association for Hydraulic Research, Bangkok, Thailand, 1975, pp. 465-476.

Thomann, R.V., Systems Analysis and Water Quality Management, Environmental Research and Applications, Inc., New York, NY, 1972.

TRACOR, Inc., "Estuarine Modeling, An Assessment," a report prepared for the Environmental Protection Agency, Feb. 1971.

Vollmers, H., "Harbour Inlets on Tidal Waters," Proceedings, Fifteenth Coastal Engineering Conference, held at Honolulu, Hawaii, July 11-17, 1976, pp. 3471-3486.

Ward, P.R.B., "Transverse Dispersion in Oscillatory Channel Flow," Proceedings, Journal of the Hydraulics Division, ASCE, Vol. 100, No. HY6, pp. 755-772, June, 1974.

Weiss, R.F., and Florsheim, B.H., The Physics of Fluids, Vol. 8, No. 9, Sept., 1965, pp. 1631-1635.

Westrich, B.J., Discussion of "Finite Element Model for Cohesive Sediment Transport," by C.R. Araithurai and R.B. Krone, "Finite Element Model for Cohesive Sediment Transport," Journal of the Hydraulics Division, ASCE, Vol. 102, HY3, pp. 323-338.

Westrich, W., "Simulation of Mass Exchange in Dead Zones for Steady and Unsteady Flow Conditions," presented at the April 12-15, 1976, International Symposium on Unsteady Flow in Open Channels, held in Newcastle-uponTyne, England.

Zienkiewicz, O.C., The Finite Element Method in Engineering Science, McGraw-Hill Publishing Co., Ltd., London, England.

APPENDICES

APPENDIX A

Derivation of the Element Coefficient Matrix

The derivation of the element coefficient matrix is presented here. This matrix is also called the steady state coefficient matrix or the stiffness matrix. From Eqs. 5.4.7 and 5.4.10

$$[K]\ \{C\}^e = \int_A \left[[N]^T \left[u \frac{\partial \hat{C}}{\partial x} + v \frac{\partial \hat{C}}{\partial y} \right] + \frac{\partial [N]^T}{\partial x} D_x \frac{\partial \hat{C}}{\partial x} + \frac{\partial [N]^T}{\partial Y} D_y \frac{\partial \hat{C}}{\partial y} \right] dA \tag{A.1}$$

where

$$C = \sum_{\alpha=1}^{6} N_\alpha C_\alpha$$

and the quantity within the brackets is representative of each line in the 6x6 matrix. Now

$$\frac{\partial N_I}{\partial L_j} = (4L_I - 1)\ \delta_{Ij} \tag{A.2}$$

$$\frac{\overline{N}_I}{L_j} = 4L_J \delta_{Kj} + 4L_K \delta_{Jj} \tag{A.3}$$

where $\delta_{\ell m}$ is the Kroenecker delta function such that

$$\delta_{\ell m} = \begin{cases} 0, & \text{if } \ell \neq m \\ 1, & \text{if } \ell = m \end{cases} \tag{A.4}$$

and $\overline{N}_I$ is the shape function for the mid-side node opposite to corner node I. Also

$$\frac{\partial L_I}{\partial x} = \frac{b_I}{2A} \tag{A.5}$$

$$\frac{\partial L_I}{\partial y} = \frac{a_I}{2A} \tag{A.6}$$

where A is the area of the element

$$a_I = X_{KI} - X_{JI} \tag{A.7}$$

$$b_I = Y_{JI} - Y_{KI} \tag{A.8}$$

APPENDIX A. (continued)

and the subscripts JI, KI indicate the J'th or K'th corner node ordered with respect to node I, i.e., ordered counter clockwise from node I, with

$$\frac{\partial N_I}{\partial x} = \sum_{j=1}^{6} \frac{\partial N_I}{\partial L_j} \frac{\partial L_j}{\partial x} \tag{A.9}$$

$$\frac{\partial N_I}{\partial y} = \sum_{j=1}^{6} \frac{\partial N_I}{\partial L_j} \frac{\partial L_j}{\partial y} \tag{A.10}$$

Then

$$\frac{\partial N_I}{\partial x} = (4L_I - 1) \frac{b_I}{2A} \tag{A.11}$$

$$\frac{\partial N_I}{\partial y} = (4L_I - 1) \frac{a_I}{2A} \tag{A.12}$$

$$\frac{\partial \overline{N}_I}{\partial x} = \frac{2}{A} (L_{JI} b_{KI} + L_{KI} b_{LI}) \tag{A.13}$$

$$\frac{\partial \overline{N}_I}{\partial y} = \frac{2}{A} (L_{JI} a_{KI} + L_{KI} a_{JI}) \tag{A.14}$$

Now

$$\frac{\partial \hat{C}}{\partial x} = \sum_{\alpha=1}^{3} \left[\frac{\partial N_\alpha}{\partial x} C_\alpha + \frac{\partial \overline{N}_\alpha}{\partial x} \overline{C}_\alpha \right] \tag{A.15}$$

and

$$\frac{\partial \hat{C}}{\partial y} = \sum_{\alpha=1}^{3} \left[\frac{\partial N_\alpha}{\partial y} C_\alpha + \frac{\partial \overline{N}_\alpha}{\partial y} C_\alpha \right] \tag{A.16}$$

Therefore

$$\frac{\partial \hat{C}}{\partial x} = \sum_{\alpha=1}^{3} \frac{1}{2A} [(4L_\alpha - 1) b_\alpha C_\alpha + 4(L_{J\alpha} b_{K\alpha} + L_{K\alpha} b_{J\alpha}) \overline{C_\alpha}] \tag{A.17}$$

$$\frac{\partial \hat{C}}{\partial y} = \sum_{\alpha=1}^{3} \frac{1}{2A} [(4L_\alpha - 1) a_\alpha C_\alpha + 4(L_{J\alpha} a_{K\alpha} + L_{K\alpha} a_{J\alpha}) \overline{C_\alpha}] \tag{A.18}$$

where J and K indicate the complimentary corner nodes to node α.

APPENDIX A. (continued)

Alternatively, at any point within the element

$$\hat{C} = \sum_{\alpha=1}^{3} N_\alpha C_\alpha + \overline{N}_\alpha \overline{C}_\alpha = \sum_{\alpha=1}^{3} L\,(2L_\alpha - 1)C_\alpha + 4L_J L_K \overline{C}_{JK\alpha} \qquad (A.19)$$

where

I identifies a corner node

J,K indicate the remaining corner nodes

$\overline{C}_{JK\alpha}$ is the concentration of the mid-side node between nodes J and K, opposite node α.

and overbars identify mid-side parameters with overbars.

Eq. A.1 may be rewritten letting I be the matrix row and α the column location

$$[k_{I\alpha}]\{C_\alpha\}^e = \int_A [\ldots(N_I u + D_x \frac{\partial N_I}{\partial x}) \frac{\partial \hat{C}}{\partial x} + (N_I v + D_y \frac{\partial N_I}{\partial y}) \frac{\partial \hat{C}}{\partial y} \ldots] \, dxdy \qquad (A.20)$$

for the corner nodes, i.e., for I = 1,2,3; α = 1,2...6 and for the mid-side nodes, i.e., for I = 4,5,6; α = 1,2...6

$$[K_{I\alpha}]\{c\alpha\}^e = \int_A [\ldots(\overline{N}_I u + D_x \frac{\partial \overline{N}_I}{\partial x}) \frac{\partial \hat{C}}{\partial x} + (\overline{N}_I v + D_y \frac{\partial \overline{N}_I}{\partial y}) \frac{\partial \hat{C}}{\partial y} \ldots] \, dxdy \qquad (A.21)$$

Substitution for the gradients of $\hat{C}$ and of N_I or $\overline{N}_I$ above and subsequent manipulation yield

$$[k_{I\alpha}]\{C_\alpha\}^e = \frac{1}{2A} [\ldots J_{I\alpha} C_\alpha + \overline{J}_{I\alpha} \overline{C}_\alpha \ldots] \qquad (A.22)$$

for corner nodes, I = 1,2,3; α = 1,2...6 and

$$[k_{I\alpha}]\{C_\alpha\}^e = \frac{1}{2A} [\ldots I_{I\alpha} C_\alpha + \overline{I}_{I\alpha} \overline{C}_\alpha \ldots] \qquad (A.23)$$

for mid-side nodes, I = 4,5,6; α = 1,2...6 where

$$J_{I\alpha} = \int_A \left([L_I(2L_I - 1)(ub_\alpha + va_\alpha) + \frac{(4L_I - 1)}{2A} (b_I b_\alpha D_x + a_I a_\alpha D_y] \cdot \right.$$
$$\left. \cdot (4L_\alpha - 1) \right) \, dxdy \qquad (A.24)$$

APPENDIX A. (continued)

$$\bar{J}_{I\alpha} = \int_A \Big\{ L_I(2L_I - 1)[4u(L_{J\alpha}b_{K\alpha} + L_{K\alpha}b_{J\alpha}) + 4v(L_{J\alpha}a_{K\alpha} + L_{K\alpha}a_{J\alpha})] + (4L_I - 1)[\frac{4b_I D_x}{2A}(L_{J\alpha}b_{K\alpha} + L_{K\alpha}b_{J\alpha}) + \frac{4a_I D_y}{2A}(L_{J\alpha}a_{K\alpha} + L_{K\alpha}a_{J\alpha})] \Big| dxdy \tag{A.25}$$

$$I_{I\alpha} = \int_A \Big[[4L_{JI}L_{KI}(ub_\alpha + va_\alpha) + \frac{2}{A} b D_x(L_{JI}b_{KI} + L_{KI}b_{JI}) + \frac{2a_\alpha D_z}{A} (L_{JI}a_{KI} + L_{KI}a_{JI})](4L_\alpha - 1) \Big] dxdy \tag{A.26}$$

$$\bar{I}_I = \int_A \Big[[4L_{JI}L_{KI}u + \frac{2}{A}(L_{JI}b_{KI} + L_{KI}a_{JI})D_x] 4(L_{J\alpha}L_{K\alpha} + L_{K\alpha}a_{J\alpha}) + [4L_{JI}L_{KI}v + \frac{2D_z}{A}(L_{JI}a_{KI} + L_{KI}a_{JI})] 4(L_{J\alpha}L_{K\alpha} + L_{K\alpha}a_{J\alpha}) \Big] dxdy \tag{A.27}$$

where double subscripts mℓ indicate that m is the m'th node ordered relative to the ℓ'th node as described for the model triangular element. Integrating eq. A.24 through A.27

$$J_{I\alpha} = \begin{cases} \frac{-A}{15}(ub_\alpha + va_\alpha) - \frac{1}{6}(b_I b_\alpha D_x + a_I a_\alpha D_z), & I \neq \alpha \\ \frac{2A}{15}(ub_\alpha + va_\alpha) + \frac{1}{2}(b_i b_\alpha D_x + a_I a_\alpha D_z), & I = \alpha \end{cases} \tag{A.28}$$

$$\bar{J}_{I\alpha} = \begin{cases} uA(C_{I\alpha}b_{K\alpha} + C_{\alpha I}b_{J\alpha}) + \frac{2}{3}b_I b_{M_{I\alpha}} D_x + vA(C_{I\alpha}a_{K\alpha} + C_{\alpha I}a_{J\alpha}) + \frac{2}{3}a_I a_{M_{I\alpha}} D_z, & I \neq \alpha \\ \frac{-A}{15}[u(b_{K\alpha} + b_{J\alpha}) + v(a_{K\alpha} + a_{J\alpha})], & I = \alpha \end{cases} \tag{A.29}$$

where

$$[C_{I\alpha}] = \frac{1}{15}\begin{bmatrix} 0 & -1 & 2 \\ 2 & 0 & -1 \\ -1 & 2 & 0 \end{bmatrix} \tag{A.30}$$

and

$$M_{3\alpha} = 3; \quad M_{4\alpha} = 2; \quad M_{5\alpha} = 1.$$

$$I_{I\alpha} = \begin{cases} \frac{A}{5}(b_\alpha u + a_\alpha v) + \frac{2}{3}(b_{KI}b_\alpha D_x + a_{KI}a_\alpha D_z), & I \neq \alpha \\ \frac{-A}{15}(b_I u + A_I v), & I = \alpha \end{cases} \tag{A.31}$$

APPENDIX A. (continued)

$$\overline{I}_{I\alpha} = \begin{cases} uA(F_{J\alpha}b_{K\alpha} + F_{\alpha I}b_{J\alpha}) + \frac{2}{3}D_x[(b_{JI} + b_{KI})(b_{K\alpha} + b_{J\alpha}) + b_I b_\alpha] + \\ vA(F_{I\alpha}a_{K\alpha} + F_{\alpha J}a_{J\alpha}) + \frac{2}{3}D_x[(a_{JI} + a_{KI})(a_{K\alpha} + a_{J\alpha}) + a_I a_\alpha], \; I \neq \alpha \\ \\ \frac{8uA}{15}(b_{K\alpha} + b_{J\alpha}) + \frac{4D_x}{3}(b^2_{K\alpha} + b_{K\alpha}b_{J\alpha} + b^2_{J\alpha}) + \frac{8va}{15}(a_{K\alpha} + a_{J\alpha}) + \\ \frac{4D_z}{3}(a^2_{K\alpha} + a_{K\alpha}a_{J\alpha} = a^2_{J\alpha}), \; I = \alpha \end{cases} \tag{A.32}$$

where

$$[F_{I\alpha}] = \frac{4}{15}\begin{bmatrix} 0 & 2 & 1 \\ 1 & 0 & 2 \\ 2 & 1 & 0 \end{bmatrix} \tag{A.33}$$

APPENDIX B. EMPIRICAL EQUATIONS FOR COMPUTING LONGITUDINAL TRANSVERSE AND VERTICAL DISPERSION COEFFICIENTS.

Number	Investigator	Equation
1	Kolomogoroff (1941), open channel flow	$D_L = cLa^{4/3}E^{1/3}$
2	Taylor (1954), pipe flow	$D_L = 10.11\ u_* R$
3	Aris (1954), supported Taylor's work	$\frac{D_L}{u_* R} = \text{constant}$
4	Thomas (1958), open channel flow	$\frac{D_L}{u_* H} = (\frac{\bar{u}}{u_*})^3 \phi(n) + \frac{u_*}{\bar{u}} \psi(n)$
5	Elder (1959), open channel flow	$D_L = 5.93\ u_* H$ $D_T = 0.23\ u_* H$
6	Parker (1961), open channel flow	$D_L = 14.28\ (2gS)^{1/2} R^{3/2}$
7	Saffman (1962), supported Aris' work	$\frac{D_L}{u_* H} = \text{constant}$
8	Krenkel (1962), open channel flow	$D_L = 9.1\ u_* H$
9	Bowden (1963), natural streams	$D_L = 0.15\ U_{max} H$

APPENDIX B. (continued)

Number	Investigator	Equation
10	Glover (1964), natural streams	$D_L = 500\ u_* H$ $D_V \approx 0.067\ u_* H$
11	Yotsukura and Fiering (1964), open channel flow (smooth)	$D_L = 13.0\ u_* H$
12	Bowden (1965), estuary and coastal flows flows	$D_L = 5.9\ u_* H = 0.26\ \bar{u} H$ for steady flows. D_L(oscilatory flow) = 1/2 D_L (steady flow)
13	Holley and Harleman (1965), natural streams	$D_L = 77\ n\ U_{max}\ Rh^{5/6}$
14	Levenspiel and Smith (1966), flow through tubes	$D_L = \frac{\bar{u}}{8} [8\sigma^2 + 1)^{1/2} - 1] L'$
15	Hays (1966), open channel flow	$D_L = 6.39\ H^{1.24} E^{0.3}$
16	Thackston (1966), natural streams	$D_L = 7.25\ u_* H\ (\frac{\bar{u}}{u_*})^{1/4}$
17	Cederwall (1967), supported Taylor's work	$D = (u'^2)^{1/2}$
18	Stiger and Siemons (1967), natural streams	$D_L = 13{,}000\ (1 - \frac{x}{L_o})^3$

APPENDIX B. (continued)

Number	Investigator	Equation
19	Fischer (1967), natural streams	$D_L = \frac{1}{A}\iint_A \{\bar{u}'' \int_0^y \frac{1}{\varepsilon y d(d)} [\int_0^y \int_0^d u''dzdy]dy\}dA$
		$D_L \simeq 0.30 \left(\frac{\overline{u''}}{u_*}\right)^2 \left(\frac{L}{R}\right)^2$
20	Sooky (1969), open channel flow	$D_L = K_i' + K' + K''$
		in which: $K_i' = 0.222 \frac{u_* Hm}{k^3 a} \alpha$
		$K' = aK''$
		$K' = \frac{1}{9} k u_* Hm$
21	Holley, et al. (1970), oscilatory channel flow	$D_T = 0.16 \left(\frac{Tu''}{B}\right)^2 u_* H$
22	Bansal (1971), natural streams	$\log_{10} \left(K \frac{v_s}{v} \frac{D_L}{VH}\right) = 6.45 - 0.762 \log_{10} \left(\frac{VH}{\nu}\right)$
		$\log_{10} \left(K \frac{v_s}{v} \frac{D_L}{u_* H}\right) = 6.467 - 0.714 \log_{10} \left(\frac{u_* H}{\nu}\right)$
		$\log_{10} \left(\frac{D_V}{\nu}\right) = -8.1 + 1.558 \log_{10} \left(\frac{VH}{\nu}\right)$

APPENDIX B. (continued)

Number	Investigator	Equation
22	Bansal (cont.)	$\log_{10}\left(\frac{D_V}{V}\right) = -8.08 + 1.89 \log_{10}\left(\frac{u_* H}{V}\right)$
		$\log_{10}\left(\frac{D_T}{vH}\right) = -3.597 + 1.378 \log_{10}(B/H)$
		$\log_{10}\left(\frac{D_T}{u_* H}\right) = -2.698 + 1.498 \log_{10}(B/H)$
23	Cristodoulou, et al. (1974), Massachusetts Bay	$\overline{D} = \sqrt{D_T D_L}$
24	Ouellet and Cerceau (1975), St. Lawrence Estuary	$D_L = 77\ n\ \lvert\overline{u}\rvert\ R^{5/6}$ in fps system
25	Vrengdenhil and Voogt (1975), Estuaries	$D_L = \frac{0.07\ \lvert u\rvert\ H\ \sqrt{g}}{c}$
26	Abbott (1977), open channel	$D_{advective} = \left[\frac{\alpha - \beta^2}{2}\right] CVH$
		$D_{rolling} = \frac{c^3}{18}\left(\frac{H}{r}\right)^2 vH$

APPENDIX C
UTILIZATION OF STUDY RESULTS

Figures 5.1 to 5.32 may be used to estimate the gross circulation and sedimentation characteristics of marina basins that are roughly rectangular in planform, have aspect ratios (L/W) between 0.3 and 3.0, an entrance width/basin length ratio (W_e/L) between 0.11 and 0.33, and have single entrances approximately 66 m wide. The effects of wider or multiple entrances can be assessed in some instances. Figures 5.1 to 5.21 may be interpolated for a particular basin aspect ratio (L/W) to yield an estimate of local non-dimensionalized velocities and sedimentation rates. Dimensionalized quantities are obtained by multiplying the local non-dimensional speed, $\sqrt{u^2 + v^2}/u_o$, by the entrance velocity, u_o, and the local non-dimensional sedimentation rate, S/u_oC_o, by the entrance velocity and entrance boundary suspended sediment concentration, C_o, for cases where C_o is less than $3x10^{-4}$kg/l. In the event that C_o exceeds $3x10^{-4}$kg/l, S/u_oC_o should be multiplied by $C_o^{7/3}$ rather than C_o. Figures 5.22 and 5.32 may be interpolated to yield estimates of the basin-averaged circulation speed and sedimentation rate as well as the percent of basin area having a particular range of circulation or sedimentation rates. Figure 5.32D can also be used to adjust the sedimentation estimates for entrance boundary velocities in excess of 0.15 m/s or for increased transverse dispersion effects (see Section 3.5). The following examples illustrate the use of the results of this study.

A. Uni-directional steady or slowly-varying channel flow

A 370m by 170 m small-boat basin is to be constructed along a river with the longer dimension parallel to the channel. Stream velocities and vertically-averaged suspended sediment concentrations are about 0.5 m/s and 10^{-3}kg/l. It is desired that circulation within the basin be optimized and that sedimentation rates be estimated.

Using a single entrance, optimum circulation will result if the entrance is centrally located in the breakwater. Its width will be determined by navigation requirements. Figure 5.14 presents the non-dimensionalized velocity and sedimentation fields in

plan view for a single centrally-located entrance and curves C4X2 and C4X2V50 of Figures 5.23A and 5.32D, respectively, indicate the relative area contained within each isopleth of Figure 5.14. Dimensionalized velocities are recovered by multiplying $\sqrt{u^2+v^2}/u_o$ by u_o=0.50 m/s but since the channel suspended sediment concentration, C_o, is greater than 3×10^{-4}kg/l, the dimensionalized sedimentation rate is recovered by multiplying S/u_oC_o by $u_oC_o^{7/3}$ wherein the dimensions of $C_o^{7/3}$ remain M/L^3. Thus, the basin-averaged circulation speed will be about 0.02 x 0.05 m/s or 0.01 m/s and the mean sedimentation rate about 5.5×10^{-8}x 0.5 m/s x $(10^{-3}$kg/l x 10^3l/m$^3)^{7/3}$ or 2.8 x 10^{-8}kg m^{-2}s^{-1}. Assuming a bulk density of 1.2 x 10^3kg/m^3 for the semi-consolidated sediment, then the basin-averaged shoaling rate would be about 8 x 10^{-4}m/yr.

If Engelund's (1974) transverse dispersion coefficients are adopted, the sedimentation rates will be higher than indicated above. From Figure 5.32D, the average sedimentation rate increases approximately 10% per order of increase in the transverse dispersion coefficient, relative to the values for case C4X2. Assuming that such behavior is independent of the magnitude of the velocity, the sedimentation rates of Figure 5.14B may be increased about 14%. Thus, the basin-averaged sedimentation rate will be about 3.2×10^{-8} kg m^{-2}s^{-1} and the shoaling rate will be about 9×10^{-4}m/yr.

For comparison, if a single entrance is located at the downstream end of the breakwater, the sedimentation rate will be minimized but the circulation will be weaker than for a centralized entrance. The velocity field is given by Figure 5.16A and dimensionalized velocities are obtained by multiplying the values shown by 0.50 m/s. Curve D4X2 of Figure 5.25A indicates that the basin-averaged velocity will be very low, about 0.002 x 0.50 m/s or 0.001 m/s, an order of magnitude lower than for a centralized entrance. Assuming that increases in the entrance velocity or transverse dispersion have similar effects for eccentric entrances as for centralized entrances, Figure 5.32D indicates that the basin-averaged sedimentation rate should be decreased about 65%. Thus,

the value of 0.35 from curve D4X2 of Figure 5.32B is reduced to 1.2×10^{-9} or about 6×10^{-10} kg $m^{-2}s^{-1}$ which is approximately two orders lower than for the centralized entrance. An intermediately positioned entrance will presumably produce correspondingly intermediate circulation and sedimentation characteristics. The exact position of the entrance will generally be determined by the disposition of docking and berthing facilities and navigation requirements.

B. Tidal Flow

An 800 m by 400 m basin is to be situated on a tidal channel where the maximum flood and ebb currents are respectively about -0.50m/s and 0.70 m/s, positive values indicating flow towards the ocean. The longer basin dimension is to be oriented parallel to the channel, suspended sediment concentrations average 10^{-4}kg/l. Estimates of the mean circulation and sedimentation characteristics for various entrance configurations are desired. Two alternative configurations are considered, first, a single centrally-located 120 m-side entrance and second, two 60-m entrances symmetrically disposed about the center of the breakwater.

The flood and ebb stages are considered separately, the analysis proceeding similar to that of the preceeding example. Estimates of circulation and sedimentation are thus obtained for each tidal stage. Finally, these values are averaged to provide estimates for the complete tidal period. It must be remembered, however, that the results of this study do not take into consideration the effects of tidal filling and emptying of the basin and hence only provide order-of-magnitude estimates.

Assuming a simple sinusoidal tide curve over each tidal stage, the stage-averaged entrance boundary velocity, u_o, will be one-half the stage maximum. For the case under consideration, the stage averages are -0.25m/s and 0.35m/s. For a single, centrally-located 120m-wide, entrance Figures 5.17 and 5.25A (curve CE4X2) describe the circulation characteristics under steady flow conditions. If Figure 5.14 with channel flow from left to right

represents flood conditions, the values shown are multiplied by the mean flood velocity, in this case -0.25 m/s. The mirror image of Figure 5.15 then represents the ebb condition and the values shown should be multiplied by the mean ebb velocity, 0.35 m/s. The summation and averaging of the magnitudes of the dimensionalized ebb and flood velocities at each point yields an estimate of the velocity averaged over the tidal cycle. Such a procedure ignores the effects of filling and emptying of the basin and thus does not take into account the partial isolation of basin waters from entrance shear effects during the basin-emptying stage. Average ebb-stage circulation may be weaker or stronger than predicted by the methods employed here, depending on the strength of the flood-induced circulation.

Curves CE4X2 in Figures 5.25A and 5.25B are treated in a similar fashion. The basin-averaged non-dimensionalized circulation speed is about 0.07 which gives average flood and ebb speeds of 0.018 m/s and 0.025 m/s, respectively, which when averaged give a tidal-mean circulation speed of about 0.021 m/s. The basin-averaged non-dimensionalized sedimentation rate for steady flows with u_o equal to 0.15 m/s is about 1.75×10^{-7}. This mean sedimentation rate must be adjusted for the effects of entrance boundary velocities different from that used in this study, i.e. 0.15 m/s in most cases. Interpolating between curves C4X2 and C4X2V50 of Figure 5.32D indicates that the basin-averaged sedimentation rates should be lowered about 18% and 36%, respectively, for the flood and ebb stages. The dimensionalized sedimentation rates for each tidal stage are then obtained by multiplying by the product of the entrance boundary velocity and the suspended sediment concentration. (If the suspended sediment concentration had been greater than 3×10^{-4} kg/l, $C_o^{7/3}$ would have been used rather than C_o.) The respective flood and ebb values are then about 1.43×10^{-7} kg $m^{-2}s^{-1}$ and 1.12×10^{-7}kg $m^{-2}s^{-1}$. Averaging these rates gives a tidal-mean sedimentation rate of 1.28×10^{-7}kg $m^{-2}s^{-1}$ or, using the semi-consolidated sediment

density of $1.2 \times 10^3 kg/m^3$, the average shoaling rate will be about $3.4 \times 10^{-3} m/yr$.

An alternate basin design is shown in Figure 5.18 with two 66 m symmetrically-disposed entrances. The analysis proceeds as described above, the values in Figure 5.18A and its mirror image being multiplied by the mean ebb and flood channel velocities. Summing and averaging these values at corresponding points provides an estimate of the tidal-mean circulation field. Figure 5.25A, curve UD4X2, indicates a basin-mean velocity of about 0.085 that is 21% greater than for the single, centrally-located entrance. Uncorrected mean flood and ebb velocities are then about 0.022 and 0.029 m/s and the tidal-mean velocity is about 0.026 m/s.

Basin-averaged sedimentation rates for this configuration are essentially identical to those of the single entrance cases (Figure 5.25B) but their spatial distribution is of course different. If the values in Figure 5.18B and its mirror (ebb) image are decreased 18% and 36%, respectively, to adjust for the differences in modeled and prototype entrance velocities, the average of the values in the two figures will yield an estimate of the spatial distribution of sedimentation rates. Again, ebb conditions in the prototype may differ from that assumed here.